Okinawa Institute of Science and Technology

Graduate University

Thesis submitted for the degree of

Doctor of Philosophy

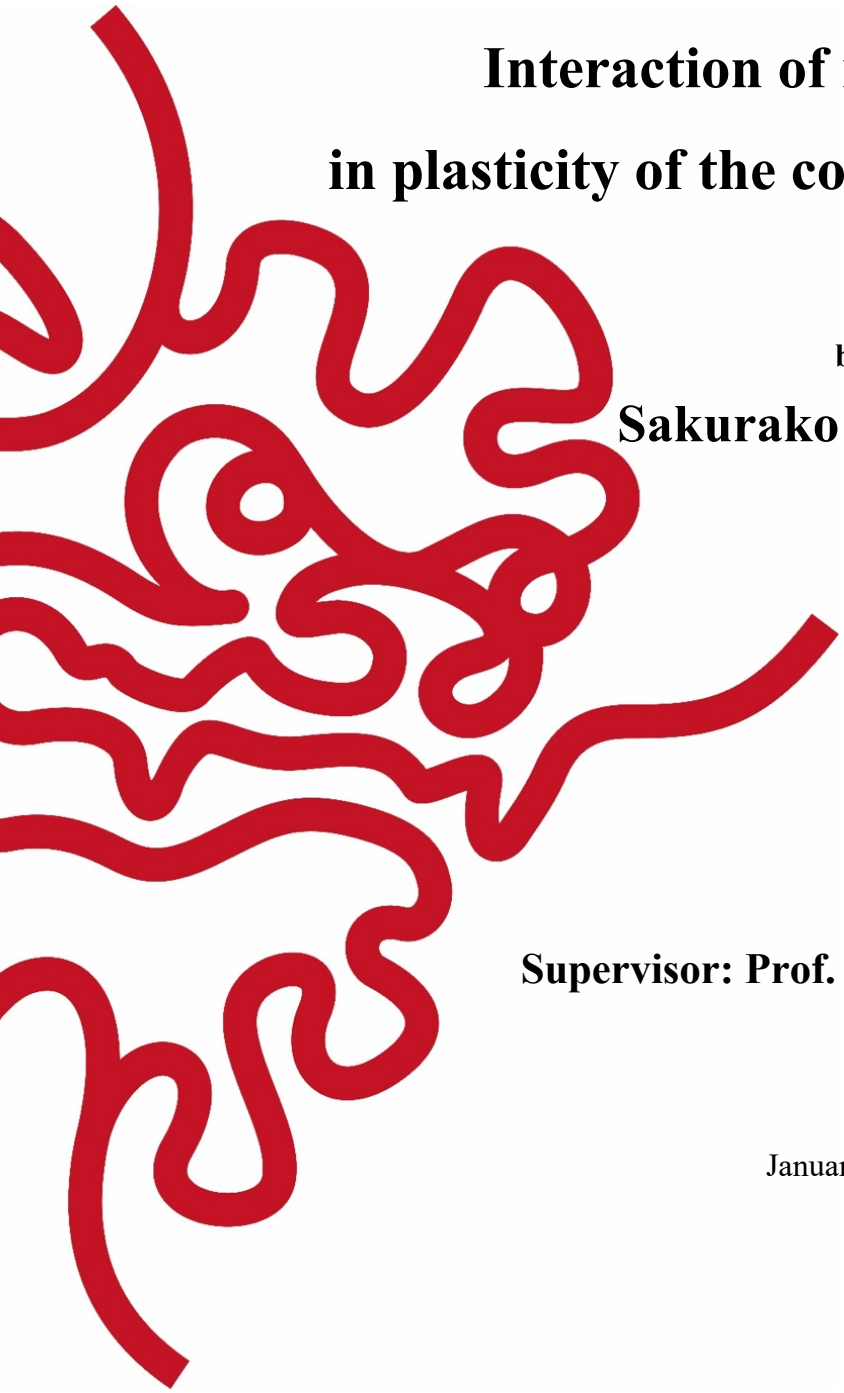

Interaction of multiple inputs in plasticity of the corticostriatal synapses

by

Sakurako Watanabe

Supervisor: Prof. Jeffery R Wickens

January 2021

Declaration of Original and Sole Authorship

I, Sakurako Watanabe, declare that this thesis entitled “Interaction of multiple inputs in plasticity of the corticostriatal synapses” and the data presented in it are original and my own work.

I confirm that:

- No part of this work has previously been submitted for a degree at this or any other university.
- References to the work of others have been clearly attributed. Quotations from the work of others have been clearly indicated and attributed to them.
- In cases where others have contributed to part of this work, such contribution has been clearly acknowledged and distinguished from my own work.
- None of this work has been previously published elsewhere.

Date: 13th January 2021

Signature: Sakurako Watanabe

Abstract

Dopamine-dependent plasticity in synapses between the cortical pyramidal neurons and the spiny projection neurons (SPNs) in the striatum is associated with reinforcement learning. Spike timing-dependent plasticity (STDP), which depends on the relative timing of pre- and postsynaptic activity, has been described in these synapses. Previously the STDP profile has been determined by testing single input-output events in isolation from the context of concurrently occurring multiple inputs into the same neuron. However, interactions among synaptic inputs at the level of the dendrites might influence STDP induction. The overall aim of this thesis is to study whether the activation of multiple synaptic inputs alters the characteristics of STDP in the corticostriatal pathway. Whole-cell electrophysiological recordings of SPNs in the dorsomedial striatum (DMS) of mouse brain slices were made in the presence of two inputs stimulated at different time points relative to postsynaptic firing. This protocol induced LTD depending on the timing of each input in SPNs expressing dopamine D1 receptors but not in SPNs expressing D2 receptors. When two inputs showed interactions, indicated by nonlinear summation of evoked EPSPs, STDP profiles were altered from those seen when single inputs were studied. In addition, pairing of two presynaptic inputs without postsynaptic firing also induced LTD, suggesting that pairing of synaptic inputs alone within a temporal window can induce associative synaptic plasticity. In separate experiments, optogenetic release of dopamine two seconds after each pairing modified STDP, depending on the input timing and interactions. Dopamine also modulated associative synaptic plasticity induced in the absence of postsynaptic firing. These results suggest that the rules for synaptic plasticity observed with multiple inputs to the same neuron are not identical to those observed when inputs are tested one at a time per neuron. This new knowledge helps to place STDP in the context of whole brain activity and adds to current understanding of associative learning in the striatum.

Acknowledgements

"Run to the rescue with love and peace will follow"
– River Phoenix

Firstly, I would like to express my gratitude to my supervisor Prof. Jeff Wickens for his intellectual inputs, continuous support, and above all patience. I would also like to thank all the former and current members of the Neurobiology Research Unit. In particular, Drs. Mayumi Shindou, Tomomi Shindou, Takashi Nakano, Atsushi Tamura, and Ms. Aya Zucca for their support on developing my electrophysiology skills. I would also like to thank Dr. Kiyoto Kurima for his continuous support on generating triple transgenic mouse line, Mr. Andrew Liu and Ms. Yumiko Akamine for their support on immunohistochemistry and cheerful company. Mr. Kavinda Liyanagama provided me with some programs for voltammetry analysis. I am also grateful to our research administrator Ms. Yukako Suzuki for her continuous administrative support.

Besides my lab colleagues, I would like to thank my mentor Prof. Gail Tripp and my thesis committee member Prof. Gordon Arbuthnott for their support and helpful comments on my thesis. My gratitude extends to the rest of OIST community, including the Animal Research Section for taking care of the animals, Dr. Paolo Barzaghi from the Imaging Section for his help on obtaining confocal microscopy images, and Dr. Darren George from Ganjuu Wellbeing Services for psychological support. Computational work in this thesis was conducted during the OIST Computational Neuroscience Course 2014. I am grateful to the support from the tutors during the workshop. In addition, I would like to thank OIST and Japan Society for the Promotion of Science (JSPS) for generous funding (Grants-in-aid for JSPS fellows, Grant No. JP17J00440).

I cannot complete my thesis without mentioning how grateful I am to my family and friends. I cannot thank my parents enough for all the support and opportunities they have given me throughout my life. Finally, and most importantly, I would like to thank my husband Viktoras and my wee Maya, without whom I could not have come this far to complete my degree.

List of Abbreviations

AC	adenylyl cyclase
ACd	dorsal anterior cingulate cortex
aCSF	artificial cerebrospinal fluid
AMPA	α-amino-3-hydroxy-5-methyl-4-isoxazolepropionic acid
AMPAR	α-amino-3-hydroxy-5-methyl-4-isoxazolepropionic acid receptor
ANOVA	analysis of variance
AP	action potential
bAP	backpropagating action potential
CaMKII	Ca^{2+}/calmodulin-dependent protein kinase II
cAMP	cyclic adenosine monophosphate
CB1R	cannabinoid type 1 receptor
CC	corpus callosum
CFE	carbon fiber electrode
ChI	cholinergic interneuron
ChR2	channelrhodopsin-2
D1R	dopamine type 1 receptor
D2R	dopamine type 2 receptor
DA	dopamine
DARPP-32	dopamine- and cAMP-regulated phosphoprotein, Mr 32 kDa
DAT	dopamine transporter
DLS	dorsolateral striatum
DMS	dorsomedial striatum
dSPN	direct pathway spiny projection neuron
eCB	endocannabinoid
eGFP	enhanced green fluorescent protein
EP	entopeduncular nucleus
EPSP	excitatory postsynaptic potential
FSCV	fast scan cyclic voltammetry
GABA	γ-aminobutyric acid
GABAR	γ-aminobutyric acid receptor
GPCR	G-protein coupled receptor
GPe	external segment of the globus pallidus
GPi	internal segment of the globus pallidus
HFS	high frequency stimulation
IP_3R	inositol triphosphate receptor
iSPN	indirect pathway spiny projection neuron
Kir	inward rectifying potassium current
L-VGCC	L-type voltage gated calcium channel
LTD	long term depression
LTP	long term potentiation
mGluR	metabotropic glutamate receptor

MPH	methylphenidate
NMDA	N-methyl-D-aspartate
NMDAR	N-methyl-D-aspartate receptor
NMDG	N-methyl-D-glucamine
PB	phosphate buffer
PBS	phosphate-buffered saline
PFC	prefrontal cortex
PKA	protein kinase A
PLd	dorsal prelimbic cortex
PPR	paired pulse ratio
RMP	resting membrane potential
SDDP	subthreshold depolarization dependent plasticity
SEM	standard error of the mean
SNc	substantia nigra pars compacta
SNr	substantia nigra pars reticulata
SPN	spiny projection neuron
STDP	spike timing dependent plasticity
STN	subthalamic nucleus
t-LTD	spike-time dependent long term depression
t-LTP	spike-time dependent long term potentiation
VGCC	voltage gated calcium channel
VS	ventral striatum

Table of Contents

List of Figures

List of Tables

Chapter 1. Statement of the problem

"Everything great that ever happened in this world happened first in somebody's imagination."
– Astrid Lindgren

1.1. Introduction

The neural mechanisms for learning and memory are of fundamental importance for adaptive behavior. In recent decades, investigation of the neurophysiological basis of learning and memory has focused on activity-dependent synaptic plasticity as the most likely neural substrate for the physical changes in the brain brought about by experience (Martin, Grimwood, & Morris, 2000). Current concepts were foreshadowed by Hebb's neurophysiological postulate, which states that "When an axon of cell A is near enough to excite cell B and repeatedly or persistently takes part in firing it, some growth process or metabolic change takes place in one or both cells such that A's efficacy, as one of the cells firing B, is increased." (Hebb, 1949). Such changes were later discovered experimentally after electrical stimulation with trains of pulses, and termed long-term potentiation (LTP) (Bliss & Lomo, 1973), soon followed by experimental reports of long-term depression (LTD) (Lynch, Dunwiddie, & Gribkoff, 1977). A particular form of synaptic plasticity – spike timing-dependent plasticity (STDP) – that depends on the relative timing of pre- and postsynaptic action potentials – has since been described (Bi & Poo, 1998; Markram, Lübke, Frotscher, & Sakmann, 1997; Song, Miller, & Abbott, 2000). Because it occurs after stimulation that mimics naturally occurring firing patterns, STDP is considered a more physiologically relevant model of Hebbian learning (Feldman, 2012). In this thesis, I focus on STDP in the synapses connecting the cerebral cortex to the striatum, a basal ganglia structure that has been implicated in reinforcement learning (Packard & Knowlton, 2002).

The nature of STDP in the corticostriatal pathway has some unique features relevant to reinforcement learning. The principal neurons of the striatum, the spiny projection neurons (SPNs) receive many inputs including cortical, thalamic and dopaminergic inputs, which are activated during learning. Dopamine is a putative reward signal that is released at the time of reward delivery (Schultz, 1997; Schultz, Dayan, & Montague, 1997). A "three-factor synaptic modification rule" has been proposed that suggests that a conjunction of cortical input and striatal output activity at the corticostriatal synapses can lead to plastic changes representing associations between situations and actions, which are strengthened by dopaminergic inputs (Wickens & Kötter, 1995).

1.2. Statement of the research problem

Despite its apparent physiological relevance, the STDP paradigm has some limitations. Experimental determination of the dependence of STDP on the exact timing of presynaptic and postsynaptic spikes has been done by testing single input-output events in isolation from the context of concurrently occurring multiple inputs into the same neuron. An underlying assumption of the STDP paradigm is that the temporal requirements determined in these isolated conditions will apply *in vivo*, in the presence of multiple inputs. Current theoretical and computational models make this assumption, despite numerous indications that interactions among synaptic inputs at the level of the dendrites are highly probable. Therefore, there is a need to investigate STDP in the context of multiple synaptic inputs

experimentally to determine whether the plasticity of each synapse depends only on the relative timing of the presynaptic and postsynaptic spikes.

The overall aim of this thesis is to study STDP in the corticostriatal pathway, focusing on whether the activation of multiple synaptic inputs alters the characteristics of STDP. Until now, studies of STDP in this pathway have employed a single stimulating electrode and examined one time point per neuron. In the thesis research, two independent stimulating electrodes were used to test two different time points in the same neuron. This approach allowed for the possibility, suggested by biophysical considerations, that multiple inputs might interact during STDP induction and produce a spectrum of plasticity contrasting with that seen when single inputs are used. This approach employing multiple inputs may bridge *in vitro* STDP studies and *in vivo* learning mechanisms.

In addition to the immediate effects of spike-timing on synaptic plasticity, the three-factor rule referred to above also suggests that the timing of presynaptic and postsynaptic spikes may be an important determinant of which synapses show dopamine-dependent plasticity. Theoretical considerations suggest that temporally related synaptic inputs may leave "eligibility traces" (Barto, Sutton, & Brouwer, 1981; Sutton & Barto, 1992). Consistent with this idea, experiments have shown that STDP between the cortex and the striatum is modulated by temporally specific dopamine release (Shindou, Shindou, Watanabe, & Wickens, 2019; Yagishita et al., 2014). However, there have been very few studies of the spike-timing dependence of eligibility traces. In the thesis research, the approach to STDP is extended by adding optogenetic activation of dopamine release to study whether multiple inputs might interact in the initiation of eligibility traces.

1.3. Outline of the thesis

Chapter 2 is a review of the literature concerning current understanding of synaptic plasticity in the corticostriatal pathway.

In Chapter 3, experimental methods to investigate potential interactions of synaptic inputs in the SPN firing and corticostriatal STDP are described. The approaches include whole cell recording of postsynaptic potentials in mouse striatal SPNs, simulation of a biophysical SPN model, a series of STDP pairing protocols, an optogenetic approach to control dopamine release, and electrochemical recordings to measure dopamine release.

In Chapter 4, the results of STDP experiments investigating differences between presynaptically induced spikes and spikes induced by direct current injection are reported and compared with the model.

Chapter 5 reports the results of STDP experiments in which two independent stimulating electrodes were used to test two different time points in the same neuron. Effects of interactions of two inputs on plasticity are presented.

In Chapter 6, the effects of retroactive application of dopamine on plasticity of multiple synaptic inputs are reported.

Finally, in Chapter 7, I discuss the findings reported in the context of current knowledge of STDP mechanisms in the striatum.

Chapter 2. Literature review

"The brain is waking and with it the mind is returning.
It is as if the Milky Way entered upon some cosmic dance.
Swiftly the head mass becomes an enchanted loom where
millions of flashing shuttles weave a dissolving pattern,
always a meaningful pattern though never an abiding one;
a shifting harmony of subpatterns."
– Sir Charles Sherrington, Man on his nature (1942)

2.1. Introduction

The research reported in this thesis is focused on the mouse striatum and in particular the synapses connecting the cerebral cortex to the striatum. The striatum is the major input structure of the basal ganglia, receiving glutamatergic inputs from the cerebral cortex and thalamus, and dopaminergic inputs from the midbrain (Gerfen & Surmeier, 2011). Many pieces of evidence suggest that the striatum plays a significant role in certain types of learning. The underlying mechanism of such learning is postulated to involve synaptic plasticity in this circuitry (Koralek, Jin, Long, Costa, & Carmena, 2012; Yin et al., 2009). However, the rules for synaptic plasticity in the striatum are not yet completely understood.

In the following review, I first describe the basal ganglia circuit and corticostriatal pathway. I then review current understanding of synaptic plasticity, in particular spike timing dependent plasticity in the corticostriatal pathway. I discuss how the electrical structure of the neuron, in particular its dendritic arborization affects integration of synaptic inputs and firing activity. Furthermore, I describe the role of neuromodulators such as dopamine in STDP. Finally, I introduce an eligibility trace hypothesis and discuss how multiple inputs would interact and enable plasticity.

2.2. Anatomy of the striatum

The striatum is usually subdivided into three main sections, dorsomedial striatum (DMS), dorsolateral striatum (DLS), and ventral striatum (VS). These regions are involved in different types of learning (Yin & Knowlton, 2006). It is not known whether synaptic plasticity follows the same rules in all striatal areas or differs according to region. On one hand, there is a degree of uniformity in the circuitry of the striatum with regard to cell types and interconnections. It has been suggested that the information processing operations of the corticostriatal circuit are reiterated throughout the striatum, but the different regions are functionally distinct because of their different connections. On the other hand, it is possible that different rules apply in different areas. There are suggestions of regional variations in the rules for synaptic plasticity (Partridge, Tang, & Lovinger, 2000). At present, the conditions required for inducing synaptic plasticity in the striatum, and their possible regional variations, are not completely understood. The research reported in this thesis focuses on synaptic plasticity in one area, the DMS (Fig.2.1). The DMS receives inputs from associative areas of the cortex such as prefrontal cortex (PFC) and is associated with goal-directed learning (Gruber & McDonald, 2012; Reig & Silberberg, 2014; Yin & Knowlton, 2006).

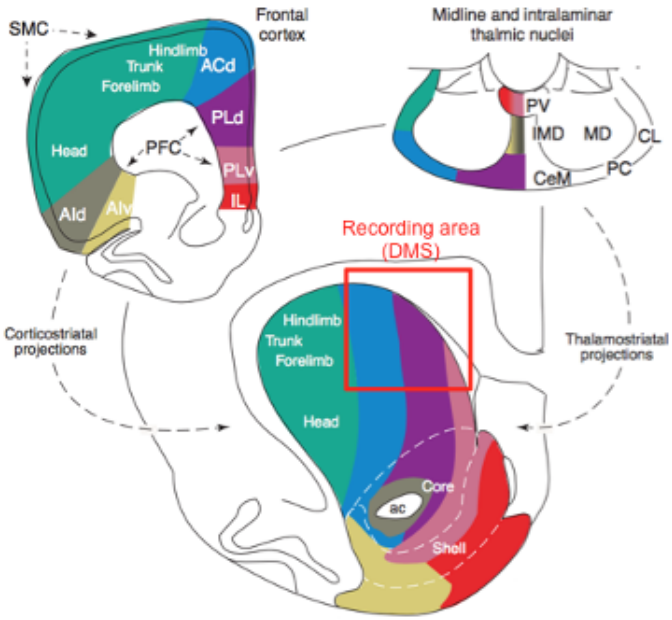

Figure 2.1. Schematic diagram of corticostriatal projection. Adapted from Voorn et al. (Voorn, Vanderschuren, Groenewegen, Robbins, & Pennartz, 2004) and modified to indicate the area of recording (DMS) for the current research (shown in red square). Of frontal cortical areas, dorsal anterior cingulate cortex (ACd; shown in blue) and dorsal prelimbic cortex (PLd; shown in purple) mainly project to the DMS.

2.3. The corticostriatal pathway

The major inputs to the striatum are from the cerebral cortex and the thalamus. As the gateway to the basal ganglia, the striatum receives inputs from all areas of the cortex (Mcgeorge & Faull, 1989) so that SPNs in the DMS receive multisensory cortical inputs (Reig & Silberberg, 2014). Up to 5000 cortical inputs converge onto a single neuron in the striatum (Kincaid, Zheng, & Wilson, 1998) and are remapped in the striatum in a mosaic (Graybiel, 1998). These inputs make monosynaptic connections with the principal neurons of the striatum, the SPNs. Thus, there is only one synapse between the input and output of the striatum, suggesting that this synapse may be a crucial determinant of the input-output relation of the striatum. The SPN output of the striatum projects back to frontal areas of the cerebral cortex via multiple basal ganglia relays, and it is thought to facilitate action (Fig.2.2) (Bolam, Hanley, Booth, & Bevan, 2000). The basal ganglia circuit diagram has been developed since, and functions of basal ganglia are not limited to motor control, but shifted to an interface between sensorimotor control and motivation, and reinforcement learning (Doya, 2007; Gerfen & Surmeier, 2011; Yin & Knowlton, 2006). Plasticity in this connection from cortex to SPNs is thus a possible basis for learning sensorimotor associations and is the focus of the present research.

While functions of the basal ganglia are vital for such motor and learning functions, dysfunctions of the basal ganglia have devastating effects on motor and cognitive functions, such as neurodegenerative diseases including Huntington's disease and Parkinson's disease.

The SPNs constitute over 90% of the neurons of the striatum (Gerfen & Surmeier, 2011). They have unique morphological and biophysical properties that give rise to sparse firing patterns, and they require convergent inputs for activation. They have densely spiny dendrites. Dorsal striatal SPNs have six primary dendrites that bifurcate twice to give rise to secondary to tertiary dendrites (Wilson, Groves, Kitai, & Linder, 1983). This huge dendritic surface area means that each SPN receives synaptic inputs from thousands of cortical and thalamic inputs. This provides a matrix of alternative input-output connections that could be strengthened or weakened during learning.

Although striatal SPNs receive numerous inputs, they typically display low firing rates because of their characteristic hyperpolarized resting membrane potentials of around -80 to -90mV set by inward rectifying K^+ current (Kir2) responsible for limiting synaptic integration (Shen et al., 2007). This holds the membrane potentials far from the firing threshold, a state termed the Down state (Wilson, 2008; Wilson & Groves, 1981). Together with slowly inactivating K^+ currents responsible for a long latency before spikes (Nisenbaum, Xu, & Wilson, 1994), SPNs show low firing rates even in response to synchronous cortical inputs (Stern, Jaeger, & Wilson, 1998; Stern, Kincaid, & Wilson, 1997). In the absence of cortical inputs, the SPNs remain essentially quiescent. This provides a basis for SPNs to serve as adaptive feature detectors with highly selective response properties.

Firing activity of the SPNs requires convergent synaptic inputs to overcome these hyperpolarizing currents. However, the corticostriatal input is anatomically sparse and low in firing rate (Turner & DeLong, 2000; Zheng & Wilson, 2002). Thus, to achieve convergent input a high degree of synchronization of cortical input is required, which may be produced by cell assemblies in the cortex representing multisensory experiences and motor intentions (Eichenbaum, 2018). Synchronization of these cortical inputs is thus an important input signal for causing the striatal neurons to fire and may also be important for engaging plasticity mechanisms (Mahon, Deniau, & Charpier, 2004). It could be anticipated from these physiological and anatomical features that activity-dependent plasticity in the corticostriatal projection might be sensitive to the precise timing of input spikes.

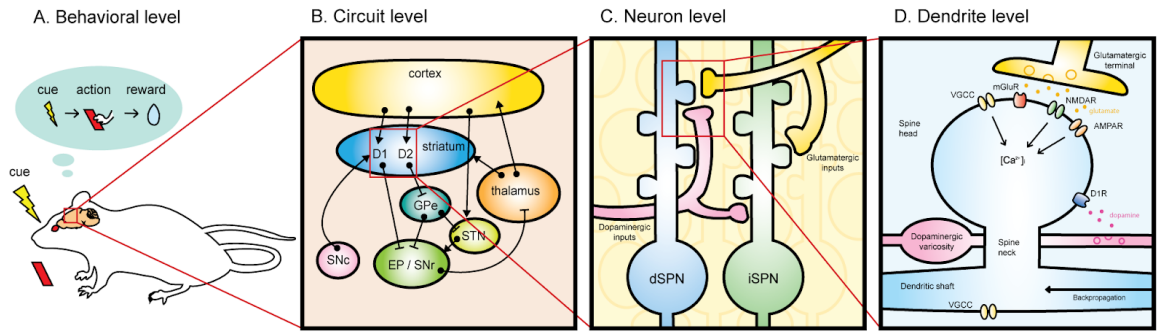

Figure 2.2. Corticostriatal pathway and reinforcement learning at different levels (A) At the behavioral level, the animal learns to associate a certain cue with an action that delivers a reward. Such a process occurs in the basal ganglia circuit. (B) A simplified diagram of the basal ganglia circuit. At the circuit level, the striatum receives inputs from the cortex and the thalamus. Within the striatum, D1R-expressing SPNs in the direct pathway (dSPN) project to the entopeduncular nucleus (EP, internal segment of the globus pallidus in primates, GPi) and the substantia nigra pars reticulata (SNr). The indirect pathway consists of D2R-expressing SPNs (iSPN) in the striatum projecting to the external segment of globus pallidus (GPe). Neurons in the GPe project to the SNr and the subthalamic nucleus (STN), which then projects to the SNr. The output nuclei of the basal ganglia project to the thalamus for motor output. The substantia nigra pars compacta (SNc) releases dopamine in the striatum. Based on (Bolam et al., 2000). (C) At the neuronal level, both dSPN and iSPN receive cortical glutamatergic inputs and dopaminergic inputs from the SNc at the same spine. (D) At the dendritic level, glutamatergic receptors, including N-methyl-D-aspartate receptors (NMDARs), α-amino-3-hydroxy-5-methyl-4-isoxazolepropionic acid receptors (AMPARs) and metabotropic glutamate receptors (mGluRs) are colocalized on the dendritic spine head together with different classes of voltage-gated Ca^{2+} channels (VGCCs). The dendritic shaft also expresses VGCCs, but the spine head and dendritic shaft are segregated by the high-resistance spine neck. Synaptic inputs result in an intracellular Ca^{2+} increase, which leads to downstream events for plasticity at individual spine heads. Dopamine released from dopamine varicosities binds to D1R (in the case of dSPN) dendritic spine and has modulatory effects.

2.4. Synaptic plasticity in general

Numerous studies over several decades have provided insight into the mechanisms for inducing and expressing synaptic plasticity. While there may be variations according to cell types, location, and connection, some generalizations are possible. Activity dependent changes in synaptic connections between two neurons were postulated by Hebb (1949) and were experimentally induced first in the hippocampus. Repeated stimulation of perforant path resulted in long-lasting potentiation of synaptic transmission (Bliss & Lomo, 1973). In the hippocampus, synaptic plasticity lasts for a few to several hours or even months, reflecting the timescale of memory functions involving consolidation of memory through protein synthesis (Frey & Morris, 1997; Martin et al., 2000).

Increase in synaptic efficacy is termed long-term potentiation (LTP). In the hippocampus, high frequency stimulation (HFS, 50 - 100 Hz) used as an induction protocol causes activation of N-methyl-D-aspartate receptors (NMDARs) by removal of Mg^{2+} block. A large increase of Ca^{2+} by entry through NMDAR underlies LTP. On the other hand, low frequency stimulation in the hippocampus causes a decrease in synaptic efficacy, termed long term depression (LTD) (Dudek & Bear, 1992). A smaller increase through voltage-gated Ca^{2+} channels (VGCC) mediates LTD. LTD is mediated by activation of postsynaptic metabotropic glutamate receptors (mGluRs) and subsequent release of endocannabinoids (eCB) from the postsynaptic neuron, acting on cannabinoid type 1 receptors (CB1R) on presynaptic neuron, resulting in the suppression of glutamate release (Mathur & Lovinger, 2012).

Elevation of intracellular Ca^{2+} is an important trigger for plasticity. However, the level of Ca^{2+} alone cannot determine the direction of plasticity (LTP or LTD). Same level of peak intracellular Ca^{2+} amplitude can induce either LTP or LTD (Nevian & Sakmann, 2006). The exact sequence of presynaptic inputs (EPSPs) and postsynaptic activity (APs) seems to activate additional mechanisms to determine the direction of plasticity.

2.5. Spike timing dependent plasticity in general

Synaptic plasticity protocols that concern the precise temporal relationship between spikes were postulated (Levy & Steward, 1983), later discovered and termed spike timing dependent plasticity (STDP) (Bi & Poo, 1998; Markram et al., 1997; Song et al., 2000). Spike timing dependent plasticity is caused by backpropagating action potentials and presynaptic inputs in dendrites (Magee & Johnston, 1997). STDP shows a Hebbian nature in many brain areas, and hence it is a candidate for a learning mechanism (Feldman, 2012).

Generally, STDP is induced by pairing presynaptic stimulation with postsynaptic depolarization for multiple times (60-100 times) at low frequency (0.1-10 Hz). The precise order of presynaptic input and postsynaptic action potential within a certain time window (tens of milliseconds timescale) determines the sign and magnitude of plasticity (Bi & Poo, 1998; Markram et al., 1997). In experimental STDP studies in areas such as the cortex and the hippocampus, when presynaptic stimulation precedes postsynaptic spiking (pre-post timing), this usually results in LTP, whereas when postsynaptic spiking is induced before presynaptic input (post-pre timing), this results in LTD (Feldman, 2012; Markram et al., 1997). This is consistent with Hebb's postulate (Hebb, 1949), as presynaptic inputs that contribute to postsynaptic firing (pre-post) are strengthened, while presynaptic inputs that occur after postsynaptic firing (post-pre) have no causal effect on postsynaptic firing and are subsequently weakened. Hence, this form of STDP is termed Hebbian STDP (Feldman, 2012). To distinguish it from HFS-driven plasticity, such STDP-driven LTP and LTD are usually termed t-LTP and t-LTD, respectively (Wickens, 2009).

2.6. Synaptic plasticity in the corticostriatal pathway

In parallel with the elucidation of the phenomena and mechanisms of LTP and LTD in other brain regions, a body of knowledge was accumulated concerning the corticostriatal pathway. This proceeded at a slower pace in part because the non-laminar anatomical structure of the striatum made the interpretation of extracellular field potentials difficult. Thus, intracellular recording methods had to be used. In addition, plasticity in the corticostriatal pathway presented a different picture from the hippocampus. The reasons for these differences are partially understood, in terms of biochemical differences, the strong influence of neuromodulators, and differences in cellular properties.

In the corticostriatal pathway, early studies showed that LTD was induced by protocols that in other areas would produce LTP. High frequency stimulation (50-100Hz) of presynaptic cortical neurons paired with postsynaptic depolarization resulted in LTD in the SPN *in vitro* (Calabresi, Maj, Pisani, Mercuri, & Bernardi, 1992). Induction of LTP was found to be possible, but required pharmacological manipulations, including Mg^{2+}-free solutions to activate NMDARs and dopamine (Calabresi, Maj, et al., 1992; Calabresi, Pisani, Mercuri, & Bernardi, 1992; Kerr & Wickens, 2001). In contrast, a similar HFS protocol *in vivo* resulted in LTP (Charpier & Deniau, 1997). In addition to *in vitro* vs. *in vivo* differences, developmental ages, regional differences (VS, DLS and DMS) (Lovinger, 2010; Partridge et al., 2000), influences of various neurotransmitter types and states of SPNs (Up vs. Down) also affect the direction of plasticity (Di Filippo et al., 2009).

2.7. Variability in *in vitro* corticostriatal STDP

In the corticostriatal pathway, STDP is probably a more physiologically relevant mechanism than HFS-induced plasticity for learning. Sparse, spike-timing phenomena are important especially because the natural *in vivo* firing rate of corticostriatal afferents (Turner & DeLong, 2000) and SPNs is quite low (0.1-10 Hz) (Wilson & Groves, 1981), which is much lower than the 50-100 Hz stimulation commonly used in HFS protocols. In addition, spatiotemporally correlated synchronized cortical inputs are necessary to make otherwise-silent SPNs fire (Mahon et al., 2004; Stern et al., 1998). Furthermore, learning involves temporally precise association of different stimuli represented in the cortex, so the timing of spikes may be logically necessary for synaptic plasticity and subsequent learning to occur (Izhikevich, 2007). However, studies to date have shown considerable variability in STDP in the corticostriatal pathway.

In vitro studies of STDP in the corticostriatal pathway show mixed profiles, as some studies show anti-Hebbian or non-Hebbian STDP, while other studies show Hebbian STDP (summarized in Table 2.1). The variety of induction protocols and the variation in results makes it very challenging for the student of striatal STDP to integrate the findings into a common and coherent picture. This variability in corticostriatal STDP may be explained by its high sensitivity to differences in experimental conditions. Such differences include use of GABA antagonists, differences in SPN cell types, regional differences, differences in the substrate activated by the electrode, developmental differences, and differences in pairing protocols.

Inhibition of the postsynaptic SPN during induction may have effects on the amount and direction of plasticity. For example, GABA antagonism contributes to differences in the direction of STDP. Fino et al. (2005) first demonstrated the anti-Hebbian rule for corticostriatal STDP *in vitro*. In their study, pre-post timing resulted in LTD, whereas post-pre timing resulted in LTP (Fino, Glowinski, & Venance, 2005). Shindou *et al.* (2011) also showed pre-post timing-induced LTD, but no plasticity after post-pre pairing (Shindou,

Ochi-Shindou, & Wickens, 2011). In contrast, in the presence of $GABA_A$-type receptor ($GABA_AR$) antagonists, Hebbian STDP was observed (Paille et al., 2013; Pawlak & Kerr, 2008; Shen, Flajolet, Greengard, & Surmeier, 2008). In the presence of GABA antagonists, Pawlak and Kerr (2008) showed that pre-post timing resulted in LTP, whereas post-pre timing resulted in LTD. $GABA_AR$-antagonists were used to control the precise timing of backpropagating action potentials (bAPs) by blocking GABAergic inhibition by interneurons and nearby SPNs. Paille *et al.* (2013) in their computational analysis suggested that GABA antagonism contributed the ratio of Ca^{2+} through NMDA and VGCC changed the equilibrium and made it more likely to undergo LTP (Paille et al., 2013). However, GABA antagonism alone may not be able to fully explain the different plasticity pictures found in corticostriatal STDP.

Different cell types also exhibit different plasticity profiles. Spiny projection neurons are classified into striatonigral neurons, involved in the direct pathway (dSPNs), and striatopallidal neurons, engaged in the indirect pathway (iSPNs). dSPNs express dopamine type one receptors (D1R), which are coupled to G_s and stimulate adenylyl cyclase (AC) to have a net excitatory effect via cAMP / PKA pathway. iSPNs express dopamine type two receptors (D2R) which are coupled to G_i and have a net inhibitory effect (Gerfen & Surmeier, 2011). Shen et al. (2008) showed in the presence of GABA inhibition that iSPNs followed the Hebbian-STDP rule, while dSPNs showed only pre-post LTP and post-pre LTD was induced only in the presence of D1R antagonist (Shen et al., 2008). Shindou et al. (2019) showed pre-post LTD in dSPNs, but no plasticity in iSPNs in the absence of GABA inhibition (Shindou et al., 2019). There are cell type differences, but differences in SPN cell types alone also cannot account for variability.

Regional differences (DLS, DMS, VS) within the striatum may also cause differences in plasticity. For example, regional differences in HFS-induced plasticity have been attributed to the heterogeneous nature of the striatum (Partridge et al., 2000). Many of the STDP studies done in the DLS show bidirectional STDP (Cui et al., 2015; Fino, Deniau, & Venance, 2009; Fino et al., 2005; Paille et al., 2013; Pawlak & Kerr, 2008; Xu et al., 2018). On the other hand, post-pre pairing at 30 ms temporal window in DMS did not induce any plasticity (Shindou et al., 2011, 2019). These findings might indicate that there are regional differences in the temporal requirements for STDP. In other brain regions, for example in the cerebellum, there are reports of regionally distinct temporal requirements for STDP. The temporal requirements for STDP in the flocculus and vermis are different, possibly due to their differences in behavioral functions (Suvrathan, Payne, & Raymond, 2016). In the flocculus, the temporal window is narrower and strict to 120 ms, whereas in the vermis, LTD with broad timing requirements was observed. Likewise, in the striatum, differences in plasticity profiles between locations of recording, such as between DLS and DMS, may be due to differences in temporal requirements. However, there have not yet been regional comparisons of the timing requirements for STDP in the striatum. People working in different regions have used different induction protocols. Thus, regional differences in timing requirements require further investigation.

In relation to the substrate activated by stimulating electrodes during induction, there is evidence that even STDP stimulation protocols may cause release of multiple neurotransmitters and neuromodulators, especially when intrastriatal stimulation is used. Thus, the positioning stimulating electrodes in different locations, such as the striatum, cortex, or corpus callosum (CC), may contribute to the difference in plasticity by activating different substrates. Similarly, the frequency of stimulation may have different effects on neuromodulator release. For example, theta stimulation within the striatum in Shen et al. (2008)'s protocol and cortical stimulation in the presence of bicuculline (Pawlak & Kerr, 2008) resulted in dopamine release (Shindou et al., 2019). These protocols induced Hebbian

STDP. Thus, stimulation-evoked dopamine release may contribute to corticostriatal Hebbian STDP when these protocols are used.

Age difference and developmental changes may also account for differences in plasticity profiles. Partridge et al. (2000) showed in HFS-induced plasticity that in DLS, there is a developmental shift from LTP to LTD with different developmental stages (P16 - 34), whereas no developmental shift was observed in the DMS (Partridge et al., 2000). Some of the corticostriatal STDP studies in the DLS were done in animals as young as one (Cui et al., 2015) or two weeks (Cui et al., 2015; Fino et al., 2009, 2005; Pawlak & Kerr, 2008; Shen et al., 2008), and differences may be due to developmental shifts. In the DLS of younger animals (P7 - 10), unidirectional, Hebbian pre-post t-LTD was observed due to lack of tonic GABA signaling, which starts to appear in the juvenile stage (Valtcheva et al., 2017). Thus, developmental stages should be taken into account when considering the different findings.

The fine structure of timing of presynaptic and postsynaptic spikes also seems to be a significant determinant of direction and magnitude of plasticity. In some protocols, this temporal structure can be described simply in terms of relative timing of pre- and postsynaptic spikes. For example, Pawlak and Kerr (2008) showed that a time window of -10 to -20 ms produced mixed results and no overall change, and that -30 ms time window was able to produce LTD. In these experiments they used a pairing frequency of 60 times at 0.1 Hz. On the other hand, Fino et al. (2005) showed no plasticity outside of the 30 ms time window with a pairing frequency of 100 times at 1 Hz. Protocol differences in terms of pairing number and frequency also contribute to the differences in STDP profile. Cui et al. (2015) showed that pre-post pairing induced LTD only when protocol was above 50 pairings. On the other hand, higher pairing number (75 - 100 pairings) and lower pairing number (5 - 10) induced post-pre LTP, but only half the cells showed post-pre LTP after 50 pairings (Cui et al., 2015).

Some protocols do not allow a simple description in terms of relative timing because they have both pre-post and post-pre components. For example, Shen et al. (2008)'s protocol actually had three EPSPs paired with three APs at 50 Hz consecutively, which means that first EPSP was given at +5 ms prior to the first AP, but the second AP followed the first EPSP 15 ms later, making -15 ms time window for the first EPSP. This protocol induced LTP in both dSPNs and iSPNs (Shen et al., 2008). Number of postsynaptic action potentials (1 AP or 3 APs) also contributes to the amount of Ca^{2+} influx and subsequent plasticity. While many studies with higher frequency (e.g. 1 - 5 Hz) only pair single APs (Fino et al., 2005; Paille et al., 2013; Shen et al., 2008), with mild frequency protocol (60 times at 0.1 Hz), pairing with single APs failed to induce plasticity, while pairing with AP triplets induced LTD (Shindou et al., 2011).

Overall, the evidence indicates that corticostriatal STDP is sensitive to subtle differences in experimental conditions. The variability observed may reflect regional, developmental, or neurochemical heterogeneity of the striatum. However, the association with distinct functional specializations remains speculative at this stage. On the other hand, an emerging understanding of dendritic processing in SPNs may provide a fundamental insight into the determinants of STDP at the synaptic level.

Publication	Induction protocol post-pre	Induction protocol pre-post	Direction of plasticity	Other conditions
Fino *et al.* (2005)	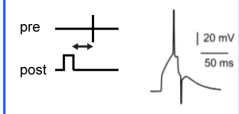 100 times @1Hz Δt= ~-30 ms	 100 times @1Hz Δt= ~+30 ms	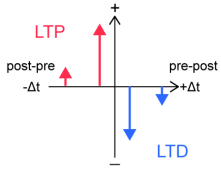	DLS rats (2-3 weeks) -87mV 32°C
Pawlak & Kerr (2008)	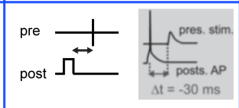 60 times @0.1Hz Δt= -10, -20, -30 ms	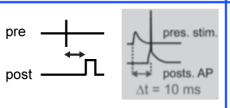 60 times @0.1Hz Δt= +10 ms	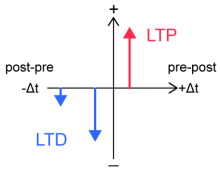	DLS rats (2-3 weeks) -83mV 31-33°C +GABA inhibition
Shen *et al.* (2008)	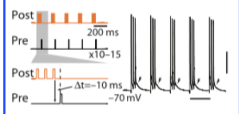 10-15 times @5Hz Δt= -10 ms	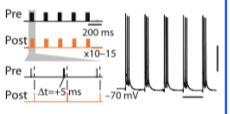 10-15 times @5Hz Δt= +5 ms	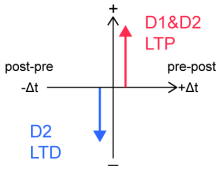	DLS&DMS mice (2-4 weeks) -70mV 22-23°C +GABA inhibition
Fino *et al.* (2009)	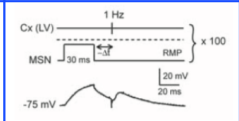 100 times @1Hz Δt= ~-110 ms	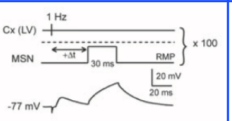 100 times @1Hz Δt= ~+110 ms	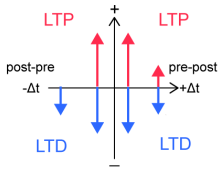	DLS rats (2-3 weeks) -73mV 32°C
Shindou *et al.* (2011)	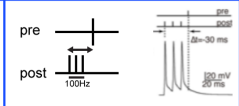 60 times @0.1Hz Δt= -30 ms	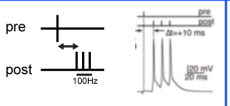 60 times @0.1Hz Δt= +10 ms	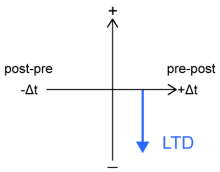	DMS mice (8 weeks) -80mV 30°C
Paille *et al.* (2013)	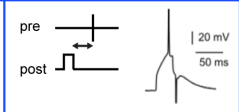 100 times @1Hz Δt= ~-25 ms	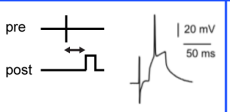 100 times @1Hz Δt= ~+30 ms	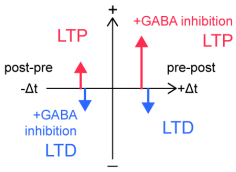	DLS rats (2-13 weeks) -72mV 34°C +GABA inhibition
Yagishita *et al.* (2014)		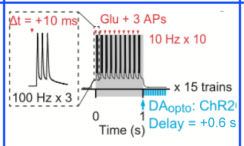 15 trains 10 bursts @0.1Hz	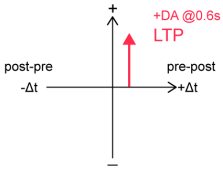	ventral striatum mice (5-7weeks) -70mV 30-32°C DA optically applied
Cui *et al.* (2015) Xu *et al.* (2018)	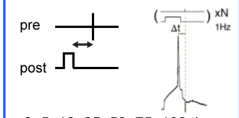 2, 5, 10, 25, 50, 75, 100 times @1Hz Δt= ~-30 ms	 2, 5, 10, 25, 50, 75, 100 times @1Hz Δt= ~+30 ms	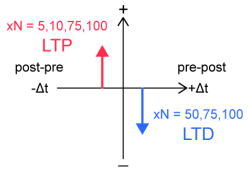	DLS rats (2-3 weeks) mice(2-3 weeks, 8-12 weeks) -78mV 34°C
Shindou *et al.* (2019)	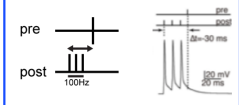 60 times @0.1Hz Δt= -30 ms	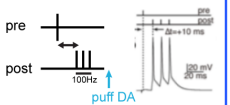 60 times @0.1Hz Δt= +10 ms	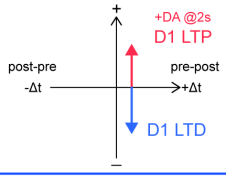	DMS mice (8 weeks) -80mV 30°C DA puff applied

Table 2.1. Summary of *in vitro* STDP studies in the corticostriatal pathway. Main results from each publication are summarized in terms of induction protocols, direction of plasticity and other conditions to note. Induction protocols specify number of pairing, frequency, number of spikes, and temporal window. Direction of plasticity showed the overall results for post-pre and pre-post timings. X-axis is roughly normalized to -50 ms to +50 ms range. Y-axis indicates the relative strength of plasticity (%

(Table 2.1. continued) change in synaptic efficacy, in potentials or currents), where + means LTP and – means LTD. Conditions describe the area of recording, animals used (age), recording voltage, recording temperature and other things to note. Figures for induction protocols were adapted and modified from the original papers.

2.8. Dendritic processing in STDP

One of the key questions in studies of synaptic plasticity concerns how synaptic change is localized to a specific subset of synapses, and how these are selected for modification from among the many thousands on each neuron. In other words, how is experience encoded in specific synapses? Several decades of study of activity-dependent changes in synaptic efficacy have indicated that the biophysical properties of dendrites and dendritic spines play a significant role in this specificity of synaptic plasticity. The general understanding of these factors has been obtained from studies in various regions such as the hippocampus and cerebral cortex. These factors take a specific form within the SPNs.

The densely spiny dendrites of the SPNs provide a favorable substrate for experience-dependent plasticity. Specificity of synaptic plasticity may in part be due to the biophysical properties of dendritic spines (Matsuzaki, Honkura, Ellis-Davies, & Kasai, 2004). Dendritic spines have highly compartmentalized structure, with clustering of different channels and receptors so that synaptic inputs to one spine can produce localized effects without influencing neighboring spines (Branco & Häusser, 2010; Gulledge, Kampa, & Stuart, 2005). Synaptic inputs cause Ca^{2+} influx by activating multiple channels, including VGCCs of L-, R- and T-types, NMDARs, α-amino-3-hydroxy-5-methyl-4-isoxazolepropionic acid receptors (AMPARs) and activating release from internal Ca^{2+} stores (Fino et al., 2009). Compartmentalization allows spatially restricted Ca^{2+} influx in individual dendritic spines upon synaptic inputs, which allow specificity of synaptic plasticity at the level of single synapses and spines (Yuste, 2013; Yuste & Denk, 1995).

In contrast to the chemical compartmentalization effects of dendritic spines due to the biophysics of diffusion, electrical current spread from spine to dendrite or dendrite to spine follows different laws. Current flowing from the synaptic channels down the spine neck to the dendrite is attenuated to a much greater degree than current flowing in the opposite direction because of the asymmetry in impedance (Araya, Jiang, Eisenthal, & Yuste, 2006). Thus, membrane potentials can differ between spines according to synaptic activity, but spines on a given dendrite will follow the dendritic membrane potential. Further complicating this structure, dendrites are not isopotential compartments and their membrane potential may vary along the length of the dendrite. An action potential may propagate along a dendrite transiently causing localized depolarization (Kerr & Plenz, 2002). Action potentials, when generated, not only propagate down the axon to transmit information to the next neuron, but they also propagate back to the dendrites via dendritic, voltage-gated Na^{+} and Ca^{2+} channels (Stuart, Spruston, Sakmann, & Häusser, 1997). Backpropagating action potentials (bAPs) cause a local supralinear depolarization in dendrites mediated by voltage-dependent Na^{+} and Ca^{2+} channels and NMDARs, termed dendritic spikes (Waters et al., 2008). This backpropagation serves as a signal to spines that reports output activity.

The combination, at individual dendritic spines, of information about synaptic inputs and action potential outputs of the entire neuron, provides a foundation for STDP. Backpropagation itself may not always provide sufficient depolarization for plasticity, but local dendritic depolarization plays a major role in distal dendrites (Feldman, 2012; Letzkus, Kampa, & Stuart, 2006). In one conception of STDP, the timing of synaptic inputs with respect to bAP, and the effect of this timing on spine Ca^{2+} concentration, is the basis for the timing dependence of plasticity. However, the mechanism is more complicated than that. Although pairing synaptic input and bAP at certain time windows resulted in sublinear (post-pre) or supralinear (pre-post) Ca^{2+} increase, the Ca^{2+} increase by itself did not determine the direction of plasticity (Nevian & Sakmann, 2004, 2006). Some other mechanism is involved in the detection of relative spike timing and its translation into STDP.

These general principles governing the induction of STDP provide initial expectations concerning STDP in the striatum. In striatal SPNs, somatic action potentials backpropagate to high-order distal dendrites (Kerr & Plenz, 2004). Shindou et al. (2011) showed that triplets of action potentials cause a supralinear increase in the local spine Ca^{2+} when paired with EPSP at pre-post timing, but not post-pre timing (Shindou et al., 2011). Striatal dendritic spines are also able to detect subthreshold local depolarizations that serve as plasticity-inducing signals, even in the absence of action potentials (Fino et al., 2009). The presence of local subthreshold depolarization at dendrites that receive synaptic inputs may be a more important trigger for plasticity than the somatic action potentials and bAPs (Hardie & Spruston, 2009; Letzkus et al., 2006).

Aside from the idealized consideration of electrical activity over the dendritic tree, in practice, experimental induction of STDP involves procedures that may engage different mechanisms from those that operate *in vivo*. Thus, the methods for experimentally inducing postsynaptic firing, be it by postsynaptic current injection or afferent stimulation, may also cause different STDP profiles (Fig.2.3). Due to the electrical and chemical compartmentalization of dendritic structures and heterogeneous distribution of backpropagation, the spatiotemporal profiles of Ca^{2+} increases in the dendrites and spines differ when the source of activation is synaptic inputs rather than somatic depolarization (Carter & Sabatini, 2004). Upon receiving synaptic inputs, local depolarization at the dendrites is much higher than somatic depolarization (Larkum & Nevian, 2008). As the temporal relationship between the input EPSP and the output action potential, represented as a Ca^{2+} signal, is a key signal for coincidence detection for plasticity (Nevian & Sakmann, 2004), different means of firing induction may have consequences for induction of synaptic plasticity. In other words, while the action potential may be seen as an all-or-none event at the outgoing axon, the way the action potential is generated makes a difference in the dendrites. Thus, it is useful to ask how the different experimental methods for firing a neuron might lead to different electrochemical effects across the dendritic arborization and at individual dendritic spines.

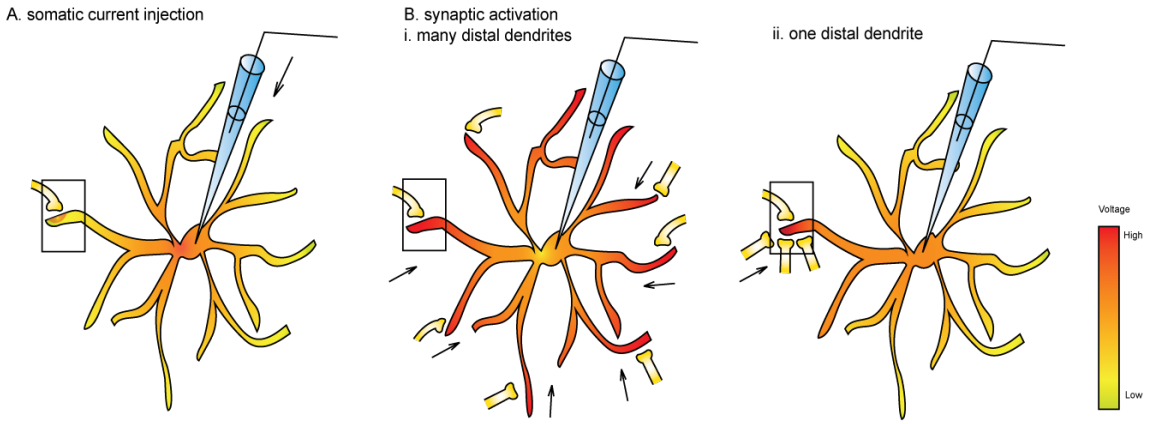

Figure 2.3. Electrical structure of an SPN and hypothetical electrical behavior of the neuron by different means of activation. (A) In conventional experimental studies including STDP, the neuron is activated by somatic current injection. A distal dendrite (highlighted inside the box) receives a backpropagating action potential, and a synaptic input from presynaptic stimulation is reflected as an EPSP. (B) Presynaptic stimulation has the following scenarios depending on the spatial distribution of the SPN dendrites and afferent axons that make synaptic contacts with them. Firing may occur by (i) synaptic activation to many dendritic processes, or by (ii) sufficient synaptic inputs to one distal dendrite. Note that at the soma, where recording takes place, the voltage may be the same between A and B, but at the dendrite (inside the box) the electric behavior may be different, especially at the level of dendritic spines.

2.9. Specificity of plasticity of multiple inputs within the STDP time window

The STDP curve describing the relationship between temporal difference of pre- and postsynaptic activity and the direction and magnitude of plasticity is based on the effects of a single stimulating electrode, tested cell by cell, at different timepoints in separate experiments (Bi & Poo, 1998; Fino, Deniau, & Venance, 2008; Pawlak & Kerr, 2008). We consider the time over which this curve is described as the STDP "window." According to the STDP concept, the occurrence, direction, and magnitude of STDP occurring within this window depends on the relative timing of inputs to the postsynaptic spike (Bi & Poo, 1998). In the typical STDP protocols used to map out the STDP curve within this window, the stimulating electrode activates a population of presynaptic inputs simultaneously. The plasticity induced by such synchronous inputs at different timepoints is then used to build up the STDP curve (Fig.2.4A). However, the curve may not be the same if there are multiple inputs acting on the dendrites in parallel (Fig.2.4B). Thus, there is a need to experimentally test an assumption of the STDP paradigm and of many computational models that the STDP curve determined using synchronous inputs at selected time points would operate the same way in the context of the inputs occurring naturally within the STDP window. Specifically, whether the STDP curve would apply in the "enchanted loom where millions of flashing shuttles weave a dissolving pattern" envisaged by Sherrington (Sherrington, 1942).

Input specificity is one of the essential characteristics required for synaptic plasticity to serve as an efficient memory mechanism. Input specificity may be defined as limiting the plasticity to the specific synapses that took part in firing the postsynaptic neuron, in the case of Hebbian plasticity. In STDP, input specificity would mean that the plasticity of synapses that are active in a certain temporal sequence with the postsynaptic spike would not be affected by other inputs that occurred at different times. Such temporal specificity implies that STDP occurs at each synapse on the basis of the temporal relationship of its activity to the postsynaptic spike, and otherwise independently of activity at other synapses.

In the striatum, input specificity of HFS-induced corticostriatal plasticity was shown by Calabresi et al. (2002) using two different stimulating electrodes in the cortex. In this study, two stimulating electrodes (test and conditioning stimulating electrodes) were inserted in the opposite side of the cortex from the recording electrode. Plasticity occurred only at the synapses that received conditioning stimuli, and not test stimuli, demonstrating an input specificity (Calabresi et al., 2002). However, of two stimuli, only one received the HFS while the other input was not stimulated. Thus, multiple inputs interleaved, but not synchronous with the stimulus, were not tested. While showing a degree of input specificity, Calabresi et al. (2002) leaves open the possibility that multiple inputs occurring within a narrow time interval may interact at the striatal SPN.

In an experiment that addressed specificity in the context of multiple input STDP, He et al. (2015) delivered in the cortex a sequence of pre-post and post-pre stimulation by stimulating one presynaptic input before and another presynaptic input after the postsynaptic spike. In this experiment, only the input that came at a specific time relative to the postsynaptic spike was strengthened by retroactive application of neuromodulators after STDP pairing. Norepinephrine application only enabled LTP in inputs by pre-post pairing but not by post-pre pairing. Also, serotonin only enabled LTD in inputs with post-pre pairing, and not pre-post pairing (He et al., 2015). However, this experiment concerns the specificity of eligibility, rather than plasticity. In the absence of neuromodulators, these protocols did not produce any plasticity in either pre-post or post-pre pairing. In addition, the two stimulated pathways were 300 μm apart, which was possible because of the laminar structure of the cortex, and their independence was confirmed by the absence of paired pulse

interactions (He et al., 2015). Therefore, potential effects of interactions of multiple inputs at dendrites in STDP have not been shown experimentally.

The foregoing indicates a lack of evidence concerning whether the specificity of STDP to specific temporal relationships is preserved in the higher traffic situation that occurs *in vivo*. The operation of STDP rules at individual synapses may not be feasible when dendrites receive multiple inputs because local electrical interactions occur among neighboring spines along a dendrite (Carter, Soler-Llavina, & Sabatini, 2007). For example, Tazerart et al. (2020) showed that stimulating an additional spine during STDP induction altered Ca^{2+} dynamics and the induction of t-LTP and t-LTD (Tazerart, Mitchell, Miranda-Rottmann, & Araya, 2020). Thus, there is a need for more experimental evidence concerning STDP under conditions of multiple inputs. The question remains open whether specificity of STDP is maintained, or how it is changed, when multiple parallel streams of inputs converge within the STDP temporal window (Fig.2.4B).

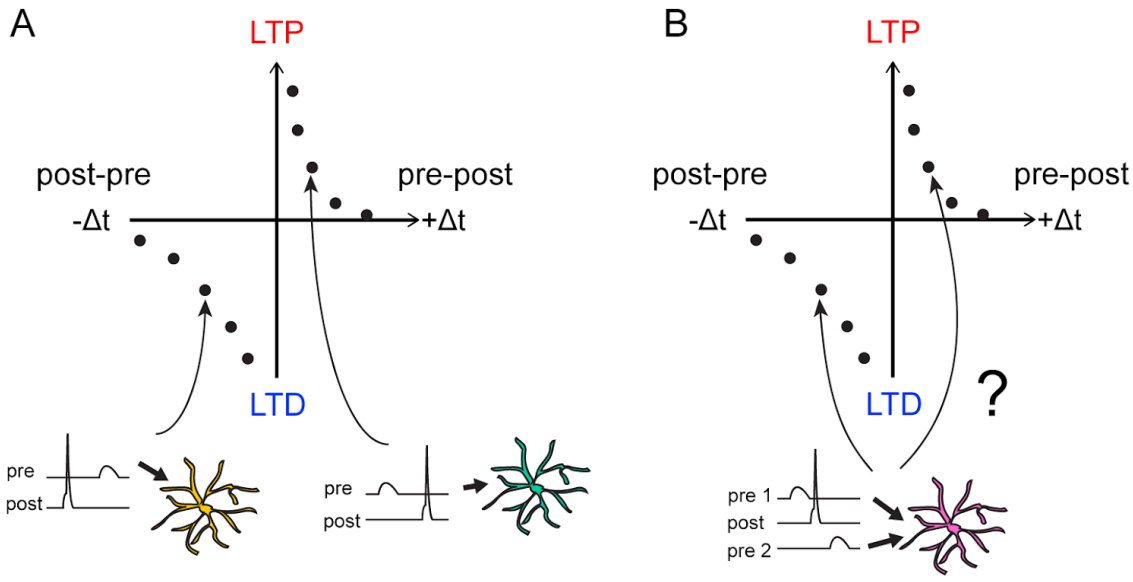

Figure 2.4. STDP curve. (A) An STDP curve is normally generated by collecting results from many STDP experiments. Each datapoint is obtained from the result in separate neurons. However, (B) if there are multiple inputs (pre 1 and 2) at different time windows relative to postsynaptic firing, it is not clear whether STDP curve would remain the same, or the inputs may interact with each other and influence STDP outcomes.

2.10. Neuromodulation of plasticity in learning

To appropriately translate activity into learned actions through plasticity, neuromodulators may need to be involved as putative key teaching signals. Neuromodulation of plasticity is a potential mechanism for reinforcement by such a teaching signal. Associative learning through modulation of activity-dependent plasticity was first described in the *Aplysia* withdrawal reflex (Carew, Hawkins, & Kandel, 1983; Hawkins, Abrams, Carew, & Kandel, 1983). Siphon stimulation paired with tail shock results in increased synaptic efficacy, termed facilitation. Activity of siphon stimulation that activates gills via motor neurons is strengthened by serotonin release from interneurons activated by tail shock. The temporal relationship between siphon stimulation and tail shock is crucial for subsequent learning to occur.

An appetitive form of learning involving dopamine has also been reported in *Aplysia* using a single-cell analog of the operant conditioning procedure (Brembs, Lorenzetti, Reyes, Baxter, & Byrne, 2002). In these experiments spontaneous bites in the absence of food were reinforced by electrical stimulation of neuron En2 which normally conveys information about the presence of food during ingestive behavior. Stimulation of neuron En2 in association with spontaneous biting caused an increase in the number of bites, which was associated with a corresponding increase in excitability of the neuron driving the biting behavior. A similar effect was produced by a puff of dopamine. However, these effects involve a cell-wide plasticity in excitability rather than changes at a specific synapse.

Like the *Aplysia* heterosynaptic plasticity, activity-dependent plasticity between the cortex and the striatum is strengthened by dopaminergic inputs (Reynolds, Hyland, & Wickens, 2001; Reynolds & Wickens, 2002; Wickens, Begg, & Arbuthnott, 1996). At a subset of synapses in the striatum, cortical glutamatergic inputs and dopaminergic inputs from midbrain dopamine neurons converge on the same dendritic spine of a SPN (Arbuthnott & Wickens, 2007; Mcgeorge & Faull, 1989; Smith & Bolam, 1990). Dendritic spine heads of SPNs mainly receive cortical glutamatergic inputs, while dopaminergic inputs terminate on the same dendrites at the spine neck (Freund, Powell, & Smith, 1984; Wilson et al., 1983). This anatomical arrangement suggests a way for dopamine to modulate the efficacy of corticostriatal synapses.

When dopamine is released in relation to synaptic activity of inputs to dSPNs, temporally specific D1R activation results in activation of a series of downstream signaling cascades responsible for LTP (Wickens & Kötter, 1995). In particular, the activity of key molecules, such as dopamine- and cAMP-regulated phosphoprotein, Mr 32 kDa (DARPP-32) and Ca^{2+}/calmodulin-dependent protein kinase II (CaMKII), seems to be involved in controlling the direction of plasticity (Nakano, Doi, Yoshimoto, & Doya, 2010; Wanjerkhede & Bapi, 2011). In addition to the temporally precise presynaptic and postsynaptic activity, a precise timing of the third factor, in this case interaction of dopamine signaling cascades in relation to the precise timing of activity dependent Ca^{2+} influx through dendritic processes, enables plasticity.

Neuromodulatory effects of dopamine are diverse and not only via direct actions on SPN physiology, but also via modulation of other neuronal populations to change synaptic plasticity. Within the striatum, many cells and axon terminals express dopamine receptors. For example, D2Rs are expressed not only on iSPNs, but also on dopaminergic terminals, cholinergic interneurons (ChI), and presynaptic cortical terminals to modulate plasticity (Augustin, Chancey, & Lovinger, 2018; Xu et al., 2018).

Dopamine neuromodulation can alter conditions to induce STDP. Dopamine can lower the minimum pairing numbers to induce plasticity in the striatum. Cui et al. (2015) described activity-dependent t-LTP after a small number (5-15) of pairings, mediated by eCBs. This

eCB-dependent t-LTP was controlled by dopamine, via D2R located presynaptically in cortical terminals (Xu et al., 2018).

At the behavioral level, dopamine release occurs in response to an unexpected reward or cue that predicts reward delivery (Schultz et al., 1997). In the case of unexpected reward, the dopamine release occurs some time after the neural activity that led to reward (Schultz, 1997; Schultz et al., 1997). In order to learn from this event, some mechanism to bridge the delay between the neural activity and the release of dopamine is required, otherwise animals would not learn from unexpected rewards. It has been proposed that an eligibility trace is involved in bridging this time delay.

2.11. Experimental evidence for eligibility traces in synaptic plasticity

During learning, reward arrives a few seconds after the action. The brain bridges this temporal gap between the action and reward. In order to form associations, "an eligibility trace" needs to be set up at the time of action, leaving a trace that decays slowly for a modulatory reinforcement signal to assign credit to the action. In theory, eligibility traces are a transient memory of past Hebbian coincidence events stored locally at the level of synapses (Frémaux & Gerstner, 2015). At the cell level, eligibility traces need to be specifically and locally activated at the time of action, and their transient expressions need to last until the arrival of the reinforcing neuromodulator a few seconds after. The requirements for eligibility traces thus include many of the same requirements as STDP.

Existence of eligibility traces in STDP has been experimentally shown by several studies. Cassenaer and Laurent (2012) showed the existence of an eligibility trace in *in vivo* mushroom body of locusts by demonstrating that neuromodulator octopamine can retroactively modulate and enable STDP when applied one second after pre-post pairing, suggesting that pairing itself turned on an eligibility trace (Cassenaer & Laurent, 2012). In the cortex, He et al. (2015) used two cortical inputs to induce cortical STDP with delayed (0-5 s) application of distinct neuromodulators. Two distinct eligibility traces for LTP and LTD were activated in a Hebbian manner (pre-post for LTP and post-pre for LTD) within the same cortical neuron, showing the input specificity of such eligibility traces (He et al., 2015). This suggests that eligibility traces may be a conserved mechanism.

In the corticostriatal pathway, Shindou et al. (2019) showed that phasic dopamine release by UV flash uncaging two seconds after the pairing of presynaptic cortical activity and postsynaptic dSPN firing induced t-LTP (Fig.2.5B). This retroactive effect of dopamine is consistent with the hypothesis of a silent eligibility trace. The nature of the trace itself is not known, but transient expression in Ca^{2+}-permeable AMPAR lasting for a few seconds after pairing events seems to be involved in the eligibility trace mechanism that is turned on by pre-post pairing (Shindou et al., 2019). Yagishita et al. (2014) also showed that pairing of glutamate uncaging and postsynaptic spikes produced t-LTP when dopamine was released 0.6 to one second after the start of pairings, but still during the pre-post pairing activity (Yagishita et al., 2014) (Fig.2.5A).

These studies show that a precise sequence of pairing (pre-post or post-pre timing) turns on a specific eligibility trace, which later actions of a neuromodulator can turn into t-LTP or t-LTD. He et al (2015) also showed that in the cortex, activation of two inputs to the same cell, in different spike timing sequences, resulted in distinct effects at each input. This suggests that even when there are multiple presynaptic inputs, the eligibility traces for different inputs are independent of each other. However, until now, such independence has not been shown for eligibility traces in the corticostriatal pathway.

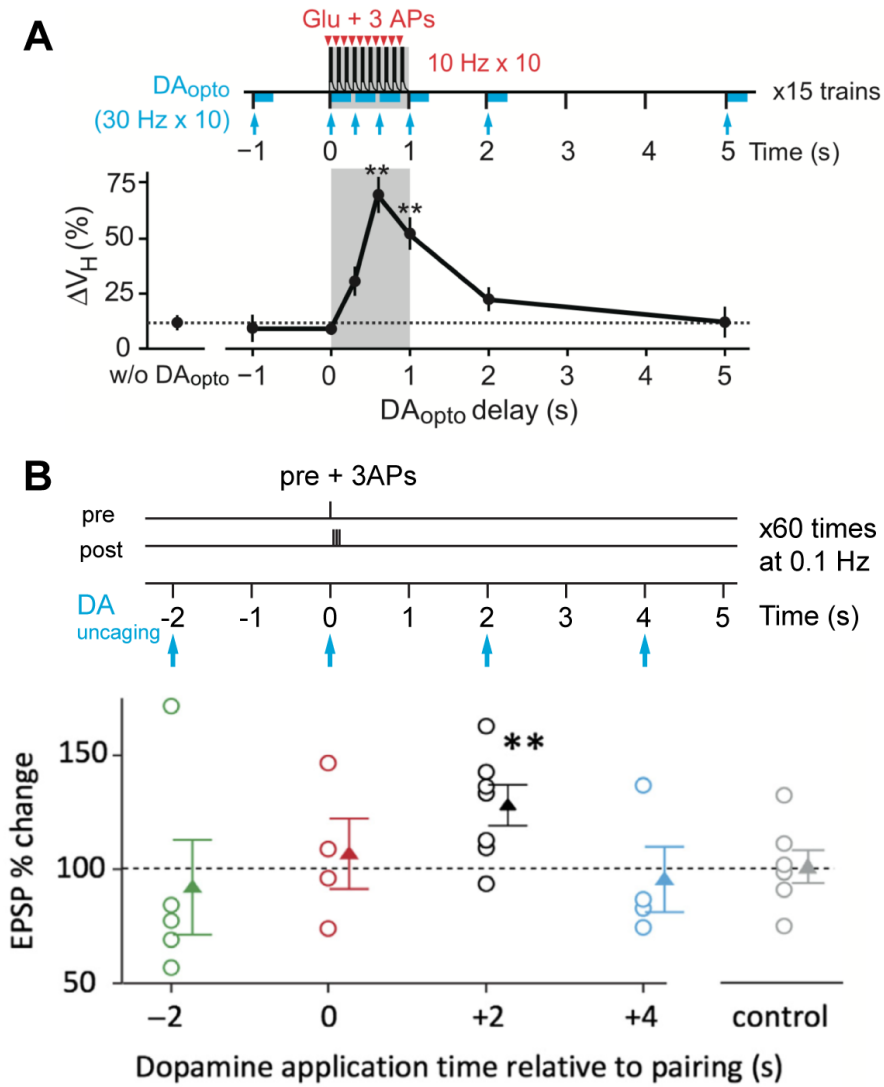

Figure 2.5. Comparison of the temporal windows for dopamine modulation of corticostriatal t-LTP. (A) In Yagishita et al. (2014), dopamine applied optogenetically during the STDP pairing protocol (0.6 - 1 s) enabled t-LTP. On the other hand, (B) in Shindou et al. (2019), application of dopamine by UV uncaging during the STDP pairing protocol did not produce plasticity, but two seconds after pairing induced t-LTP, showing an eligibility trace. Adapted and modified from Yagishita et al. (2014) and Shindou et al. (2019).

2.12. Conclusion of the literature review and research questions

Timing is one of the important variables in activity dependent plasticity, not only in relation to spike timing in STDP protocols, but also in relation to the timing of neuromodulatory inputs. The formation of associations based on temporal correlations is fundamental to intelligent behavior. However, our current understanding of the temporal requirements for synaptic plasticity are largely based on studies in which a single set of synaptic inputs is activated in synchrony. In the living brain, each neuron receives a multitude of synaptic inputs distributed in time, and in space over its dendritic arborization. Whether the ideal STDP curves that are obtained by studying one input at one time point generalize to the situation in the living brain is an open question. This question can be broken down into a number of more specific questions, as follows.

Firstly, does the way the postsynaptic neuron is caused to fire, whether by convergent synaptic inputs or current injection via an electrode, influence the STDP curve? In the living brain, a postsynaptic neuron fires when the net excitatory input from presynaptic neurons exceeds threshold. However, in STDP studies, postsynaptic firing is normally induced by somatic current injection. Based on our understanding of the electrical properties of dendrites as reviewed above, we might expect that these different routes to action potential firing would be associated with different patterns of STDP. To address this question, in Chapter 4, I report on experiments and computer simulations in which postsynaptic action potential firing is brought about by stimulation of cortical afferent fibers rather than current injection, and how this way of firing the postsynaptic neuron affects STDP.

Secondly, do multiple synaptic inputs occurring in sequence, before and after the spike of a given postsynaptic neuron, display the same STDP as synaptic inputs tested in isolation at corresponding time points in different neurons? In the brain, synaptic plasticity occurs in the context of multiple asynchronous inputs. However, most studies of STDP are based on combining results from multiple neurons, in each of which only one particular spike timing was tested. It is not clear, however, whether the STDP curve obtained by this method of stimulating one input and one time point per neuron would be the same as if multiple timepoints were tested using different inputs to the same neuron. The literature reviewed suggests that the interaction of multiple inputs occurring within the STDP time window might alter the STDP curve because of interactions among inputs on connected parts of the dendritic tree. In Chapter 5, I address this issue by testing the effects of stimulating two inputs to the same neuron at different spike timing.

Thirdly, experiments testing the eligibility trace hypothesis in the striatum have, like STDP experiments, usually involved a single time point per neuron. After pre-post pairing, application of dopamine two seconds after pairing enabled STDP, specifically t-LTP, in the striatum (Shindou et al., 2019). However, pairing of glutamate uncaging and postsynaptic spikes produced potentiation only when dopamine was released during the pairing (Yagishita et al., 2014). In the cortex, He et al. (2015) showed that different timepoints for induction of eligibility could result in different effects of the subsequent application of distinct neuromodulators. The spike timing requirements for induction of the eligibility trace have not been explored in the striatum. In Chapter 6, I report the effects of retroactive application of dopamine by optogenetics on two sets of synaptic inputs to the same neuron at different timepoints in relation to the postsynaptic spikes.

Chapter 3. Materials and methods

"It has long been an axiom of mine that
the little things are infinitely the most important"
– Sir Arthur Conan Doyle, A Case of Identity (1891)

3.1. Introduction

The purpose of this chapter is to describe materials and methods used in Chapters 4, 5, and 6.

3.2. Animals

3.2.1. D1/D2 eGFP transgenic animals (Chapters 4 & 5)

To identify dopamine D1 or D2 receptor SPN subtypes during whole-cell recording, BAC transgenic mice that expressed enhanced green fluorescent protein (eGFP) on D1 or D2 receptors were used (Gong et al., 2003). Juvenile to adult (1-4 months old) male BAC transgenic mice (Drd1a- or Drd2-eGFP) bred from Tg (Drd1a-eGFP)118Gsat/Mmnc (MMRRC bioresource facility, University of Missouri/Harlan, USA) and Tg (Drd2-eGFP) 118Gsat/Mmnc (MMRRC bioresource facility, University of North Carolina, USA) on Swiss Webster background (total n = 155) were used for experiments in Chapter 4. These D1-eGFP and D2-eGFP mice were further backcrossed with C57BL/6 mice to generate D1/D2-eGFP mice on C57BL/6 background. Adult (2-4 months old) male D1/D2-eGFP mice on C57BL/6 background (total n = 147) were used for experiments in Chapter 5.

3.2.2. Generation of triple transgenic animals (Chapter 6)

In order to achieve optogenetic stimulation of selective dopamine neurons while identifying SPN cell types, triple transgenic mice were generated. Dopamine transporter (DAT)-Cre (B6.SJL- Slc6a3$^{tm1.1(cre)Bkmn}$/J, JAX stock No. 006660) mice were crossed with Ai32 (RCL-ChR2 (H134R) / EYFP) mice (B6;129S-Gt *(ROSA)*$^{26Sor\ tm32(CAG-COP4*H134R/EYFP)Hze}$/J, JAX stock No. 012569), to express channelrhodopsin-2 (ChR2) specifically in DAT-expressing neurons. In order to identify dSPN cell types, DAT-Cre; Ai32 mice were further crossed with Drd1a-tdTomato mice (B6. Cg-Tg (Drd1a-tdTomato) 6Calak/J, JAX stock No. 016204). Specifically, a variant of ChR2 with H134R mutation was used, which has a reduced desensitization and increased light sensitivity with a peak response around 450 nm and slightly less temporal precision than ChR2 (Lin, 2011). These triple transgenic Ai32 +/-:: DAT-Cre +/-::Drd1a-tdTomato +/- mice were hereby referred to as RDT mice. Adult (2-5 months old) DAT-Cre +/- /Ai 32 +/- double transgenic animals (n = 8) and triple transgenic RDT mice (n = 10) were used to verify dopamine release in the striatal brain slices. Adult (2-5 months old) RDT mice (n = 218 total, both male and female were used) were used for plasticity experiments in Chapter 6.

3.2.3. Ethical considerations

In all experiments, animals were treated with every caution to minimize the suffering and number of animals to be used in experiments. Animals were treated in accordance with the protocols approved by the Okinawa Institute of Science and Technology Animal Care

and Use Committee (ACUC approved protocols No. 2015-123, 2017-174 & 2019-281), fully accredited by AAALAC International.

3.3. Slice preparation

Animals were deeply anesthetized with isoflurane (Abbott), quickly decapitated and the brains removed. Slices containing the cortex and the striatum were cut in an oblique plane, 45° rostral-up to the horizontal to maintain the intact corticostriatal projection (Shindou et al., 2011; Fig.3.1). Brains were sliced at 300 µm using a VT1000S microtome (Leica) at a rate of 0.04-0.05 mm s^{-1} at 40-50 Hz with N-methyl-D-glucamine (NMDG)-based artificial cerebrospinal fluid (aCSF). NMDG-aCSF contained the following (in mM): 93.0 NMDG, 2.5 KCl, 1.2 NaH_2PO_4, 30.0 $NaHCO_3$, 20.0 HEPES, 25.0 glucose, 5.0 sodium ascorbate, 2.0 thiourea, 3.0 sodium pyruvate, 10.0 $MgCl_2$, 0.5 $CaCl_2$, with the pH adjusted to 7.3-7.4 using HCl, saturated with 95% O_2/5% CO_2 (Ting, Daigle, Chen, & Feng, 2014). Slices were individually placed on a filter paper (10.0 µm Omnipore membrane filters) and transferred to a holding chamber for incubation in oxygenated standard aCSF maintained at 36°C for 1 h, after which they were kept in a holding chamber containing oxygenated aCSF at room temperature until recording. Standard aCSF contained (in mM) 120.0 NaCl, 2.5 KCl, 2.0 $CaCl_2$, 1.0 $MgCl_2$, 25.0 $NaHCO_3$, 1.25 NaH_2PO_4, and 15.0 glucose with constant oxygenation (95% O_2/5% CO_2). During recording, single slices were transferred to the stage of an upright manual fixed stage microscope with infrared differential interference contrast microscopy (BX51WIF, Olympus, Japan) and perfused at 3 mL min^{-1} with oxygenated standard aCSF at room temperature for Chapter 4, and at 28 – 32°C for Chapters 5 & 6, with a temperature controller (TC-324C single channel temperature controller, Warner instrument).

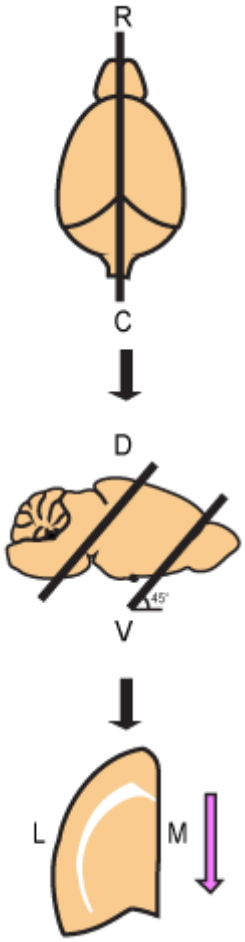

Figure 3.1. Schematic diagram to dissect the mouse brain to preserve corticostriatal projection. The brain was first cut in half rostrocaudally (R: rostral, C: caudal). The half hemisphere was then cut in an oblique plane, 45° rostral-up to the horizontal. D: dorsal, V: ventral. Brains were then sliced with microtome in the direction indicated by the pink arrow. M: medial, L: lateral.

3.4. Electrophysiology

Whole-cell recordings from SPNs in the DMS were obtained with a MultiClamp 700B amplifier (Molecular Devices) and a Digidata 1440A (Molecular Devices) running Clampex 10.5 software. Patch pipettes (Rt = 2 - 5 MΩ, borosilicate glass pipettes, 1.5 OD x 0.86 ID x 100 L mm, GC150F-10, Harvard Apparatus), connected to the headstage (CV-7B, Axon Instruments), were filled with internal solution containing the following (in mM): 143.0 K-gluconate, 12.5 HEPES, 1.5 $MgCl_2$, 4.0 ATP, 0.3 GTP, 12.5 phosphocreatine, and 0.5% biocytin, and the pH was adjusted to 7.2-7.4 using KOH. The final osmolality was 280-300 mOsm L^{-1}. Current-clamp recordings were filtered at 10 kHz and sampled at 100 kHz.

3.4.1. Stimulation electrodes for afferent firing induction protocol (Chapter 4)

For electrical stimulation, two sets of bipolar electrodes were gently inserted in the corpus callosum (CC) between the cortex and the DMS. The CC contains many cortical afferent fibers projecting to the striatum (Molyneaux, Arlotta, Menezes, & Macklis, 2007; Sohur, Padmanabhan, Kotchetkov, Menezes, & Macklis, 2014). Two sets of bipolar electrodes were separated at least 150 – 200 μm apart and were connected to constant current stimulators (model DS3, Digitimer Ltd). Firing properties of action potentials using (a) direct current injection and (b) electrical stimulation with the bipolar electrode were compared. Recorded variables were resting membrane potential before (100 ms before the first stimulation) and after (700 ms after the last stimulation) stimulation, peak amplitude, threshold, rise time, spike height and spike half width. Spike height was defined as the difference between the peak amplitude and the resting membrane potential before, as the stimulus interval was too small for the cell to repolarize. Threshold was defined as the voltage value at which the slope of depolarization exceeded 40 V s^{-1} (Wickens & Wilson, 1998). Rise time was calculated as the time of peak subtracted by the time of threshold. Half width was obtained at 50% of the peak.

3.4.2. Afferent-induced STDP protocol (Chapter 4)

After stimulation protocols verified the independence of two electrical inputs, synaptic STDP protocol proceeded. The current intensity for one stimulator was adjusted to evoke a unitary EPSP of about 0.5 - 4 mV in size. The current intensity for the other stimulator was also adjusted to reliably produce three consecutive spikes. The experiment proceeded as follows. Firstly, the baseline EPSP was obtained by giving electrical stimulation at 0.05 Hz for 10 min. Then, a synaptic input and a triplet of synaptically evoked spikes at 50 Hz were paired at either 10 ms before the first spike (Δt = +10 ms) or 10 ms after the third spike (Δt = -50 ms). Pairing was repeated 60 times at 0.1 Hz (Pawlak & Kerr, 2008; Shindou et al., 2011). After pairing, EPSPs were recorded and monitored continuously at 0.05 Hz for 20 min.

3.4.3. Two-input STDP protocol (Chapter 5 & 6)

For electrical stimulation, two sets of bipolar electrodes (custom array of two SNEX-100 platinum iridium concentric bipolar electrodes, tip diameter 100 μm, aligned with 300 – 400 μm tip distance, Microprobes) connected to constant current stimulators (STG4008, Multi Channel Systems) were gently inserted in the layer V of the cortex, to avoid activating thalamostriatal afferents, in contrast to CC stimulation used in Chapter 4. Two sets of electrodes were separated at least 150 – 200 μm apart. Each set of electrodes were used to

evoke EPSPs in SPNs, one as S1, and the other as S2. Stimulus intensity was 20 – 1600 μA, and the duration was 0.2 – 0.5 ms to induce EPSPs. Interactions of two inputs were tested before proceeding to STDP experiments. Individual EPSPs from S1 and S2 inputs were recorded with sufficient (500 ms) interval at 0.05 Hz. Then, S1 and S2 were simultaneously stimulated at 0.05 Hz (combined EPSP) and compared against the arithmetic sum of S1 and S2 EPSP, using the mean over 10 traces. Cells were divided into three categories, namely, cells showing sublinear, linear, or supralinear summation (described later in results). After paired pulse ratio (PPR) measurement (50 ms apart, 10 sweeps at 0.1 Hz), baseline EPSP was recorded at 0.05 Hz for 10 min, with 500 ms interval between S1 and S2. During the pairing protocol, S1 input was followed by action potential triplets (at 50 Hz) 10 ms before the first spike, which was then followed by S2 inputs arriving 10 ms after the third spike (50 ms after the first spike). To induce action potentials, 1000 – 3100 pA current was injected for 1 ms each. Pairing was repeated 60 times at 0.1 Hz (Pawlak & Kerr, 2008; Shindou et al., 2011). After pairing, both S1 and S2 EPSPs were recorded and monitored continuously for 20 min at 0.05 Hz.

3.4.4. Pharmacological manipulation for 2-input STDP protocol (Chapter 5)

Previously, Shindou et al. (2019) showed that application of a D1R agonist (0.5 – 1 μM SKF-81297) during pre-post pairing STDP protocol in the presence of L-type voltage gated calcium channel (L-VGCC) blocker (10 μM nimodipine) to block LTD induction, induced LTP (Shindou et al., 2019). Therefore, to test whether the combination of L-VGCC blocker and D1R agonist could preferentially modulate only pre-post input when there is another input at post-pre timing, nimodipine (10 μM, Sigma) and D1R agonist SKF-81297 (0.5, 1, 3 μM, Sigma) were bath applied by switching to aCSF containing these agents five minutes prior to the start of pairing protocol so that the pharmacological agents were available during the pairing protocol (Shindou et al., 2019). With the rate of perfusion (3 ml/min), it takes about two min. to reach the recording chamber, an additional min. to fill the recording chamber, and two more minutes were added to allow diffusion of the chemicals into the slice. Drug-containing aCSF were applied for the total of ten minutes, after which it was switched back to the regular aCSF.

3.4.5. STDP protocol with optogenetic dopamine release (Chapter 6)

STDP protocol remained the same as 2-input STDP in Chapter 5. For optical stimulation, Hg lamp (Olympus U-RFL-T, 100W) with fluorescent filter (U-MWIB3, 460 – 495 nm excitation, 510 nm IF emission, 505 nm mirror, Olympus) was equipped with a shutter (VMM-T1 Shutter driver/timer, Uniblitz). Blue light stimulation was done through x40 objective lens. During each pairing, blue light was stimulated two seconds after the beginning of pairing, by opening the shutter for 20 ms repeated twice at 20 Hz using STG4008 stimulator. After pairing, both S1 and S2 EPSPs were recorded and monitored continuously for 20 min at 0.05 Hz.

3.4.6. Inclusion criteria for electrophysiology data

Cells that showed fluctuations of membrane potentials or input resistance by more than 20% were excluded from the analysis.

3.5. Computational model (Chapter 4)

A biophysically detailed multi-compartment model of an SPN was based on a previously published model by Wolf et al. (2005). The model in the NEURON simulation environment was downloaded from Model DB (the details are available from the link: https://senselab.med.yale.edu/ModelDB/showmodel.cshtml?model=112834#tabs-1).
NEURON 7.3 was used for simulation in the McIntosh environment (Mac OS X 10.9.5, 2.8 GHz, X86_64, 16GB).

The parameters were based on previous studies and modified accordingly to match our experimental results (Moyer, Wolf, & Finkel, 2007; Wolf et al., 2005).

The original model was for the ventral striatum (Wolf et al., 2005), but further modified to match the morphology of SPNs in the dorsal striatum. Based on morphological observations of dorsal striatal SPNs (Wilson, 1992), six primary dendrites were inserted instead of four in the original model. Each dendrite bifurcated twice to give rise to secondary and tertiary dendrites (6 primary, 12 secondary, and 24 tertiary dendrites in total).

For intrinsic currents and synaptic currents, mod files were modified to fit the experimental conditions and later modifications by the authors (Moyer et al., 2007) as follows. Other parameters remained the same as the original Wolf model (Wolf et al., 2005). Briefly, the original model of 189-compartments included all reported species of calcium currents and calcium-dependent potassium currents. Full list of parameters can be found in their original publication (Wolf et al., 2005). In addition, the model was stylized to reduce the computational load of explicitly modeling spines. Instead, dendritic length and diameter were adjusted to compensate for additional membrane area attributable to dendritic spines (Wolf et al., 2005).

naf.mod: qfact 3 to 1, gnabar 1.5 to 1.875 to 3, mvhalf -23.9 to -25.9, hvhalf -62.9 to -64.9
nap.mod: qfact 3 to 1, gnabar 4e-5 to 5e-5 then to 4.2e-4
kaf.mod: qfact 3 to 1, gkbar 0.21 to 0.36
kas.mod: qfact 9 to 3, gkbar 0.01 to 0.0104
kir.mod: qfact 0.5 to 0.1667
krp.mod: qfact 3 to 1, gkbar 0.001 to 0.002
bkkca.mod: qfact 3 to 1, gkbar 0.001 to 0.12
skkca.mod: celsius to 22, gkbar 0.175 to 0.1885, then to 0.02 // to account for AHP
caL.mod: qfact 3 to 1, pbar 6.7e-6 to 6.7e-5
caL13.mood: qfact 3 to 1, pcaLbar 1.7e-6 to 3.19e-5
can.mod: qfact 3 to 1, pbar 10 fold increase
caq.mod: qfact 3 to 1, pcaqbar 10 fold increase
car.mod: qfact 3 to 1, pcarbar 10 fold increase
cat.mod: qfact 3 to 1, pcatbar 10 fold increase, to 7.6e-6, instead of 4e-6

To account for temperature difference (as recordings were done at room temperature for experiments in Chapter 4), the temperature coefficient (Q-factor) was changed from 3 to 1 for all channels and receptors.

GABA.mod: qfact 3 to 1
NMDA.mod: qfact 3 to 1
AMPA.mod: qfact 3 to 1

3.6. Fast scan cyclic voltammetry for dopamine detection (Chapter 6)

For the detection of dopamine in brain slices, custom-made carbon fiber electrodes (CFE) and commercially available CFE (diameter 10 µm, length 250 µm, CF10-250, World

Precision Instruments) were used. A custom-made CFE consisted of a bundle of carbon fibers of 7 µm diameter and 250 µm length (Goodfellow Cambridge) in a glass micropipette (Harvard Apparatus), with no electrode conditioning (Fuller et al., 2019). Electrodes were connected to the headstage (CV-7B/EC, gain modified to increase the current range to ± 2 µA, Axon Instruments) and FSCV was performed with a MultiClamp 700B amplifier (Molecular Devices) and a Digidata 1440A (Molecular Devices) running Clampex 10.5 software. The applied waveform was from -0.3 V to +1.3 V, then back to -0.3V over 9 ms interval. CFEs were inserted into the DMS of the acute brain slices from DAT-Cre / Ai32 mice (n = 8) or RDT mice (n = 10). Calibration was done with 2 µM increments of 2 µM dopamine-HCl added to aCSF. For the sole purpose of confirming the dopamine release, a linear relationship between the peak current and concentration was assumed instead of principle component regression methods to estimate the amount of dopamine. Stimulation and recording sites were around the same area as the STDP experiments.

3.7. Histology and visualization of recorded neurons

3.7.1. Morphological reconstruction of SPNs (Chapter 4)

After the experiments, recorded slices were kept in 4% paraformaldehyde in 0.1 M phosphate buffer (PB) at 4°C overnight, then rinsed with PB for 30 min before being replaced by 30% sucrose solutions for at least one hour to overnight. Slices were then reacted with 1:500 streptavidin-conjugated Alexa 488 in 0.4% Triton X in PB for 1 hr at room temperature. After being rinsed with PB, mounted and cover slipped, neurons were visualized with a confocal laser-scanning microscope (LSM510, Zeiss) to identify their morphological structures.

3.7.2. Double labeling of recorded neurons with biocytin and GFP (Chapter 5)

After the experiments, slices were kept in 4% paraformaldehyde in 0.1 M PB at 4°C overnight. They were rinsed with PB for 30 min before being replaced by 20% sucrose in phosphate-buffered saline (PBS) solution overnight. Slices were incubated with perm/quench solution (50 mM NH_4Cl, 0.2% saponin in 1 M PBS) for 15 min and then with blocking solution (5% goat serum, 0.02% saponin, 0.02% NaH_3 azide in 1 M PBS) for 1 h. After washing with PBS, they were reacted with primary antibody (1:20000 rabbit-anti-GFP, G10362, Life Technologies) in PGAS solution (0.2% fish gelatin, 0.02% saponin, 0.02% NaH_3 azide in 1 M PBS) overnight at 4°C. After three washes in PBS, they were reacted with secondary antibodies (1:500 goat-anti-rabbit 488, A11008, Invitrogen & 1:500 CF633 Streptavidin, Cat 29037, Biotium) in PGAS solution for 4 h at 25°C. After being rinsed with PBS, mounted and cover slipped, neurons were visualized with a confocal laser-scanning microscope (LSM880 for Fig.5.1D & LSM510 for Fig.5.1E, Zeiss) to confirm cell types by double labeling. 40x/NA 1.3 oil objective (for Fig.5.1D) and 20x/NA 1.3 objective (for Fig.5.1E) were used for the acquisition. The two channels were acquired in line sequential mode using a BP 465-505 - LP 525 filter in emission (MBS 488/561/633). ZEN 2.3 software was used for both acquisition and image post-processing and images were analyzed with Image J.

3.8. Data analysis and statistical analysis

Axograph X was used for off-line analysis. Electrophysiological data obtained with Axograph X were analyzed with Prism 8 (Graphpad) and SPSS 21 (IBM). For synaptic plasticity analysis, normalized EPSPs were calculated as % of baseline (baseline was the

mean over the 5-min period before pairing) and the mean normalized EPSP over the last 5-min of recording were compared against the baseline, using paired-sample t-tests. After testing for normality with one-sample Kolmogorov-Smirnov tests, paired-sample t-tests, within-subject ANOVA, and/or two-way repeated measures ANOVA were used for comparing firing properties as appropriate unless otherwise specified. For multiple comparisons, p-values were adjusted using a Bonferroni correction to avoid problems of multiplicity, ensuring that the overall probability of a type I error remained the same.

Chapter 4. Properties of afferent induced spikes and their effects on STDP

"I have never tried that before,
so I think I should definitely be able to do that."
– Astrid Lindgren, Pippi Långstrump

4.1. Introduction: different firing induction mechanisms

In synaptic plasticity protocols, timing of firing of presynaptic and postsynaptic neurons determines the direction of plasticity. In these experiments, postsynaptic firing has been elicited by current injection. In the intact brain, however, postsynaptic firing is caused by convergent afferent activity exceeding an action potential threshold. There is a possibility that the experimental induction of STDP using current injection may be different from the plasticity that occurs during learning in the intact brain. These ways of firing a cell may be associated with different dendritic responses. This raises the question whether STDP induction has the same properties when the postsynaptic spike is caused by afferent activities as when it is caused by somatic current injection. The electrical structure of a neuron reflects how the neuron is made to fire, either by direct current injection to the soma or by presynaptic stimulation. Upon receiving synaptic inputs, local depolarization at the dendrites is much higher than by somatic depolarization (Larkum & Nevian, 2008). The electrical structure of neurons from distal dendrites to soma determines how activity originating in different compartments is integrated by the neuron. Due to the electrical compartmentalization of dendritic structures and heterogeneous distribution of backpropagation, the spatiotemporal profiles of Ca^{2+} increases in the dendrites and spines would differ when the source of activation is synaptic inputs rather than somatic depolarization (Carter & Sabatini, 2004). Synaptically induced activity may trigger graded potentials, local spikes, or somatic spikes that propagate along dendrites. Somatic current injection causes similar phenomena, but it may produce profound differences in current spread compared to dendritic synaptic inputs. As the temporal relationship between the input EPSP and the output spiking, represented as a Ca^{2+} signal, is a key signal for coincidence detection for STDP (Nevian & Sakmann, 2006), different means of firing induction may have consequences for the induction of plasticity.

To investigate the difference in STDP due to differences in the method of firing the postsynaptic cell, I tested how summation of multiple inputs occurred and caused output spike activity using electrophysiological studies and a computational model. Firstly, electrophysiological recordings were performed in the SPNs to compare firing properties between the firings induced by postsynaptic current injection and by dendritically integrated synaptic inputs from stimulation of cortical afferents. A biophysical SPN model was also used to monitor voltage and Ca^{2+} influx during firing induced by postsynaptic current injection and by afferent stimulation. Secondly, using two sets of electrodes to electrically stimulate cortical afferents, an STDP protocol was developed, in which one stimulation caused afferent induced spike activity, while another stimulation caused an EPSP.

4.2. Methods

Materials and methods including animals and slice preparation, stimulation protocol, afferent-induced STDP protocol, computational model, and histological methods are described in detail in Chapter 3.

4.3. Results

4.3.1. Electrophysiological characterization of SPNs

Medium spiny projection neurons in the DMS were visually identified as either a dSPN or iSPN by the presence of the GFP signal under the microscope during recording. Cells were electrophysiologically confirmed as SPNs by their long latency before a first spike and inward rectification (Fig.4.1).

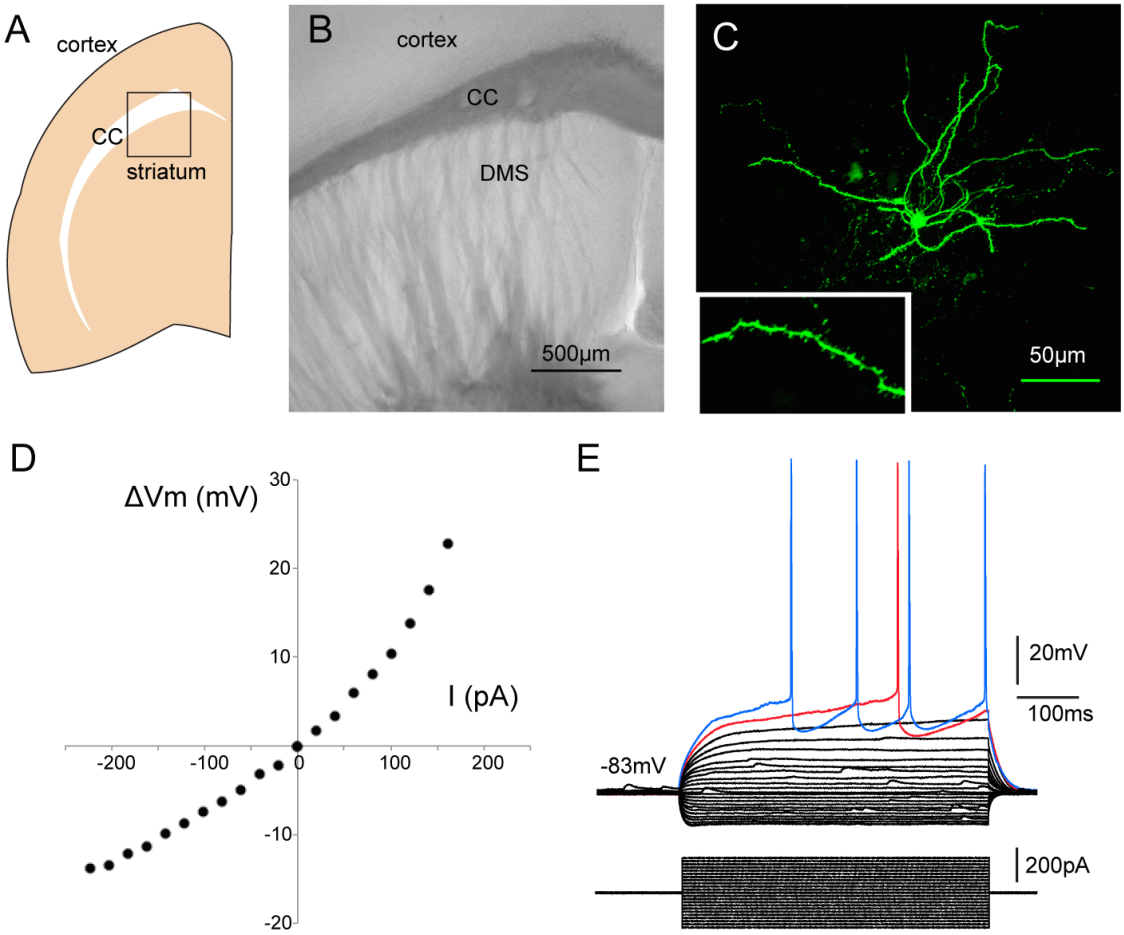

Figure 4.1. Electrophysiological characterization of SPNs. (A) Schematic diagram showing the area of recording. (B) Microphotograph of a prepared brain slice shows the area of presynaptic stimulation and recording. The holes indicate where the bipolar electrode was inserted in the corpus callosum (CC). Recording was done in the DMS. Scale bar = 500 µm. (C) Microphotograph of an iSPN injected with biocytin after recording, showing characteristic dendritic arborization and spines. Scale bar = 50 µm. (D) Current (I) and voltage (Vm) relationship (I-V curve). (E) Voltage responses to depolarizing and hyperpolarizing currents (in 20 pA steps).

4.3.2. Properties of afferent induced spikes

To see whether dendritically evoked spikes are indeed different from somatically induced spikes, firing properties of action potentials using (a) direct somatic current injection and (b) electrical stimulation of cortical afferents were compared using action potential triplets, standard firing inputs used for in vitro corticostriatal STDP studies (e.g. Shen et al., 2008; Shindou et al., 2011; Yagishita et al., 2014). Neurons (n = 17, including both dSPNs and iSPNs) were activated to fire a train of three action potentials at 50 Hz by current injection to the soma via the recording electrode or by afferent stimulation through the bipolar electrode. Current intensity was adjusted to evoke action potential triplets (Fig.4.2A). For somatic current injection, current intensity was 700 - 1250 pA for 2 ms each, and for synaptic (afferent) stimulation, 180 - 2700 μA was injected to the bipolar electrode for 0.2 - 0.6 ms each. Each dataset was obtained by averaging values from three consecutive successful spikes over ten sweeps at 0.05 Hz (Fig.4.2B&C).

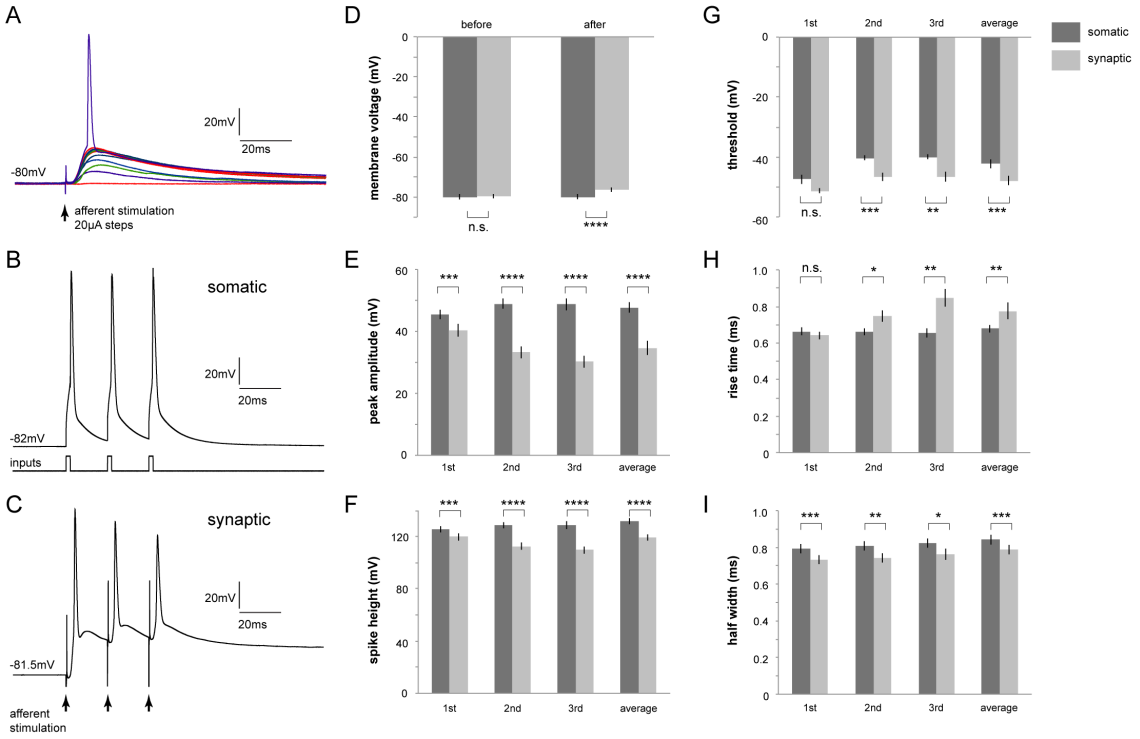

Figure 4.2. Differences in firing properties of SPNs activated by direct somatic current injection and by afferent (synaptic) stimulation. (A) A sample trace showing that increasing current intensity through the bipolar electrode (from 50 to 270 μA in 20 μA steps for 0.2 ms) resulted in cumulative EPSP amplitude and gradually a spike. (B) An example trace averaging ten sweeps of action potential triplets caused by somatic current injection (1500 pA for 2 ms). (C) An example trace showing an average of ten sweeps by upward pulse at 950 μA for 0.4 ms, caused by afferent stimulation (indicated by black arrows). (D) Membrane potentials (mV) 100 ms before firing (before) and 700 ms after the inputs (after). (E) Peak amplitudes (mV). (F) Spike heights (mV). (G) Spiking threshold (mV). (H) Rise time (ms). (I) Spike half-width (ms). Bars indicate mean ± standard error of the mean (SEM) from the first (1st), second (2nd) and third (3rd) spikes and average of three spikes in cells fired by somatic current injection (dark gray) and by presynaptic stimulation (light gray). *: $p < 0.05$, **: $p < 0.01$, ***: $p < 0.001$, ****: $p < 0.0001$ and n.s.: not significant.

Firing properties showed significant differences between somatically and synaptically induced spikes (summarized in Table 4.1). Membrane potentials did not differ between somatic and synaptic stimulation methods 100 ms before ($t_{(16)} = 0.61$, $p = 0.553$; Fig.4.2D). However, membrane potential was significantly more depolarized when cells were activated synaptically, even 700 ms after the inputs, than somatically activated spikes ($t_{(16)} = 5.95$, $p = 0.00002$). Peak amplitude was significantly smaller for synaptically induced spikes than somatically induced spikes ($t_{(16)} = 14.19$, $p < 0.00001$; Fig.4.2E), resulting in significantly smaller respective spike heights ($t_{(16)} = 14.65$, $p < 0.00001$; Fig.4.2F). The threshold was generally significantly lower when cells were activated synaptically ($t_{(16)} = 4.80$, $p = 0.000198$; Fig.4.2G), consistent with *in vivo* studies (Wickens & Wilson, 1998). However, unlike the previous study, there was no significant correlation between the threshold and current intensity injected for somatic activation (Pearson's Correlation, $r = -0.27$, $n = 17$, n.s.), although experimental conditions were different. Rise time also showed significant differences for the second and third spikes ($t_{(16)} = 3.69$, $p = 0.002$; Fig.4.2H). The spike half width was also significantly smaller for synaptically stimulated spikes ($t_{(16)} = 4.74$, $p = 0.00022$; Fig.4.2I).

In addition to differences between firing methods, significant differences were observed between spike numbers from the first through to the third, for both somatically and synaptically induced spikes. Somatically induced spikes had cumulative peak amplitude from the first through to the third spikes ($F = 4.47$, $p < 0.05$; Fig.4.2E), whereas the peak amplitude showed a decrease through the three spikes when induced synaptically ($F = 71.19$, $p < 0.001$; Fig.4.2E). The same trend was observed in respective spike heights (Fig.4.2F). The threshold also became significantly higher during the three spikes for both somatic and synaptic stimulation ($F = 25.61$, $p < 0.001$ and $F = 7.77$, $p < 0.01$, respectively; Fig.4.2G). No significant change in rise time was observed for somatically evoked spike triplets ($F = 0.159$, n.s.; Fig.4.2H), but there was a significant change in rise time for synaptically-evoked spike triplets ($F = 31.17$, $p < 0.001$; Fig.4.2H). Spike half width was also significantly different between three spikes by somatic activation ($F = 3.55$, $p < 0.05$), but not by synaptic activation ($F = 2.52$, n.s.; Fig.4.2I). In summary, firing properties differed not only between the two activation methods, but also between the triplets of action potentials.

Table 4.1. Firing properties of spiny projection neurons between somatic and synaptic (afferent) activation

		somatic				afferent		
membrane potential (mV)	before	-79.9	±	1.2	n.s.	-79.6	±	1.2
	after	-79.8	±	1.2	****	-76.4	±	1.2
peak amplitude (mV)	1st	45.5	±	1.6	***	40.4	±	2.1
	2nd	48.9	±	1.6	****	33.3	±	2.0
	3rd	48.7	±	1.9	****	30.3	±	2.0
	average	47.7	±	1.0	****	34.6	±	1.3
spike height (mV)	1st	125.4	±	2.4	***	119.9	±	2.9
	2nd	128.8	±	2.4	****	112.7	±	2.8
	3rd	128.7	±	2.8	****	109.7	±	2.8
	average	127.6	±	1.5	****	114.1	±	1.7
threshold (mV)	1st	-47.5	±	1.5	n.s.	-51.3	±	0.8
	2nd	-40.3	±	0.8	***	-46.7	±	1.4
	3rd	-40.0	±	0.8	**	-46.5	±	1.7
	average	-42.6	±	0.8	***	-48.2	±	0.8
rise time (ms)	1st	0.66	±	0.02	n.s.	0.64	±	0.02
	2nd	0.66	±	0.02	*	0.75	±	0.03
	3rd	0.65	±	0.02	**	0.85	±	0.05
	average	0.66	±	0.01	**	0.75	±	0.02
spike half width (ms)	1st	0.79	±	0.02	***	0.73	±	0.02
	2nd	0.81	±	0.03	**	0.74	±	0.02
	3rd	0.82	±	0.03	*	0.76	±	0.03
	average	0.81	±	0.01	***	0.75	±	0.01

Table 4.1. Firing properties of SPNs between somatic and synaptic (afferent) activation. Data are shown as mean ± SEM (paired sample t-test, n = 17). Except for membrane potential and overall average, p-values were adjusted using a Bonferroni correction (R=3). *: $p < 0.05$, **: $p < 0.01$, ***: $p < 0.001$, ****: $p < 0.0001$ and n.s.: not significant.

4.3.3. *In silico* dorsal striatal SPNs show differences in voltage responses and Ca^{2+} dynamics at the level of distal dendrites

In order to compare electrical behavior at the dendrite level during firing induced by somatic current injection and by afferent stimulation, a detailed biophysical model of an SPN (Wolf et al., 2005) was adjusted to match our experimental conditions. The present model captured the physiological characteristics of SPNs, namely, inward rectification and a delay before a first spike, consistent with the *in vitro* experimental recordings (Fig. 4.3B&C). Use of the model enabled monitoring of responses to triplets of action potentials elicited by somatic and synaptic stimulation in different compartments of soma, proximal, mid and distal dendrites, as indicated by the colored dots (Fig.4.3A). Stimulus intensity was adjusted to evoke three spikes. For somatic current injection, 1700 pA was injected into the soma for 3 ms for 3 times at 50 Hz. For synaptic stimulation, 120 synapses (48 AMPARs, 48 NMDARs and 24 GABARs) in distal dendritic compartments were activated for three times at 50 Hz. Voltage responses in the soma during action potential triplets were similar to the experimental results (Fig.4.3D). When voltage responses were monitored in different compartments, behavior at the distal dendrite looked profoundly different, with more than 30 mV difference in peak amplitude (Fig.4.3D, bottom right). I then monitored Ca^{2+} dynamics in the same compartments (Fig.4.3E). Again, Ca^{2+} influx in distal dendrites shows profoundly larger (more than 10-fold) responses in synaptically activated spikes than in somatically activated spikes (Fig.4.3E, bottom right). Peak Ca^{2+} concentration was approximately 1.2 μM when three APs were induced synaptically, but less than 0.1 μM when three APs were induced somatically. This is in contrast to Shindou et al. (2011)'s peak Ca^{2+} measurement (0.80 μM) in the adjacent dendritic shaft when three APs were induced somatically (Shindou et al., 2011).

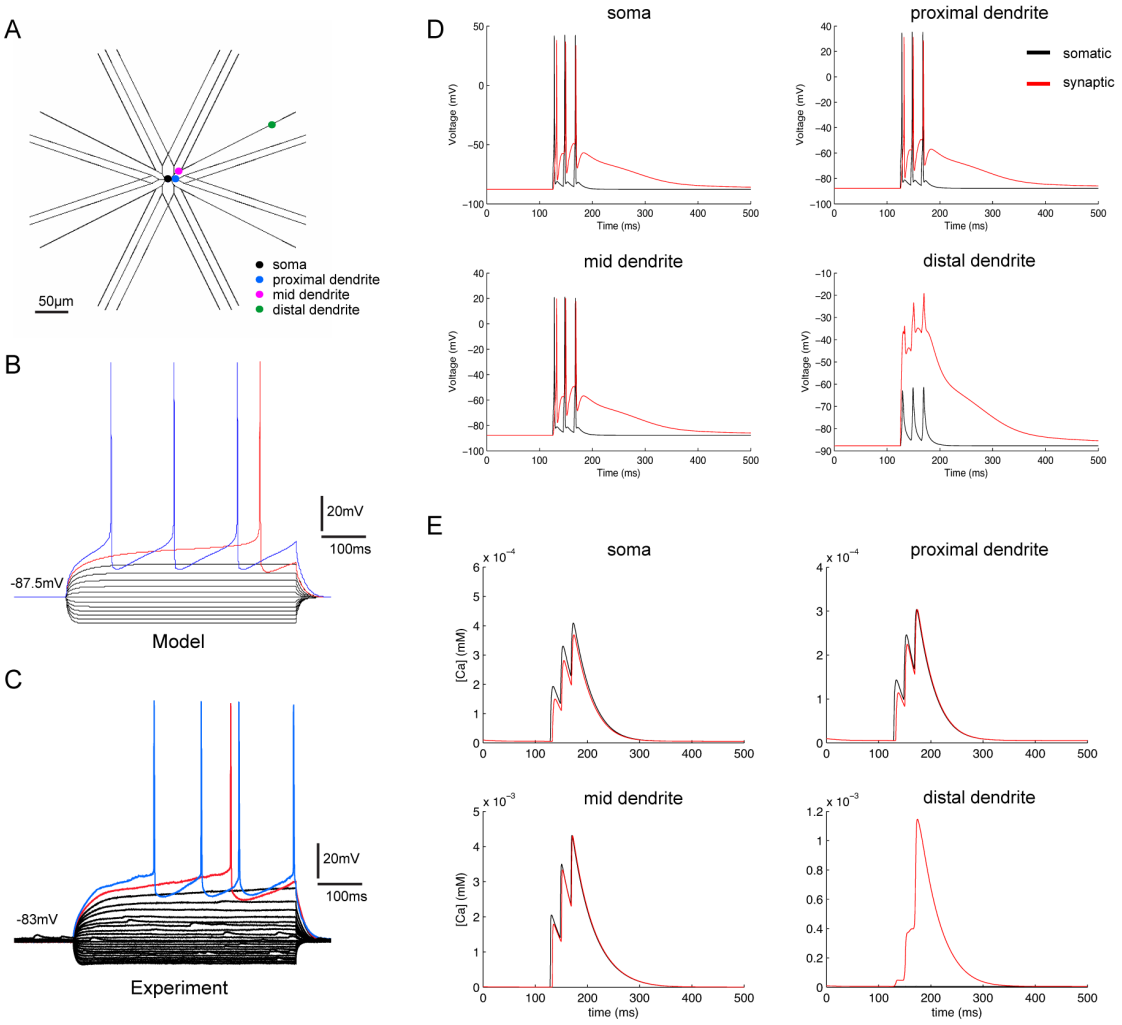

Figure 4.3. A computational model of a dorsal striatal SPN and its responses to somatically and synaptically induced action potential triplets at the level of soma and dendrites. (A) Morphology of the model SPN. Colored dots indicate the location of recording in soma (black), proximal dendrites (blue), mid dendrite (red) and distal dendrite (green). (B&C) Voltage responses of the model SPN (B) in comparison to experimental result (C) upon injection of depolarizing and hyperpolarizing currents. (D) Voltage responses upon somatic (black) and synaptic (red) stimulation in soma (top left), proximal dendrite (top right), mid dendrite (bottom left) and distal dendrite (bottom right). (E) Ca^{2+} influxes to soma, proximal, mid and distal dendrites during firing inducing inputs.

4.3.4. STDP with afferent-induced firing caused LTD in dSPNs

To induce afferent-induced spiking and evoke EPSPs separately, two sets of bipolar electrodes (S1 & S2) were used to independently activate cortical axons projecting to the same SPN. S1 stimulation served as a conditioning stimulus to evoke EPSPs, while S2 stimulation was used to induce spike triplets (Fig.4.4A&B). Before proceeding to STDP experiments, independence of two or more stimuli was tested by summation methods. If the arithmetic sum of all the stimuli is roughly equal to the combined stimulus, independence of inputs was assumed (Polsky, Mel, & Schiller, 2004). Normalized EPSPs were calculated as % change from the baseline 5-min period. The normalized EPSPs before pairing and 15-min after the pairing (last 5 min of the recording period) were compared. When there was a statistically significant difference ($p < 0.05$) between the means of normalized EPSP before and after pairing, then synaptic plasticity was assumed to have occurred. For the afferent activity induced STDP, results from 20 cells (n = 12 for dSPNs, n = 8 for iSPNs) from 15 animals were included for analysis. As different SPN cell types showed different plasticity profiles (Shen et al, 2008), afferent-induced STDP was tested in both dSPNs and iSPNs. In dSPNs, pre-post pairing ($\Delta t = +10$ ms, n = 7) resulted in LTD (normalized EPSP was 75.7 ± 7.0 %, $t_{(6)} = 3.46$, $p = 0.013$; Fig. 4.4C), whereas post-pre pairing ($\Delta t = -10$ ms from the last spike, n = 5) showed a non-significant slight decrease (normalized EPSP was 73.3 ± 11.1 %, $t_{(4)} = 2.42$, $p = 0.073$; Fig. 4.4D). In iSPNs, no plasticity was observed after pre-post paring (normalized EPSP was 87.3 ± 9.8 %, $t_{(5)} = 1.30$, $p = 0.251$, n = 6; Fig.4.5A). There were only two samples of iSPNs receiving post-pre pairing, and normalized EPSP after post-pre pairing was 86.4 % and 80.5% of the baseline. The sample size is too small to perform a statistical test (Fig.4.5B). However, LTD only after pre-post pairing in dSPNs and absence of plasticity, at least after pre-post pairing in iSPNs are consistent with the results from the previous study using the same frequency protocol (60 times at 0.1 Hz) using somatic current injection as firing methods (Shindou et al., 2011, 2019).

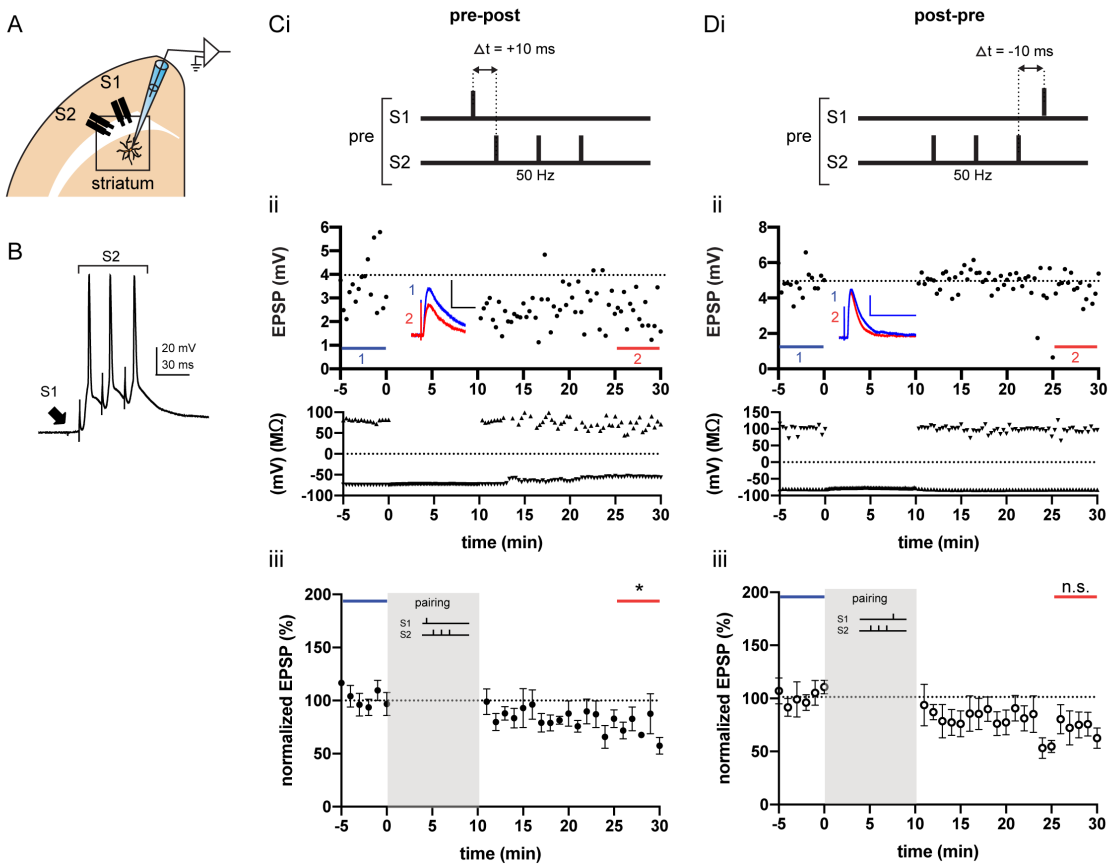

Figure 4.4. STDP with afferent-induced firing in dSPNs.(A) Schematic diagram showing the location of two bipolar electrodes in the CC. (B) An example trace showing EPSP from S1 input and action potential triplets from S2 input. (C) Pre-post and (D) post-pre pairing. (i) STDP protocol, indicating the timing of S1 input and S2 input inducing action potentials. (ii) Representative examples of changes in EPSP amplitude (mV, filled circles, top), input resistance (Ri, MΩ, upright triangles, middle), and resting membrane potential (RMP, mV, downward triangles, bottom). Sample traces show averages of EPSP over 5 min. before (blue, 1) pairing and after (red, 2) pairing. Scale bars = 2 mV (vertical) and 50 ms (horizontal). Dotted line indicates the baseline EPSP. (iii) Group averages of normalized EPSPs in (Ciii) pre-post (n = 7) and (Diii) post-pre (n = 5) pairing. Pre-post pairing induced LTD, but post-pre pairing caused no plasticity in dSPNs. Data displayed as mean over 1 min. ± SEM. *: $p < 0.05$, n.s.: not significant.

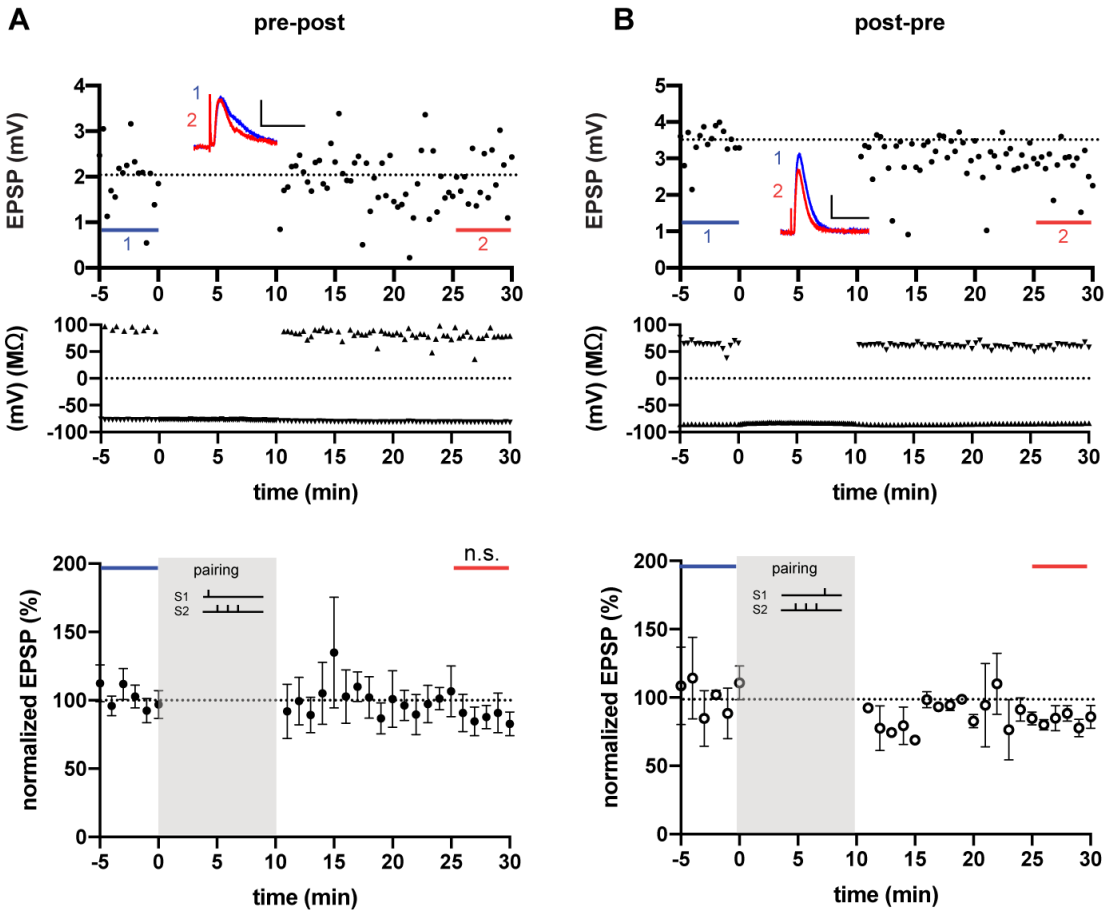

Figure 4.5. STDP with afferent-induced firing in iSPNs. (A) Pre-post pairing. Top traces are representative examples of changes in EPSP amplitudes (mV), Ri (MΩ), and RMP (mV). Sample traces show averages of EPSP over 5 min. before (blue, 1) pairing and after (red, 2) pairing. Scale bars = 1 mV (vertical) and 50 ms (horizontal). Dotted line indicates the baseline EPSP. Bottom traces show the group averages of normalized EPSPs in pre-post (n = 6) pairing. (B) Post-pre pairing. Representative examples (top) and group averages (n = 2, bottom). No plasticity was induced after pre-post pairing in iSPNs. Data displayed as mean over 1 min. ± SEM. n.s.: not significant. Data displayed as mean over 1 min. ± SEM.

4.4. Discussion

In this chapter, electrophysiological recordings and analysis with a computational model showed that spikes induced by postsynaptic current injection differed significantly from spikes induced by afferent activity. Electrical stimulation of multiple synaptic inputs was sufficient to cause output spiking activity in the postsynaptic SPNs, suggesting that this method of causing spiking could be used in STDP protocols as an alternative to somatic current injection. The computational model predicted higher Ca^{2+} influx during afferent induced spikes in distal dendrites, compared to the Ca^{2+} influx caused by spikes evoked by somatic current injection, suggesting that there may be differences in plasticity in the two conditions. When tested experimentally, however, STDP induced by afferently stimulated spikes showed a unidirectional, pre-post LTD in dSPNs. The properties of this form of STDP were consistent with a previous study using a similar pairing protocol, but with firing induced by postsynaptic current injection (Shindou et al., 2011, 2019). These results indicate that postsynaptic cell firing induced by somatic current injection is as effective as firing induced by convergent afferent stimulation in inducing STDP.

Properties of spikes induced by afferent activity differed significantly from spikes induced by postsynaptic current injection in several parameters that might affect Ca^{2+} influx. Afferent activity-induced spikes had a significantly lower peak amplitude, shorter spike half width, and on average lower threshold. However, in both distal dendrites and soma, the afferent activity caused a pronounced depolarizing envelope. This depolarizing envelope might have reduced the availability of rapidly inactivating Na^{+} currents contributing to the spikes, which could explain the lower peak amplitude and shorter half width. However, it might also have increased activation of non-inactivating Ca^{2+} currents. The Ca^{2+} influx depends on several factors, including the anatomical density and state of activation or inactivation of channels, and the membrane potential driving force relative to the equilibrium potential for Ca^{2+} (Hille, 2001). A computational model was needed to take account of these factors and estimate their net effect when working together during spiking activity.

The computational model was based on a previously published model of an SPN (Wolf et al., 2005). It reproduced the main features of the membrane potential trajectories for somatic current injection and afferent synaptic stimulation. In addition, it provided a prediction of the membrane potential in the distal dendrites, which was not accessible experimentally. This prediction showed a much larger depolarization in response to afferent stimulation than somatic current injection, and also predicted a great Ca^{2+} influx in the distal dendrites. However, the model did not include the mechanisms for translating the Ca^{2+} influx into synaptic plasticity, seen in some other models (Evans, Maniar, & Blackwell, 2013; Jędrzejewska-Szmek, Damodaran, Dorman, & Blackwell, 2017). In addition, the Ca^{2+} concentration in distal dendrites in the model was lower than previously measured peak Ca^{2+} concentration in dendritic shafts when three APs were induced somatically (Shindou et al., 2011). Therefore, there is a need to employ a better model to capture Ca^{2+} dynamics as well as plasticity.

Experimentally, the afferent stimulation and somatic current injection protocols produced similar synaptic plasticity. Pre-post stimulation caused LTD and post-pre stimulation caused no change. Taken together, these results seem to suggest that the timing of the synaptic activity relative to the postsynaptic spike plays a greater role in determining the plasticity than the characteristics of the spike itself, or even the amount of Ca^{2+} entry. This surprising result is consistent with Nevian and Sakmann (2006), who showed that it was the relative timing of the input and spike rather than the Ca^{2+} levels that determined the direction of synaptic change.

Afferent stimulation as a means to produce spikes also has its problems. Although synaptically induced spikes may reflect more precisely the firing mechanism in the brain, strong electrical stimulation of the CC causes current spread and recruits many cortical afferents. With a simple two-electrode condition, it is impossible to monitor the extent of current spread and the number of axons that are recruited and activated. In addition, as the CC also contains thalamostriatal afferents, strong stimulation may also activate thalamic inputs to the SPN. Furthermore, although the independence of two EPSPs from the two electrodes was verified prior to the STDP pairing, stimulation of intensity sufficient to cause firing may have also recruited some of the same cortical axons that were stimulated by the electrode serving as a test input. Therefore, interactions of the suprathreshold stimulus and the test stimulus during pairing cannot be strictly ruled out. Strong stimulation may also activate other afferents and neural populations, including dopamine fibers. A similar level of electrical stimulation (100 – 1000 μA steps for 0.6 ms each) via a bipolar electrode placed in the CC resulted in a small but noticeable dopamine release using fast-scan cyclic voltammetry (data not shown).

Taking account of these findings, it was decided to use somatic current injection to produce the postsynaptic spikes in later experiments. In order to control non-specific activation of other neurons, for later experiments (Chapters 5 & 6) the electrodes were placed in the layer V of the cortex to avoid activating thalamic afferents and stimulated with lower stimulus intensity to minimize the chance of overlap in current spreads. Finally, the possibility that the characteristics of the postsynaptic spike play a minor role compared to the timing of the inputs suggested that control experiments in which there was no postsynaptic spiking should also be conducted.

In summary, STDP paired with spikes induced by afferent stimulation results in a similar plasticity profile as STDP paired with spikes induced by somatic current injection. Despite the difference in electrical and chemical behavior, STDP induced by afferently stimulated spikes showed pre-post LTD in dSPNs, consistent with the results using a similar standard STDP protocol paired with firing induced by postsynaptic current injection (Shindou et al., 2011, 2019). Considering the nonspecific effects of afferent stimulation-evoked spikes due to a large current spread, a standard STDP protocol paired with firing induced by postsynaptic current injection shall be used from the next chapters (Chapters 5 & 6). This chapter has looked at integration of afferent inputs at the dendrites in terms of spiking activity. In the next chapter (Chapter 5), potential interactions of afferent inputs at the dendrites at the subthreshold level are investigated. More precisely, two inputs to the same neuron are used to test the effects of timing in the context of multiple inputs on STDP.

Chapter 5. Interaction of multiple presynaptic inputs and their effects on STDP

"when you have eliminated the impossible,
whatever remains, however improbable, must be the truth"
– Sir Arthur Conan Doyle, The Sign of the Four (1890)

5.1. Introduction

Standard STDP protocols use single simultaneous presynaptic inputs paired with postsynaptic firing. The STDP curve describing the relationship between temporal difference of pre- and postsynaptic activity and the direction and magnitude of plasticity is based on the single inputs tested in each cell in separate experiments (Fino et al., 2008; Pawlak & Kerr, 2008). Such computations occur at the level of individual dendritic spines, but dendrites receive multiple inputs which interact with neighboring spines at the subthreshold level (Carter et al., 2007). These interactions of multiple inputs may contribute to and alter plasticity profiles of corticostriatal STDP.

In the current sets of experiments, I investigated the ability of a single neuron to process two contiguous inputs as separate plasticity-inducing inputs, depending on their timing relative to postsynaptic firing. Using two sets of bipolar electrodes to induce EPSPs at different timings in a single SPN, a 2-input STDP protocol was applied to both dSPNs and iSPNs. Interactions of two EPSPs were analyzed in terms of their summation profiles. Cells were categorized into three groups, namely, sublinear, linear, and supralinear summation. In the case of sublinear summation, two stimulation electrodes activate some overlapping cortical axons, then the combined EPSP by simultaneous stimulation would be smaller than the sum of two individual EPSPs. Passive membrane properties of dendrites may also contribute to the sublinear summation due to reduced driving force decreasing the synaptic current of the concurrent input (Tran-Van-Minh et al., 2015). However, considering the strong contribution of Kir current in SPN dendrites, active membrane properties would overcome such a reduction. In the case of linear summation, two stimuli activate independent sets of cortical axons, which then innervate different branches of dendrites, then the arithmetic sum of two individual EPSPs would be roughly equal to an EPSP evoked by two simultaneous inputs (Polsky et al., 2004). In the case of supralinear summation, if two inputs innervate axons arriving on the same dendritic branch, then the combined EPSP may be supralinear, depending on the strength and place of stimulation (Dorman, Jędrzejewska-Szmek, & Blackwell, 2018; Kamijo et al., 2014; Polsky et al., 2004). This categorization does not exclude the possibility that apparent linearity could theoretically arise from the combination of sublinearity (by sharing of some axons) and supralinearity.

In addition, I looked at the interactions of multiple inputs in the absence of postsynaptic spiking. STDP can also be induced by pairing with postsynaptic cell depolarization at the subthreshold level (Fino et al., 2009). It may be possible that depolarization caused by another synaptic input could induce plasticity. I then tested whether pairing of multiple presynaptic inputs at SPN dendrites could also provide sufficient plasticity signals. Two inputs were paired to test whether their interactions would induce plasticity in the absence of postsynaptic action potentials.

5.2. Methods

Materials and methods including animals and slice preparation, electrophysiological methods, 2-input STDP protocol, and immunohistochemical methods are described in detail in Chapter 3.

5.3. Results

Data obtained from 82 cells in separate brain slices from 73 animals that met the aforementioned inclusion criteria were used for analysis. The number of cells used in each set of experiments in this chapter is summarized in Table 5.1. After two sets of electrodes were placed in the layer V of the cortex (Fig.5.1A), cells were visually identified under the microscope as either a dSPN or iSPN by the presence or absence of fluorescent signal during recording. Examples of cells that were confirmed retrospectively with double labeling of GFP and biocytin are shown in Fig.5.1D and E. With whole-cell recordings, cells were electrophysiologically confirmed as SPNs by their long latency before a first spike and inward rectification.

Table 5.1. List of experiments with the number of cells in each condition.

List of experiments	# of cells	EPSP summation profiles				Figure #
		sublinear	linear	supra-linear	not tested	
2-input STDP	**30**	**9**	**11**	**4**	**6**	
dSPNs	20	7	6	4	3	5.2 – 5.5
iSPNs	10	2	5	0	3	5.6
2-input STDP + nimo&SKF (dSPNs)	**20**	**6**	**8**	**6**		5.9
60 pairings, 1 µM SKF	11	2	7	2		5.7
31 pairings, 0.5 µM SKF	7	3	1	3		5.8
60 pairings, 3 µM SKF	2	1	0	1		
2-input STDP without APs	**25**	**15**	**8**	**2**		
dSPNs	19	13	5	1		5.10 – 5.12
iSPNs	6	2	3	1		5.13
control (dSPNs & iSPNs)	**7**	**2**	**2**	**3**		5.14
total # of cells	**82**	**32**	**29**	**15**	**6**	
%	100%	39%	35%	18%	7%	

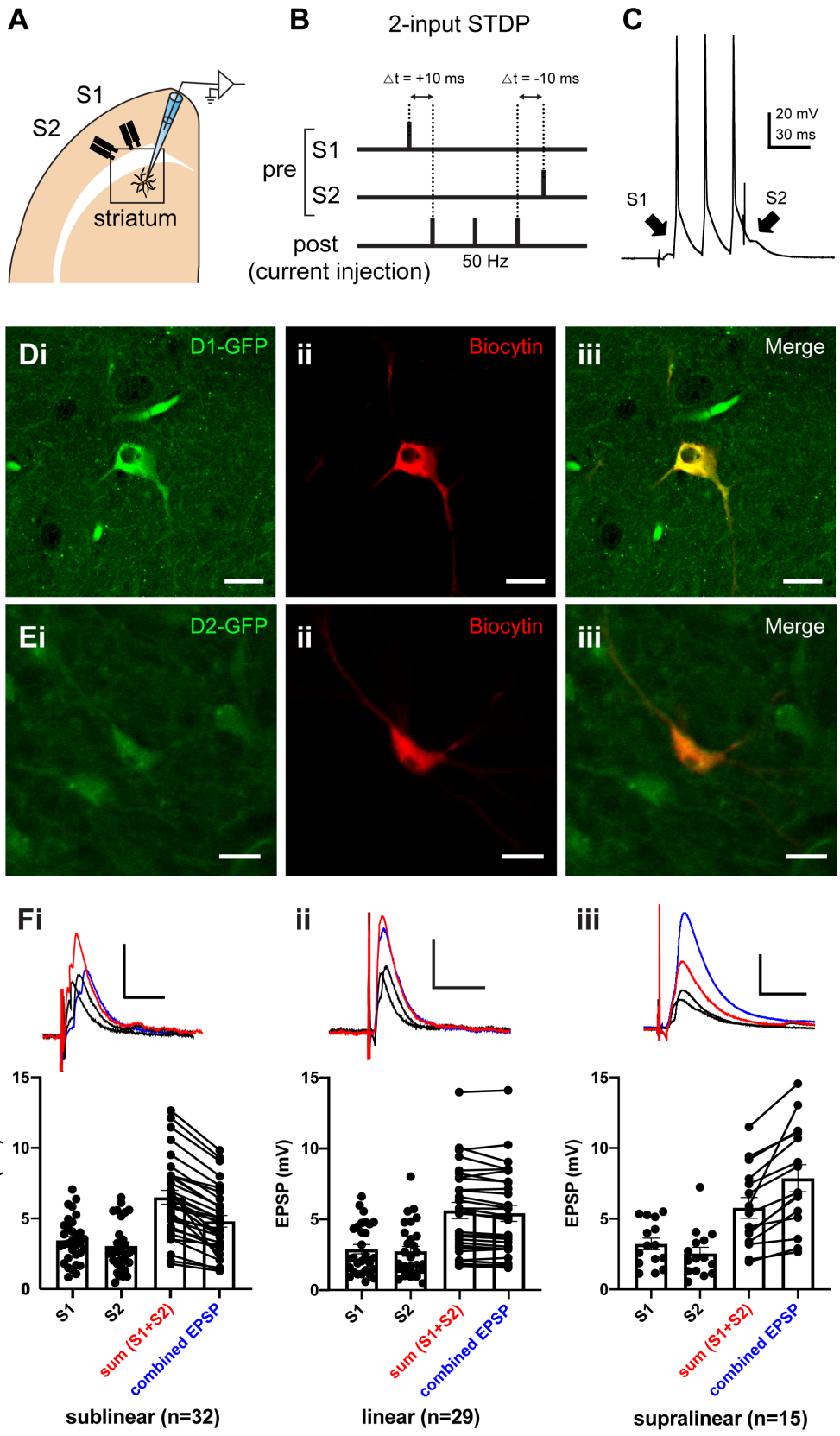

Figure 5.1. Experimental procedures for 2-input STDP protocol. (A) Schematic diagram showing the location of two bipolar electrodes inserted in the cortex layer V and the location of recording. (B) Two electrodes were used to induce unitary EPSPs at different timings (S1 & S2), and spikes (3 spikes at 50 Hz) were induced by postsynaptic current injection to the recorded neuron with a temporal window of ±10 ms. (C) A sample trace shows two inputs (S1 & S2) arriving at different timings in

(Figure 5.1. continued) relation to spikes (right). (D, E) Double labeling of the recorded neurons to confirm cell type of the recorded neuron. (D) dSPN cell type was confirmed by the labelling of (i) D1-GFP neuron enhanced with GFP antibody (green). (ii) Recorded neuron filled with biocytin reacted with CF633 streptavidin (red). (iii) Merged images. (E) iSPN cell type was confirmed by (i) D2-GFP neuron enhanced with GFP antibody (green). (ii) Recorded neuron filled with biocytin reacted with CF633 streptavidin (red). (iii) Merged images. Scale bars = 10 μm. (F, top) Sample EPSP traces of two EPSPs (black), arithmetic sum of two EPSPs (blue), and EPSP induced by combined simultaneous stimulation (red). Scale bars = 3 mV (vertical), 20 ms (horizontal). (F, bottom) Recorded cells were classified into three categories that showed (i) sublinear (n = 32), (ii) linear (n = 29) or (iii) supralinear (n = 15) summation. Black dots indicate individual values. Bars represent mean ± SEM. Cells in which linearity was not tested (n = 6) were included only in pooled data analysis.

5.3.1. Two EPSPs show three forms of interactions: sublinear, linear, and supralinear summations

Prior to synaptic plasticity experiments, independence of two inputs by two sets of stimulating electrodes was tested. For electrical stimulation, two sets of bipolar electrodes (custom array of two SNEX-100 PI concentric bipolar electrodes, Microprobes) connected to constant current stimulators (STG4008, Multi Channel Systems) were gently inserted in the layer V of the cortex (Fig.5.1A). Each set of electrodes were used to evoke EPSPs in SPNs, one as S1, and the other as S2. Interactions of two inputs were tested before proceeding to STDP experiments. Individual EPSPs from S1 and S2 inputs were recorded with larger (500 ms) interval at 0.05 Hz sufficient to avoid any interaction. Then, S1 and S2 were simultaneously stimulated at 0.05 Hz (combined EPSP) and compared against the arithmetic sum of S1 and S2 EPSP, using the mean over 10 traces. Cells were divided into three categories, namely, cells showing sublinear, linear, and supralinear summation (Fig.5.1F). Sublinear summation was defined as the combined EPSP by simultaneous stimulation below 90% of the arithmetic sum of the two EPSPs. Linear summation was defined as 90% ≤ combined EPSP < 110% of the arithmetic sum. Supralinear summation was assumed to have occurred when combined EPSP was 110% or larger than the arithmetic sum. In all the STDP experiments described in this chapter using two inputs (n = 82), in which summation of two inputs was tested (total n = 76 for both dSPNs and iSPNs, as summation profile was not tested in six pairs), sublinear summation was most prevalent, found in 32 cases (39%), while linear summation comprised 35% (29 out 82), followed by supralinear summation, which was found only in 18% of all the cases (15 out of 82).

5.3.2. Two-input STDP in dSPNs shows different plasticity profiles depending on summation profiles

A total of 30 cells (dSPNs and iSPNs) from 30 animals were exposed to 2-input STDP protocols (Fig.5.1B & C). For synaptic plasticity analysis, the mean normalized EPSPs over the last 5-min of recording (red line in Fig.5.2) were compared against the baseline (blue line in Fig.5.2). Different cell types (dSPNs and iSPNs) and cells with different summation profiles (sublinear, linear, and supralinear) were analyzed separately. In dSPNs, when inputs with linear summation (n = 6; Fig.5.2) were analyzed, only pre-post pairing showed LTD (normalized EPSP became 79.4 ± 2.8 % of the baseline, mean EPSP reduced from 3.0 ± 1.0 mV to 2.3 ± 0.8 mV, $t_{(5)} = 7.28$, p = 0.002). After post-pre pairing, there was a slight non-significant decrease in normalized EPSP (80.9 ± 8.3 %, $t_{(5)} = 2.30$, p = 0.14, n.s). Mean EPSP before pairing was 3.0 ± 1.1 mV and after pairing was 2.6 ± 0.8 mV. This plasticity profile is consistent with our previous STDP results with one pairing input (Shindou et al., 2011, 2019).

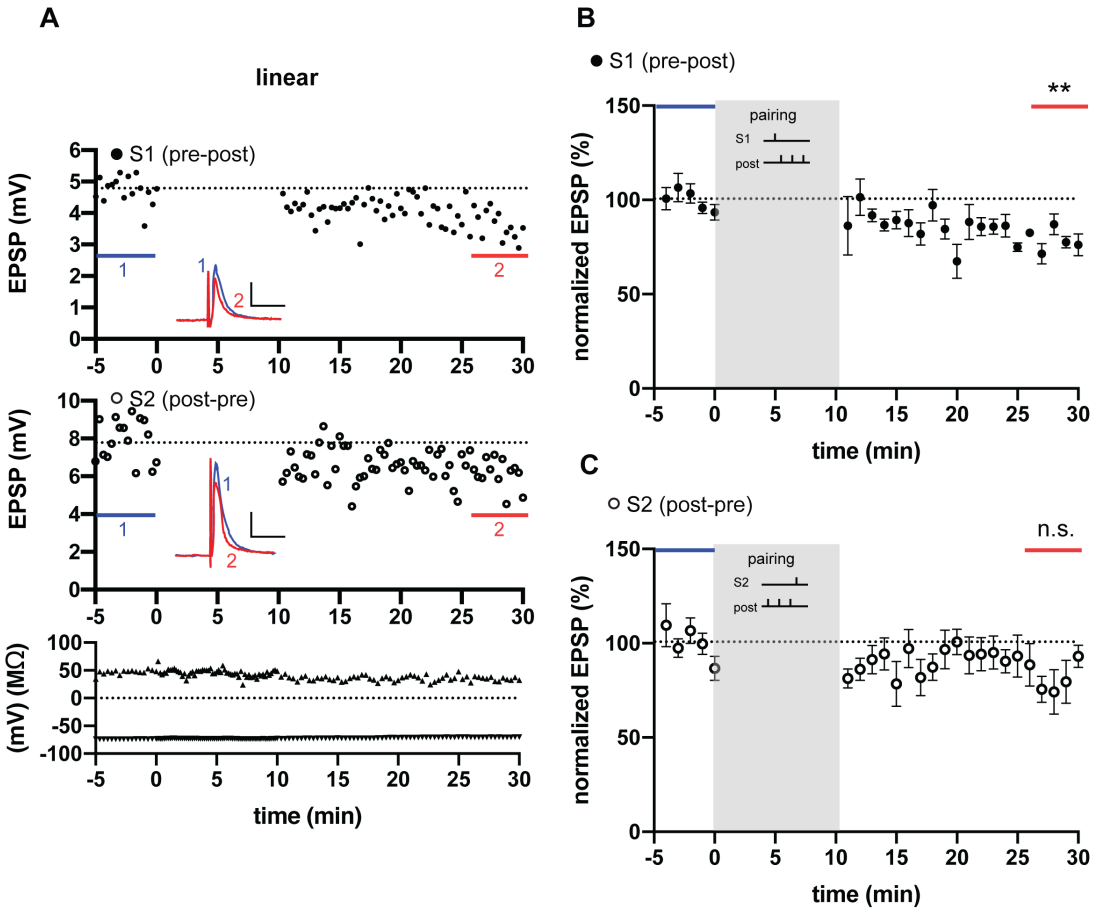

Figure 5.2. Two-input STDP in dSPNs with inputs that showed linear summation. (A) Representative examples of changes in S1 EPSP amplitude (mV, filled circles, top) and S2 EPSP amplitude (mV, open circles, middle), input resistance (Ri, MΩ, upright triangles, bottom), and resting membrane potential (RMP, mV, downward triangles, bottom). Sample traces show averages of EPSP over 5 min before pairing (blue, 1) and over last 5 min of pairing (red, 2). Scale bars = 2 mV (vertical) and 50 ms (horizontal). (B, C) Group averages (n = 6), in which each dot indicates the mean normalized EPSPs over 1 min. period ± SEM. Pre-post pairing induced LTD, but post-pre pairing caused no plasticity in dSPNs with linearly summating inputs. **: $p < 0.01$, n.s.: not significant.

Interestingly, when inputs that showed sublinear, linear, or supralinear summation were analyzed separately, different plasticity profiles were observed. When inputs with sublinear summation (n = 7) were analyzed, no plasticity was observed after pre-post pairing (95.2 ± 19.6 %, mean EPSP was 2.6 ± 0.4 mV before and 2.2 ± 0.5 mV after, $t_{(6)} = 0.24$, $p = 0.816$, n.s.; Fig.5.3). Significant LTD was induced after post-pre pairing (77.7 ± 3.5 %, mean EPSP was reduced from 3.5 ± 0.8 mV to 2.8 ± 0.7 mV, $t_{(6)} = 6.47$, $p = 0.002$; Fig.5.3). In addition, inputs with supralinear summation (n = 4) showed no plasticity after pre-post pairing (normalized EPSP was 83.0 ± 6.4 %, $t_{(3)} = 2.63$, $p = 0.078$, n.s., mean EPSP size before pairing was 2.7 ± 0.8 mV and 2.4 ± 0.9 mV after pairing). However, post-pre pairing resulted in a significant LTD (normalized EPSP after pairing was 66.1 ± 3.6 %, $t_{(3)} = 9.49$, $p = 0.004$; Fig.5.4). Mean EPSP decreased from 2.7 ± 1.0 mV to 1.7 ± 0.7 mV after pairing. Together, these results show that inputs with non-linear summation cause different STDP profiles (LTD after post-pre pairing; Fig.5.3C & Fig.5.4C) from inputs with linear summation (Fig.5.2).

Overall, in all dSPNs (n = 20, regardless of linearity of inputs, including 3 cells for which linearity was not tested), no plasticity was observed after pre-post timing in S1 EPSPs (Fig.5.5A). Mean S1 EPSP was slightly reduced from 2.9 ± 0.4 mV to 2.4 ± 0.3mV (normalized EPSP was 84.6 ± 7.4 % of the baseline) but the difference was not statistically significant ($t_{(19)} = 2.07$, $p = 0.052$, n.s). On the other hand, after post-pre timing, there was a significant LTD (74.1 ± 3.8 %, $t_{(19)} = 6.91$, $p = 0.000002$). Mean S2 EPSP was reduced from 3.1 ± 0.5 mV to 2.4 ± 0.4 mV. In summary, while independent (linearly summating) inputs (n = 6) showed LTD after pre-post pairing and not after post-pre pairing (Fig.5.5B), interacting (sublinearly or supralinearly summating) inputs (n = 11) showed no plasticity after pre-post pairing (normalized EPSP was 90.9 ± 12.4 % of the baseline, $t_{(10)} = 0.74$, $p = 0.48$), but LTD after post-pre pairing (normalized EPSP was 72.5 ± 10.8 % of the baseline, $t_{(10)} = 8.47$, $p < 0.0001$) (Fig.5.5C).

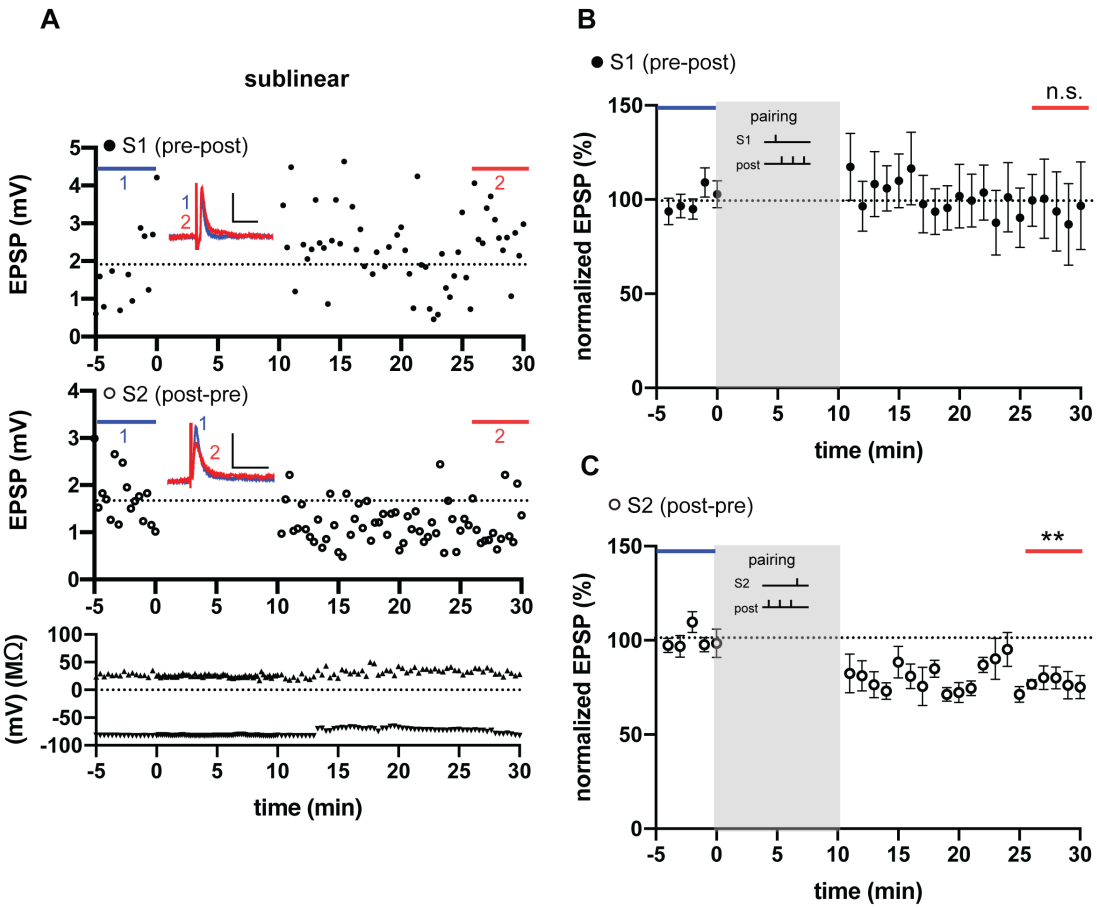

Figure 5.3. Two-input STDP in dSPNs with inputs that showed sublinear summation. (A) Representative examples of changes in S1 EPSP amplitude (mV, filled circles, top) and S2 EPSP amplitude (mV), Ri (MΩ), and RMP (mV). Sample traces show averages of EPSP over 5 min before pairing (blue, 1) and over last 5 min of pairing (red, 2). Scale bars = 1 mV (vertical) and 50 ms (horizontal). (B, C) Group averages (n = 7), in which each dot indicates the mean normalized EPSPs over 1 min. period ± SEM. Pre-post pairing caused no plasticity, but post-pre pairing caused LTD in dSPNs with sublinearly summating inputs. **: $p < 0.01$, n.s.: not significant.

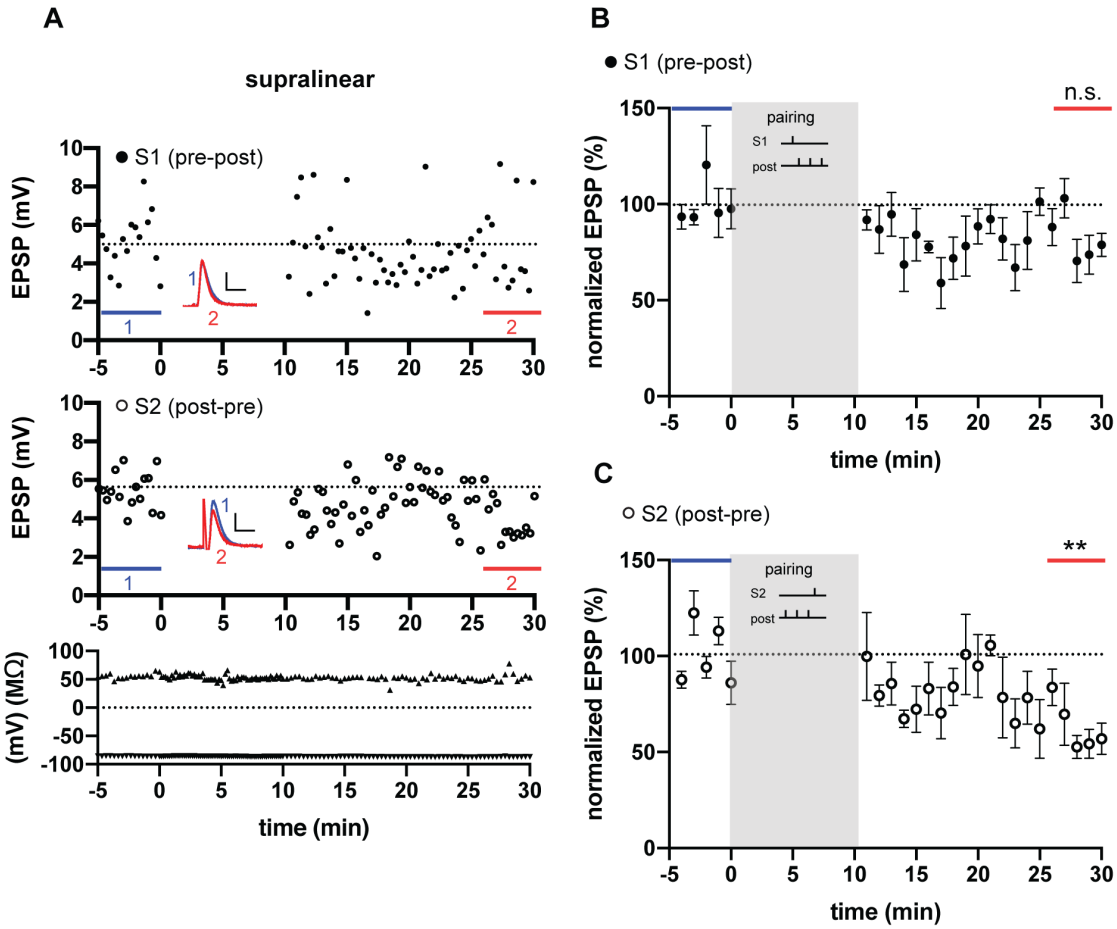

Figure 5.4. Two-input STDP in dSPNs with inputs that showed supralinear summation. (A) Representative examples of changes in S1 EPSP amplitude (mV, filled circles, top) and S2 EPSP amplitude (mV), Ri (MΩ), and RMP (mV). Sample traces show averages of EPSP over 5 min before pairing (blue, 1) and over last 5 min of pairing (red, 2). Scale bars = 2 mV (vertical) and 20 ms (horizontal). (B, C) Group averages (n = 4) of S1 EPSP (B) and S2 EPSP (C), in which each dot indicates the mean normalized EPSPs over 1 min. period ± SEM. Pre-post pairing caused no plasticity, but post-pre pairing caused LTD in dSPNs with supralinearly summating inputs. **: $p < 0.01$, n.s.: not significant.

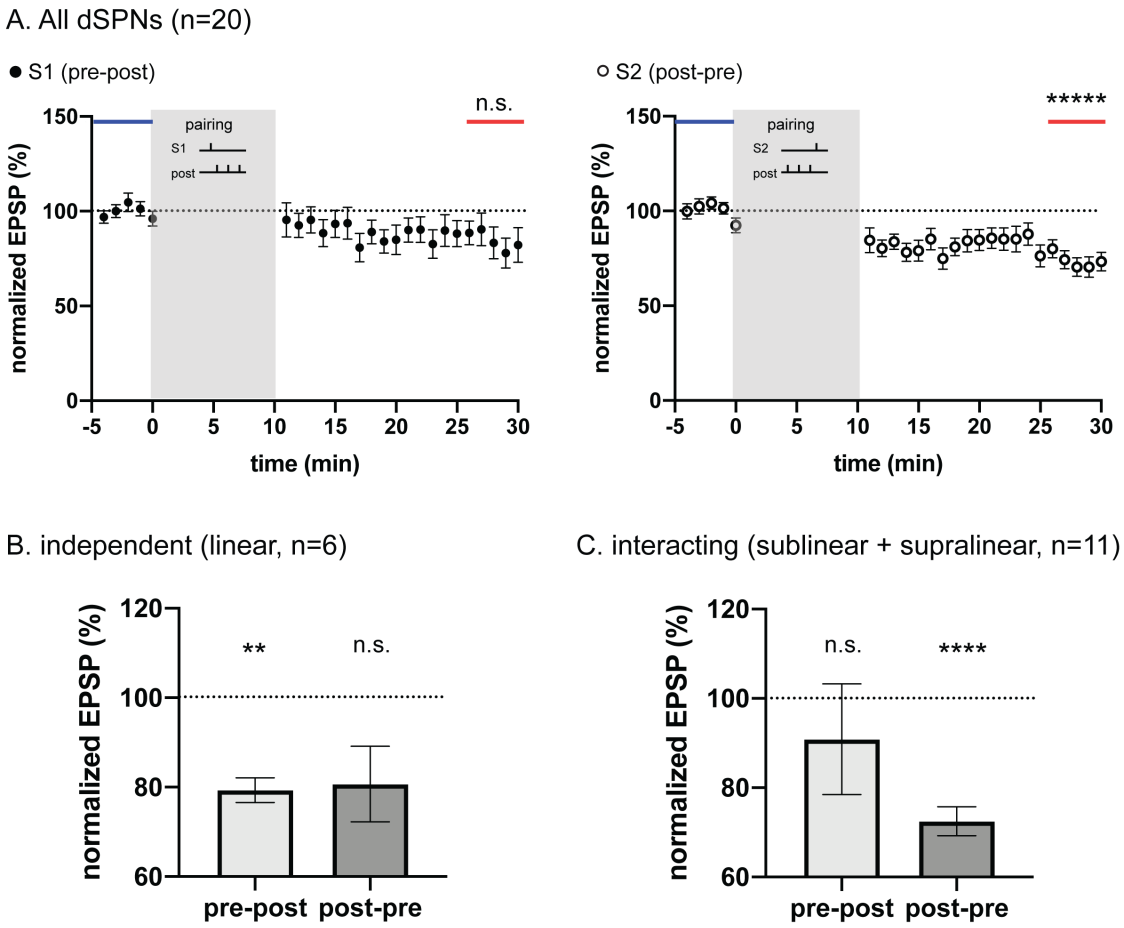

Figure 5.5. Two-input STDP in dSPNs. (A) Averages over all dSPNs (n = 20, regardless of linearity of inputs, including 3 cells for which linearity was not tested) of normalized EPSPs in S1 input (pre-post timing, left) and S2 input (post-pre timing, right). When all dSPNs were analyzed together, LTD was induced after post-pre pairing. Data displayed as mean ± SEM. (B) Summary bar graph of two-input STDP in dSPNs with independent (linearly summating) inputs (n = 6). LTD was induced after pre-post pairing. (C) Summary bar graph of two-input STDP in dSPNs with interacting (sublinearly or supralinearly summating) inputs (n = 11). LTD was induced after post-pre pairing. **: $p < 0.01$, ****: $p < 0.0001$, *****: $p < 0.00001$, n.s.: not significant.

5.3.3. No plasticity was observed in iSPNs regardless of independence of inputs

In contrast to dSPNs, which showed significant LTD, no significant plasticity was observed in iSPNs (n = 10) after pre-post (90.0 ± 11.2 %, mean EPSP decreased from 2.5 ± 0.4 mV to 2.0 ± 0.3 mV $t_{(9)} = 0.90$, p = 0.394, n.s.) or post-pre pairing (84.9 ± 9.6 %, mean EPSP was reduced from 3.2 ± 0.4 mV to 2.5 ± 0.3 mV, $t_{(9)} = 1.56$, p = 0.152, n.s.; Fig.5.6). Similarly, when only the inputs with linear summation (n = 5) were analyzed, no significant change was observed after pre-post (94.1 ± 3.8 %, mean EPSP was 2.7 ± 0.6 mV before and 2.4 ± 0.5 mV after, $t_{(4)} = 1.56$, p = 0.194, n.s.) or post-pre (normalized EPSP was 98.0 ± 9.1 %, mean EPSP was 3.4 ± 0.6 mV before and 3.2 ± 0.4 mV after, $t_{(4)} = 0.22$, p = 0.838, n.s.) pairing. Lack of synaptic plasticity in iSPNs in this protocol is consistent with our previous study (Shindou et al., 2019).

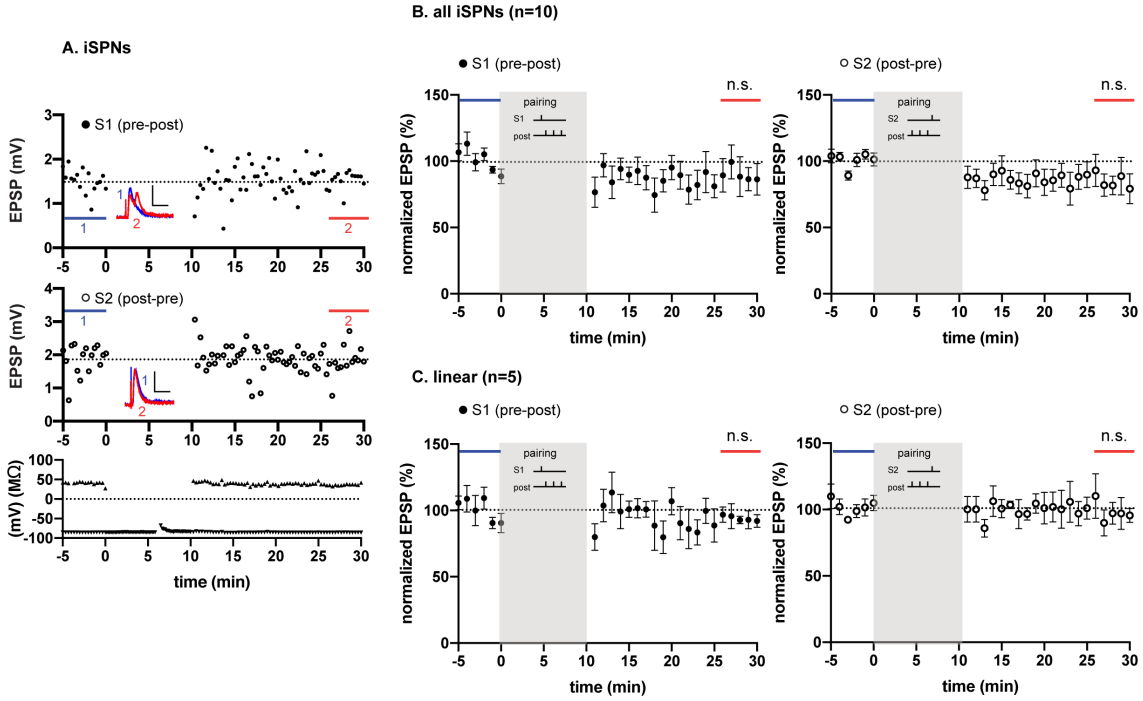

Figure 5.6. Two-input STDP in iSPNs. (A) Representative examples of changes in S1 and S2 EPSP amplitude (mV), Ri (MΩ), and RMP (mV). Sample traces show averages of EPSP over 5 min before pairing (blue, 1) and over last 5 min of pairing (red, 2). Scale bars = 1 mV (vertical) and 20 ms (horizontal). (B) Mean normalized EPSPs in all iSPNs (n = 10), and in (C) inputs that showed linear summation (n = 5). No plasticity was induced in iSPNs after pre-post or post-pre paring. Data displayed as mean ± SEM. n.s.: not significant.

5.3.4. Application of dopamine agonist in the presence of Ca^{2+} channel blocker during 2-input STDP

The results presented so far in this chapter show that LTD was induced after the 2-input STDP protocol, but not LTP. Dopamine is a neuromodulator necessary for plasticity induction, in particular for LTP (Pawlak & Kerr, 2008; Shen et al., 2008). Previously, Shindou et al. (2019) demonstrated that application of a D1 agonist (0.5 – 1 μM SKF-81297) during the pre-post pairing protocol (31 or 60 pairings, at 0.1 Hz) in the presence of L-VGCC blocker (10 μM nimodipine) to block LTD induction, induced LTP. Therefore, I tested whether nimodipine and SKF-81297 could preferentially modulate only pre-post input when there is contiguous input at post-pre timing. Twenty cells from 16 animals received the 2-input STDP protocol in the presence of nimodipine and SKF-81297 during pairing with varying concentration and pairing numbers. Firstly, nimodipine (10 μM) and SKF-81297 (1 μM) were bath applied during pairing (60 times at 0.1 Hz, total 10 min). This protocol failed to show LTP. Instead, pre-post pairing caused no plasticity, whereas post-pre pairing caused LTD (Fig.5.7). After pre-post pairing, normalized S1 EPSP remained unchanged (100.4 ± 18.5 % of the baseline, $t_{(10)} = 0.022$, $p = 0.983$, n.s.). S1 EPSP was 1.5 ± 0.3 mV before pairing, and 1.3 ± 0.2 mV after pairing. After post-pre pairing, S2 EPSP showed a significant decrease (normalized EPSP was 78.4 ± 4.6 % of the baseline, $t_{(10)} = 4.69$, $p = 0.002$). S2 EPSP decreased from 1.3 ± 0.2 mV to 1.0 ± 0.2 mV.

Next, fewer pairings (31 times) and lower (0.5 μM) SKF-81297 concentration were tested (n = 7). No plasticity was induced after pre-post pairing, but LTD was induced after post-pre pairing (Fig.5.8). S1 EPSP remained unchanged (normalized EPSP was 85.2 ± 7.5 % of the baseline, $t_{(6)} = 0.986$, $p = 0.094$, n.s.). S1 EPSP before pairing was 3.4 ± 0.9 mV, and 2.7 ± 0.7 mV after pairing. On the other hand, S2 EPSP showed a significant decrease (normalized EPSP was 77.4 ± 6.9 % of the baseline, $t_{(6)} = 3.255$, $p = 0.034$). S2 EPSP reduced from 2.2 ± 0.5 mV to 1.6 ± 0.3 mV. The frequency of action potential triplets used in this protocol (50 Hz) was lower than our previous study (100 Hz in Shindou et al., 2019), which may have been insufficient to induce LTP. Nevertheless, these results suggest that blockade of L-VGCC and dopamine agonism did not change overall plasticity profile of 2-input STDP.

Different concentrations of SKF-81297 (0.5 or 1μM) and different pairings (31 or 60 times at 0.1 Hz) showed a similar plasticity profile (LTD by post-pre pairing; Fig.5.7 & Fig.5.8). As described earlier in 5.3.2., inputs with different summation profiles may show different responses to pharmacological manipulation and may exhibit different plasticity profiles. To reveal whether there was any difference between inputs with different summation profiles, these cells were analyzed together and further investigated in terms of summation profiles. Two cells with higher SKF-81297 concentration (3 μM) were also included in this analysis. When analyzed together, linearly summating inputs (n = 8) showed robust LTD after both pre-post (normalized EPSP was 77.7 ± 4.0 % of the baseline, $t_{(7)} = 5.515$, $p = 0.002$) and post-pre timing (normalized EPSP was 77.2 ± 4.0 % of the baseline, $t_{(7)} = 5.659$, $p = 0.002$) (Fig.5.9A). Mean S1 EPSP was reduced from 1.9 ± 0.5 mV to 1.4 ± 0.4 mV, while mean S2 EPSP reduced from 1.4 ± 0.3 mV to 1.1 ± 0.2 mV.

In contrast, sublinearly summating inputs (n = 6) showed no overall plasticity (Fig.5.9B). After pre-post pairing, S1 EPSP showed no significant change (normalized EPSP was 85.2 ± 9.9 % of the baseline, $t_{(5)} = 1.5$, $p = 0.194$, n.s.). Mean EPSP before pairing was 2.4 ± 0.9 mV and after pairing was 1.8 ± 0.6 mV. Post-pre pairing also caused no significant change in S2 EPSP (normalized EPSP was 79.5 ± 10.0 % of the baseline, $t_{(5)} = 2.047$, $p =$

0.096, n.s.). Mean EPSP before pairing was 1.6 ± 0.6 mV and after pairing was 1.2 ± 0.4 mV.

Supralinearly summating inputs (n = 6) showed a different plasticity profile (Fig.5.9C). After pre-post pairing, a slight but non-significant increase was observed (normalized EPSP was 113.9 ± 34.1 % of the baseline, $t_{(5)} = 0.407$, $p = 0.701$, n.s.). Mean S1 EPSP before pairing was 2.5 ± 0.8 mV and after pairing was 2.2 ± 0.7 mV. On the other hand, post-pre pairing resulted in a significant decrease in normalized EPSP (76.6 ± 4.7 % of the baseline, $t_{(5)} = 4.948$, $p = 0.008$). Mean S2 EPSP before pairing was 1.9 ± 0.4 mV and after pairing was 1.3 ± 0.2 mV.

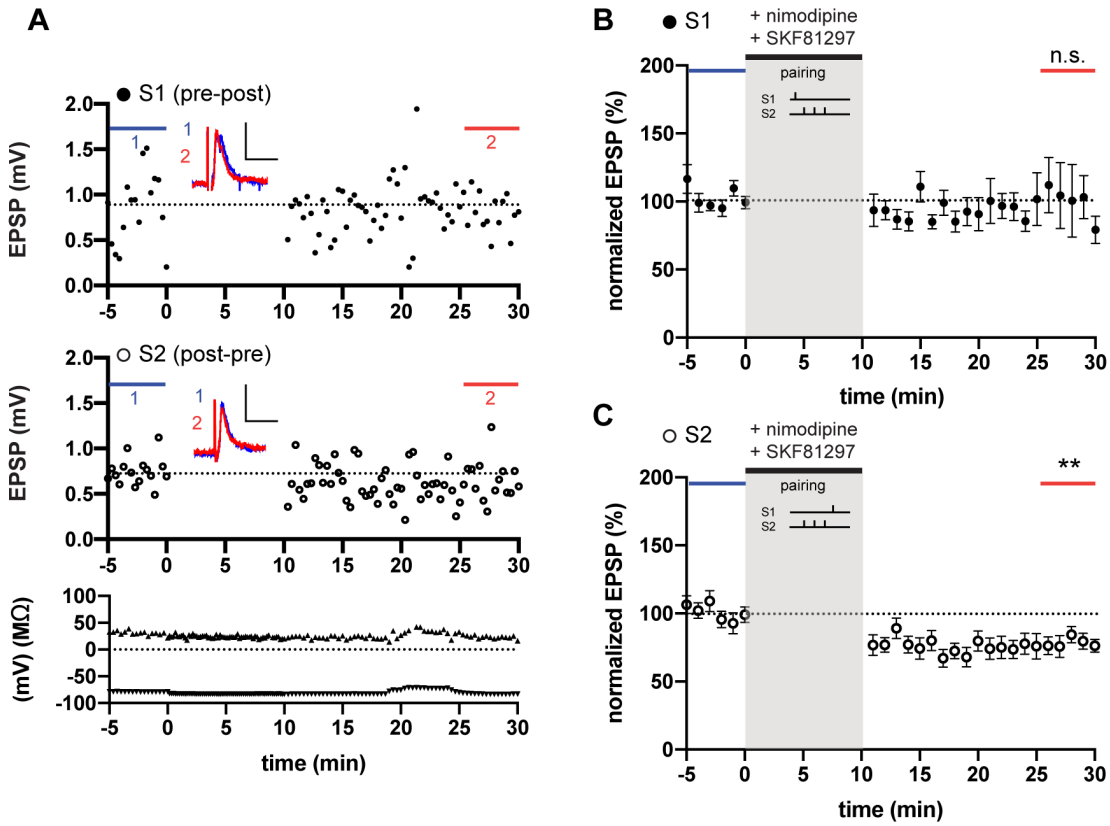

Figure 5.7. Two-input STDP in dSPNs with application of nimodipine and SKF-81297. (A) Representative examples of changes in S1 and S2 EPSP amplitude (mV), Ri (MΩ), and RMP (mV). Sample traces show averages of EPSP over 5 min before pairing (blue, 1) and over last 5 min of pairing (red, 2). Scale bars = 0.5 mV (vertical) and 50 ms (horizontal). (B) Group averages (n = 11) showing mean normalized S1 EPSPs and (C) S2 EPSPs. Black line indicates the application of nimodipine (10 μM) and SKF-81297 (1 μM) during pairing (60 times at 0.1 Hz). Pre-post pairing caused no plasticity, whereas post-pre pairing caused LTD. Data displayed as mean ± SEM.**: $p < 0.01$, n.s.: not significant.

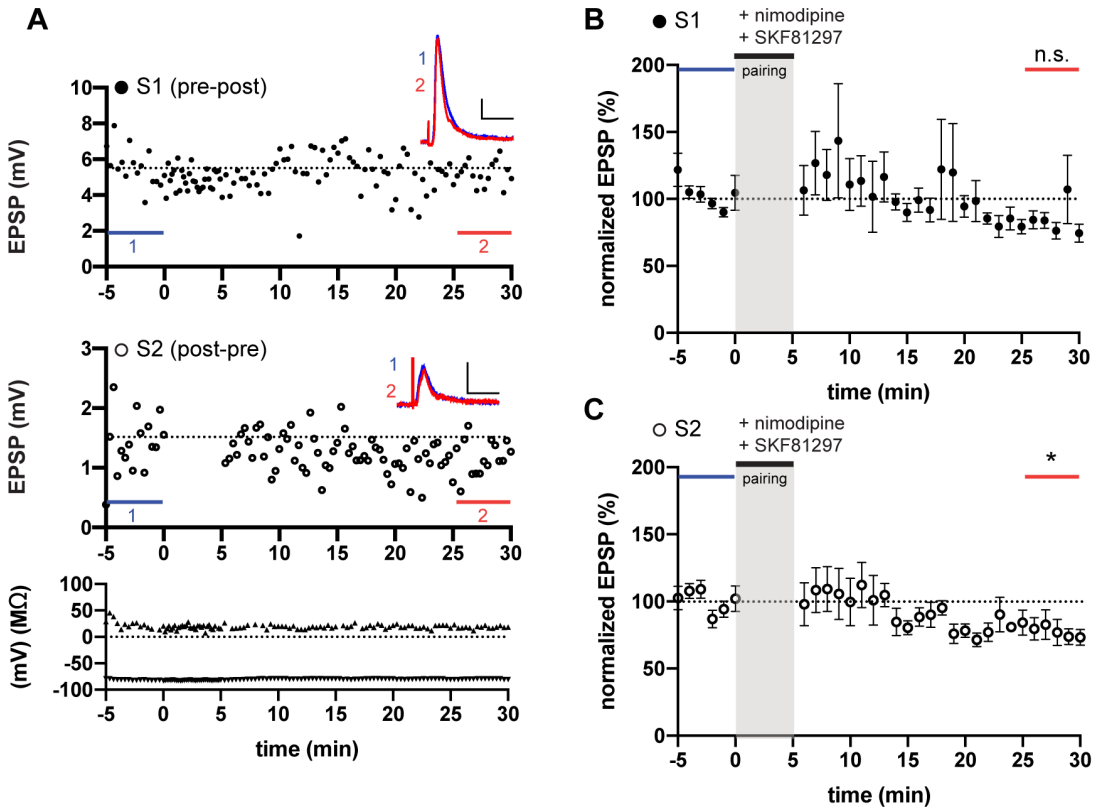

Figure 5.8. Two-input STDP in dSPNs with application of nimodipine and SKF-81297 with fewer pairing numbers. (A) Representative examples of changes in S1 and S2 EPSP amplitude (mV), Ri (MΩ), and RMP (mV). Sample traces show averages of EPSP over 5 min before pairing (blue, 1) and over last 5 min of pairing (red, 2). Scale bars = 1 mV (vertical) and 50 ms (horizontal). (B) Group averages (n = 7) showing mean normalized S1 EPSPs and (C) S2 EPSPs. Black line indicates the application of nimodipine (10 μM) and SKF-81297 (0.5 μM) during pairing (31 times at 0.1 Hz). Pre-post pairing caused no plasticity, whereas post-pre pairing caused LTD. Data displayed as mean ± SEM. *: $p < 0.05$, n.s.: not significant.

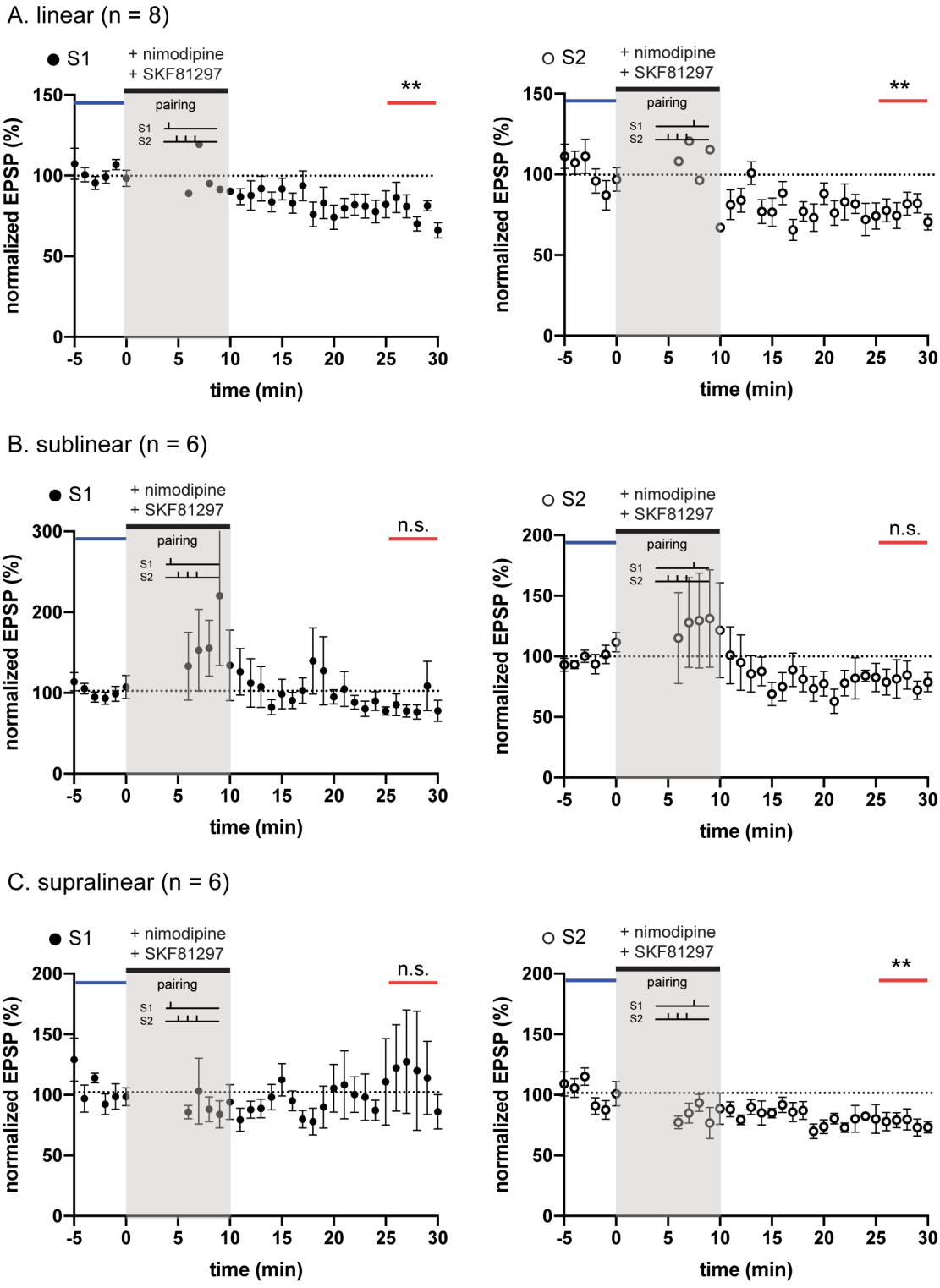

Figure 5.9. Two-input STDP in dSPNs with application of nimodipine and SKF-81297 in cells showing linear, sublinear, or supralinear summation. Group averages in (A) linear summation (n = 8), (B) sublinear summation (n = 6), and (C) supralinear summation (n = 6) groups showing mean normalized S1 EPSPs and S2 EPSPs. Black line indicates the application of nimodipine (10 μM) and SKF-81297 (0.5, 1, or 3 μM) during pairing (31 or 60 times at 0.1 Hz). Inputs with different summation (Figure 5.9. continued) profiles showed different plasticity profiles. Data displayed as mean ± SEM. **: $p < 0.01$, n.s.: not significant.

5.3.5. LTD was observed in dSPNs after pairing of two presynaptic inputs without postsynaptic firing

To test whether interactions of presynaptic inputs at SPN dendrites in the absence of postsynaptic spiking activity could provide a sufficient plasticity induction signal, I then investigated whether the two inputs (S1 and S2) in close temporal proximity have affected each other and contributed to plasticity. To test this, the 2-input STDP protocol was repeated, but this time no postsynaptic current injection was used to induce action potentials (Fig. 5.10A). S1 input and S2 input were paired at the same interval (60 ms) for 60 times at 0.1 Hz. 25 cells in separate brain slices from 22 animals received this protocol.

Surprisingly, without pairing with postsynaptic action potentials, pairing two presynaptic inputs alone caused LTD in dSPNs. STDP profiles were then analyzed depending on different summation profiles. Inputs with linear summation (n = 5) showed LTD only in S2 inputs (Fig.5.10B-D). S1 EPSP showed a non-significant decrease from 3.6 ± 0.3 mV to 2.7 ± 0.3 mV (77.0 ± 9.1 % of the baseline EPSP, $t_{(4)} = 2.54$, $p = 0.064$, n.s.). S2 EPSP showed a significant decrease from 2.8 ± 0.8 mV to 2.1 ± 0.6 mV (74.6 ± 5.8 % of the baseline EPSP, $t_{(4)} = 4.35$, $p = 0.024$,).

For nonlinearly summating inputs, inputs with sublinear summation (n = 13) showed robust LTD in both S1 and S2 inputs (Fig.5.11B-C). S1 EPSP reduced from 2.8 ± 0.3 mV to 2.0 ± 0.3 mV, which is 69.6 ± 4.2 % of the baseline EPSP, indicating a robust LTD ($t_{(12)} = 7.25$, $p = 0.00002$). Likewise, S2 EPSP decreased from 3.1 ± 0.4 mV to 1.9 ± 0.3 mV, which was statistically significant (63.2 ± 4.7% of the baseline EPSP, $t_{(12)} = 7.77$, $p = 0.00001$). There was only one case of supralinear summation, but this cell also showed a decrease in EPSPs (Fig.5.11A). S1 EPSP decreased from 4.7 to 2.2 mV (47.4 % of the baseline), whereas S2 EPSP decreased from 4.1 to 3.2 mV (78.8 % of the baseline).

Overall, in all dSPNs (n = 19), pairing of two inputs induced significant LTD in both S1 and S2 inputs (Fig.5.12). S1 EPSP was reduced from 3.1 ± 0.2 mV to 2.2 ± 0.2 mV, which is 70.4 ± 3.9 % of the baseline EPSP, indicating a robust LTD ($t_{(18)} = 7.64$, $p = 0.0000002$). S2 EPSP was also reduced from 3.0 ± 0.3 mV to 2.1 ± 0.2 mV, which was statistically significant (67.0 ± 3.7% of the baseline EPSP, $t_{(18)} = 8.81$, $p = 0.0000002$). These results suggest that pairing multiple synaptic inputs alone can induce synaptic plasticity in the absence of postsynaptic spikes.

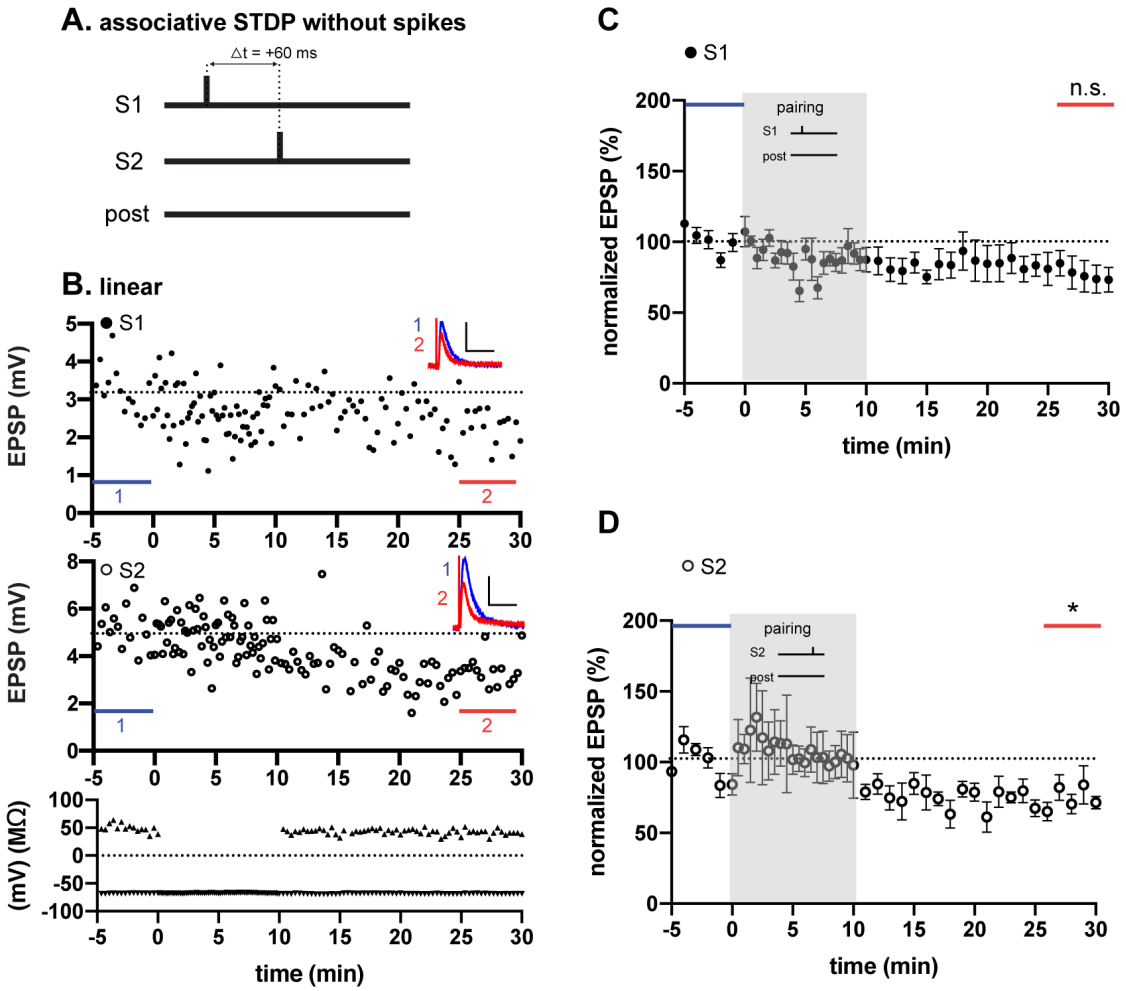

Figure 5.10. Associative STDP in dSPNs after pairing of two EPSPs in the absence of spikes. (A) S1 and S2 EPSPs were paired at 60 ms interval without pairing with spikes. In dSPNs that showed linear summation of two inputs, (B) representative example of result showing S1 and S2 EPSP amplitude (mV), Ri (MΩ), and RMP (mV). Sample traces show averages of EPSP over 5 min before pairing (blue, 1) and over last 5 min of pairing (red, 2). Scale bars = 2 mV (vertical) and 50 ms (horizontal). (C, D) Mean (± SEM) normalized EPSPs in dSPNs with linear inputs (n = 5) in (C) S1 and (D) S2 inputs. Pairing two presynaptic inputs alone caused LTD in S2 inputs. *: $p < 0.05$, n.s.: not significant.

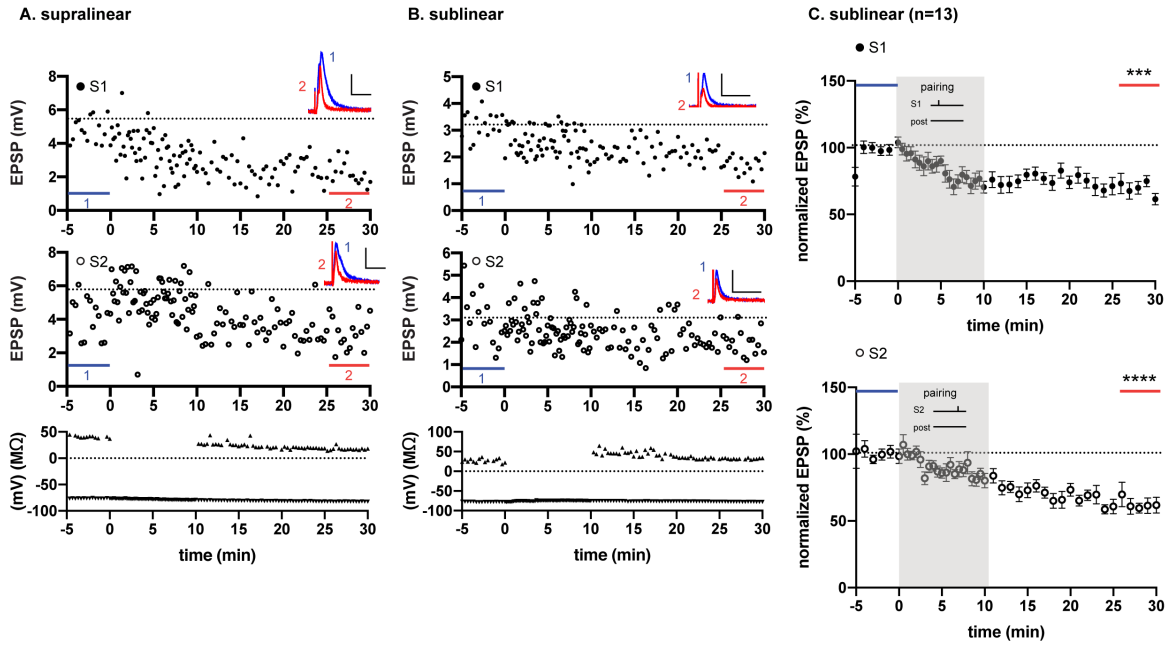

Figure 5.11. Associative STDP in dSPNs with inputs that showed nonlinear summation. (A) representative example of result that showed supralinear summation. Results show S1 and S2 EPSP amplitude (mV), Ri (MΩ), and RMP (mV). Sample traces show averages of EPSP over 5 min before pairing (blue, 1) and over last 5 min of pairing (red, 2). Scale bars = 2 mV (vertical) and 50 ms (horizontal). (B) representative example of result that showed sublinear summation. Scale bars = 2 mV (vertical) and 50 ms (horizontal). (C) Mean (± SEM) normalized EPSPs in dSPNs with sublinear summation (n = 13) in S1 (top) and S2 (bottom) inputs. Pairing two presynaptic inputs alone caused LTD in both S1 and S2 inputs. ***: $p < 0.001$, ****: $p < 0.0001$.

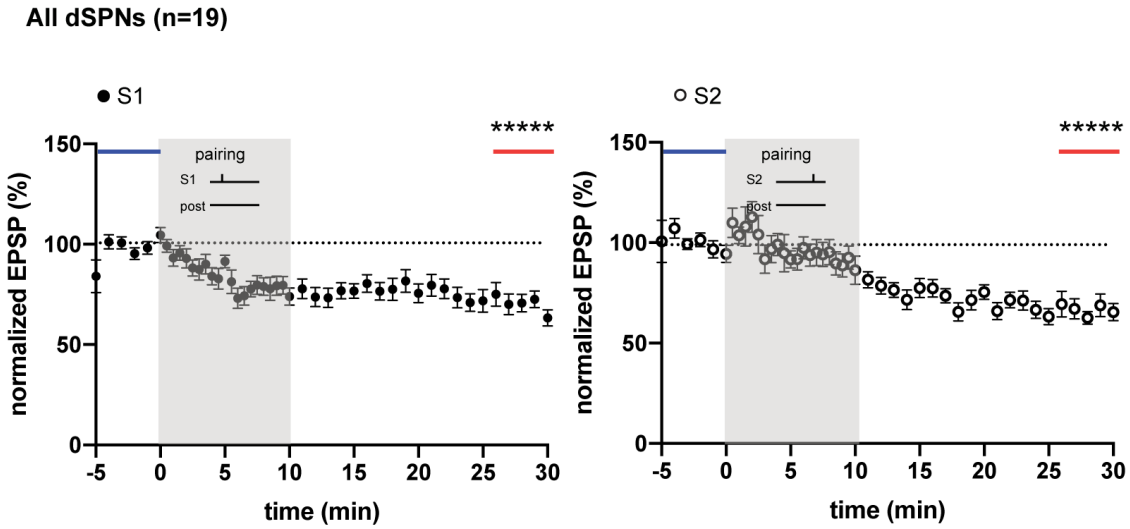

Figure 5.12. Associative STDP in dSPNs.(A) Averages over all dSPNs (n = 19) of normalized EPSPs in S1 input (pre-post timing, left) and S2 input (post-pre timing, right). Data displayed as mean ± SEM. When all dSPNs were analyzed together, LTD was induced in both S1 and S2 inputs. *****: $p < 0.00001$.

5.3.6. No plasticity was observed in iSPNs after two presynaptic inputs without postsynaptic firing

In the case of iSPNs (n = 6), the 2-input STDP protocol without postsynaptic firing did not produce any plasticity, consistent with the earlier results of 2-input STDP in iSPNs (Fig.5.13). Although there was a trend toward a decrease, S1 EPSP showed no significant change (78.3 ± 8.5% of the baseline, $t_{(5)} = 2.56$, $p = 0.102$). S1 EPSP was 2.5 ± 0.4 mV before pairing and 2.0 ± 0.4 mV after pairing. S2 EPSP also showed no significant change (76.9 ± 9.3 % of the baseline EPSP, $t_{(5)} = 2.47$, $p = 0.112$). S2 EPSP changed slightly from 1.3 ± 0.2 mV to 1.0 ± 0.1 mV.

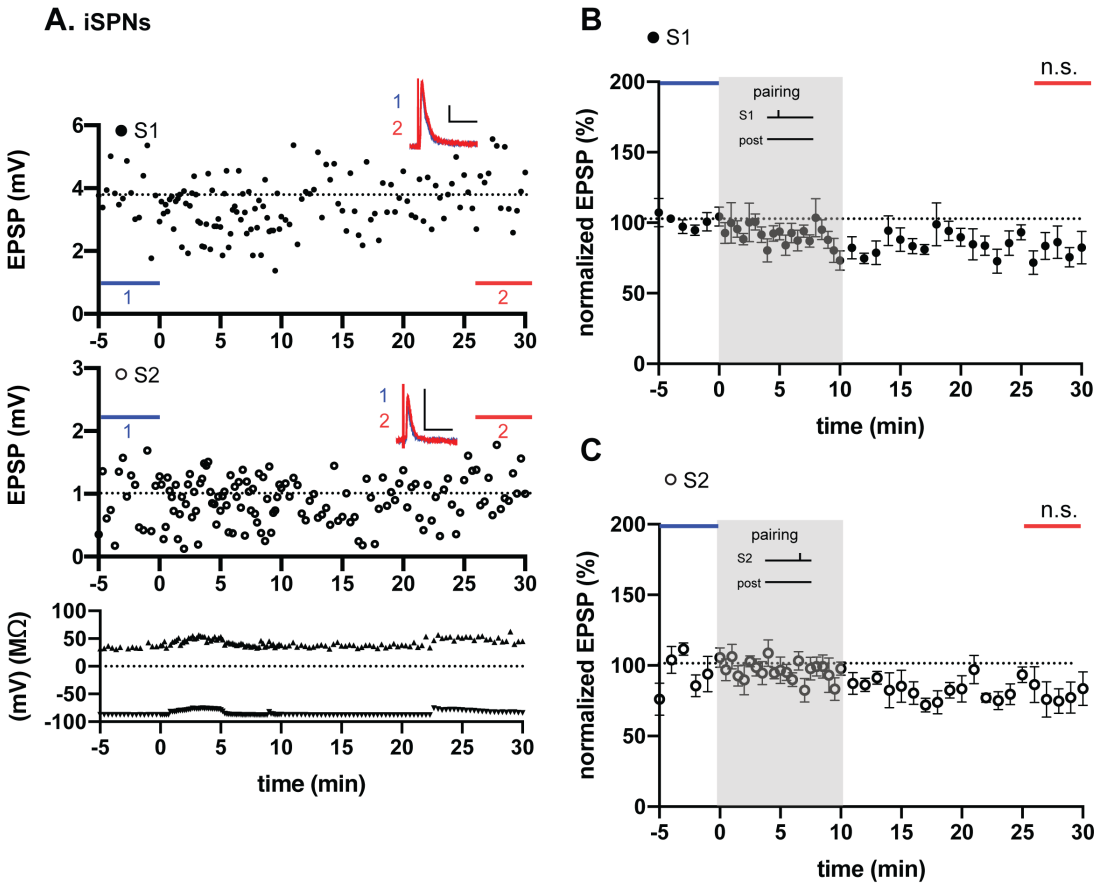

Figure 5.13. Associative STDP in iSPNs. (A) Representative examples of changes in S1 and S2 EPSP amplitude (mV), Ri (MΩ), and RMP (mV). Sample traces show averages of EPSP over 5 min before pairing (blue, 1) and over last 5 min of pairing (red, 2). Scale bars = 1 mV (vertical) and 50 ms (horizontal). (B, C) Mean normalized EPSPs in all iSPNs (n=6), in S1 (B) and S2 (C) inputs. No plasticity was induced after pairing of two inputs in iSPNs. Data displayed as mean ± SEM. n.s.: not significant.

5.3.7. Control experiments with a larger temporal window caused no plasticity

To exclude the possibility that the EPSP was decreasing with time regardless of pairing, the next experiment was carried out as a control experiment with a time interval outside of the STDP window (Δt = 500 ms). Control experiments were done in seven cells from five animals. After pairing with a 500 ms time window, no plasticity was observed (Fig.5.14). S1 EPSP slightly decreased to 87.5 ± 9.2%, but it was not statistically significant ($t_{(6)} = 1.36$, $p = 0.222$). S1 EPSP was 2.8 ± 0.5 mV before pairing and 2.3 ± 0.4 mV after pairing. S2 EPSP also remained unchanged (92.7 ± 9.8% of the baseline, $t_{(6)} = 0.747$, $p = 0.483$). S2 EPSP was 3.4 ± 0.8 mV before pairing and 3.2 ± 0.9 mV after pairing. EPSPs showed a slight trend to decrease across recording, but none of the changes were statistically significant. This control experiment confirmed that LTD by two associative inputs was not due to degradation of cell quality with time and that a shorter temporal window (Δt = 60 ms) enabled plasticity.

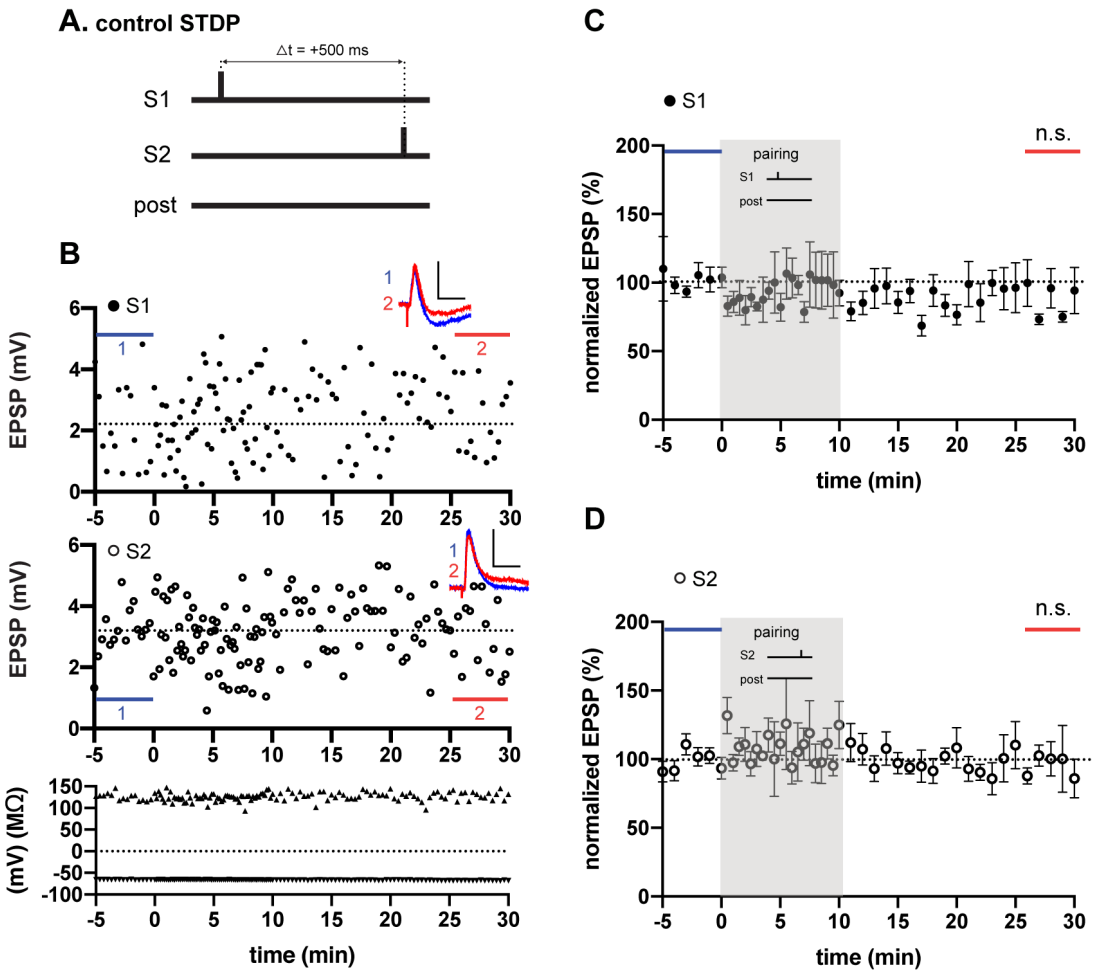

Figure 5.14. Control experiments with two inputs. (A) Control experiment with two inputs paired at 500 ms interval. (B) Representative plot shows S1 and S2 EPSP amplitudes (mV), Ri (MΩ), and RMP (mV). Sample traces show averages of EPSP over 5 min before pairing (blue, 1) and over last 5 min of pairing (red, 2). Scale bars = 2 mV (vertical) and 50 ms (horizontal). (C, D) Average traces (n = 7) of mean normalized EPSP in S1 (C) and S2 (D) inputs. No plasticity was induced after paring of two inputs at 500 ms time window. Data displayed as mean ±SEM. n.s.: not significant.

5.4. Discussion

The experiments of this chapter aimed to test whether STDP changes would show specificity of plasticity in the case of multiple inputs to the same postsynaptic cell. The results showed that specificity of plasticity in dSPNs depended on the timing of inputs relative to firing even when there were two different inputs to the single postsynaptic neuron. However, the relative timing of inputs was not the only factor determining the direction and extent of synaptic plasticity; the input summation linearity was also a factor. Cells with linear summation of two input signals showed pre-post LTD. On the other hand, cells with nonlinearly summating inputs showed the opposite profile, in that no plasticity was observed after pre-post pairing and Hebbian LTD occured after post-pre pairing. A surprising finding was that pairing two contiguous inputs without postsynaptic spikes also induced robust LTD, but with a different profile from 2-input STDP. In particular, cells with linearly summating inputs showed LTD in the later input, while cells with non-linearly summating inputs showed LTD in both inputs. The type of postsynaptic neuron was also a powerful determinant of STDP: the plasticity described occurred only in dSPNs, and none of the current protocols induced plasticity in iSPNs.

The STDP seen with two inputs to a single cell was similar to that seen with a single input, in the case of linear summation of the inputs. In this linear case, LTD occurred in the input that was exposed to pre-post stimulation, the same as when only one input to a cell is tested (Fino et al., 2005; Paille et al., 2013; Shindou et al., 2011, 2019). Thus, the STDP was not altered by the occurrence of subsequent input at post-pre timing. It appears that in the linear summation case, the plasticity signal was independently processed for separate inputs to the same cell. This implies that the cells were able to respond to two plasticity signals with different relative timing, provided the inputs are independent.

On the other hand, when tested with two inputs, cells with nonlinearly summating inputs showed a different plasticity profile from cells tested with only one input. In the case of both sublinear and supralinear summation, no plasticity was induced by pre-post pairing, and LTD was caused by a later input at post-pre timing. These results contrast strongly with what has been observed when only one input is tested: namely LTD after pre-post pairing and no change after post-pre pairing (Shindou et al., 2011, 2019). Possible explanations for this difference will be considered in the General discussion (Chapter 7).

STDP experiments with interactions of two inputs served as a simplified model of learning in the brain, which needs to tackle both spatial and temporal credit assignment. The brain needs to select the most relevant features while ignoring the irrelevant features (a kind of spatial specificity), but it also needs to assign values for actions that finish before the reward arrival (temporal specificity). Such function of selecting relevant stimuli seems to occur in the PFC and interactions between the PFC subregions (Stolyarova, 2018). The current experiments stimulated multiple sites of the PFC axons projecting to the DMS, and their temporal differences relative to SPN firing were indeed reflected as differences in plasticity.

Corticostriatal STDP is known to be dopamine dependent (Pawlak & Kerr, 2008; Shen et al., 2008). However, when the 2-input STDP protocol was applied in the presence of a dopamine agonist, together with an L-VGCC blocker to block LTD, no LTP was observed, in contrast to an earlier result with single input (Shindou et al., 2019). The combination of 2-input appeared to have the effect that a global increase in basal dopamine level by bath application of a D1 agonist during pairing was not sufficient to induce LTP. This may be related to the previously described eligibility trace, that is induced by and persists after pairing of synaptic events and enables dopamine effects on plasticity. Based on these findings, in the next chapter (Chapter 6), the effect of having two inputs on the eligibility

trace will be tested, using optogenetic methods to control precise and endogenous release of dopamine. Since no plasticity was observed in iSPNs with the current protocols, in Chapter 6, synaptic plasticity is only investigated in dSPNs.

Chapter 6. Dopamine retroactively modulates plasticity of two different inputs

"Just that," said the fox. "To me, you are still nothing more than a little boy
who is just like a hundred thousand other little boys.
And I have no need of you.
And you, on your part, have no need of me.
To you, I am nothing more than a fox like a hundred thousand other foxes.
But if you tame me, then we shall need each other.
To me, you will be unique in all the world.
To you, I shall be unique in all the world . . ."
– Antoine de Saint-Exupery, The Little Prince (1943)

6.1. Introduction

In Chapter 5, a 2-input STDP protocol was found to induce different plasticity profiles (LTD or no plasticity) depending on the timing of the inputs relative to firing of the postsynaptic neuron (pre-post or post-pre). In the present chapter, I tested whether multiple synaptic inputs will be modulated differentially by dopamine, depending on their relative timing. These experiments address a possible link between the so-called "eligibility trace" and STDP.

The eligibility trace hypothesis was proposed as a solution to the distal reward problem, the temporal gap between the neural activity that led to a reward, and the release of dopamine upon obtaining the reward. This problem was originally formulated as a criticism of Thorndike's "Law of Effect", which implied retroactive working of the effect (Waters, 1934). However, recent studies have shown that such retroactive effects occur in dopamine-dependent STDP. For example, pre-post pairing that normally produces t-LTD, resulted in t-LTP if dopamine was applied two seconds after the pairing (Shindou et al., 2019). Other experiments, however, showed that pairing of glutamate uncaging and postsynaptic spikes produced t-LTP only when dopamine was released during the pairing (Yagishita et al., 2014) (Chapter 2, Fig.2.5). In the cortex, He et al. (2015) showed that the retroactive application of distinct neuromodulators differentially modulates specific time points for STDP induction. The forgoing experiments have focused on the retroactive effects of the neuromodulators: there is a need to understand the timing requirements for induction of the eligibility trace.

In this chapter, interactions of dopamine and multiple synaptic inputs were investigated using electrochemical, electrophysiological and optogenetic approaches in dSPNs in the DMS. Firstly, dopamine release by optical stimulation was measured by fast scan cyclic voltammetry and its immediate effects on EPSP amplitudes was tested. Secondly, to test whether optogenetic application of dopamine could reproduce the results with UV uncaging (Shindou et al., 2019), pre-post pairing STDP protocol (one presynaptic stimulation, 60 times at 0.1 Hz) was followed by optogenetic application of dopamine two sec. after each pairing. Thirdly, the optical stimulation protocol was also applied during post-pre pairing protocol to test whether dopamine can retroactively modulate STDP by post-pre pairing. Fourthly, optogenetically controlled dopamine release was tested in the 2-input STDP protocol. Finally, effects of temporally controlled release of dopamine on associative STDP protocol with two conditioning inputs in the absence of postsynaptic spikes were investigated.

6.2. Methods

Methods including generation of triple transgenic animals, slice preparation, fast scan cyclic voltammetry (FSCV) for dopamine detection, optical stimulation protocol, and STDP protocol with temporally controlled dopamine release are described in detail in Chapter 3.

6.3. Results

For FSCV, data from 18 animals were used for analysis. For plasticity experiments, data obtained from 59 cells from 53 animals that met the aforementioned inclusion criteria were used for analysis. List of STDP experiments done in this chapter is summarized in Table 6.1. For both FSCV and electrophysiology, cells were visually identified under the microscope as a dSPN by the presence of red fluorescence during recording. With whole-cell recordings, cells were electrophysiologically confirmed as SPNs by their long latency before a first spike and inward rectification.

Table 6.1. List of experiments with the number of cells in each condition.

List of experiments	# of cells	Figure #
pre-post STDP + optoDA	**12**	6.3.
post-pre STDP + optoDA	**6**	6.4.
2-input STDP + opto DA	**21**	6.8.
sublinear	10	6.6.
linear	5	6.5.
supralinear	6	6.7.
associative STDP + optoDA	**20**	6.12.
sublinear	9	6.10.
linear	7	6.9.
supralinear	4	6.11.
total # of cells	**59**	

6.3.1. Verification of dopamine release upon optical stimulation

After calibrating the CFE (Fig.6.1A-C), the concentration of dopamine was measured with FSCV using the same stimulation protocol for STDP experiment (2x 10 ms pulses at 20 Hz, repeated at 0.1 Hz, Fig. 6.1D&E). Sufficiently measurable amount of dopamine was released by the stimulation throughout the visual field, with slight gradient from the right to left (Fig. 6.1F). In addition, to confirm that only optical stimulation releases dopamine, dopamine release was measured upon electrical and optical stimulation. Electrical simulation within the striatum at theta frequency (Shen et al., 2008) was shown to induce measurable dopamine release, while cortical stimulation with a bipolar electrode did not cause dopamine release in the striatum (Shindou et al., 2019). Using the same pairing protocol (60 times at 0.1 Hz) as STDP experiments, no measurable dopamine was observed after cortical stimulation with two sets of bipolar electrodes with different stimulus intensities (200 – 800 μA) (Fig.6.1H). Upon optical stimulation, however, dopamine was released at the concentration of $[DA]_{peak}$ = 112.3 ± 16.5 nM (n = 9). When cortical stimulation was combined with optical stimulation it resulted in a similar peak of dopamine concentration ($[DA]_{peak}$ = 134.2 ± 22.7 nM, n = 9). In order to confirm that it was dopamine, DAT blocker methylphenidate (MPH, 10 μM) was bath applied during optical stimulation. During 5 min. of MPH application, $[DA]_{peak}$ was doubled (217.7 ± 44.8 nM, n = 9) from the baseline. This significant increase ($t_{(8)}$ = 3.43, p = 0.009) was irreversible after 10 min of wash (MPH vs. wash, $t_{(7)}$ = 1.978, p = 0.088; Fig.6.1I).

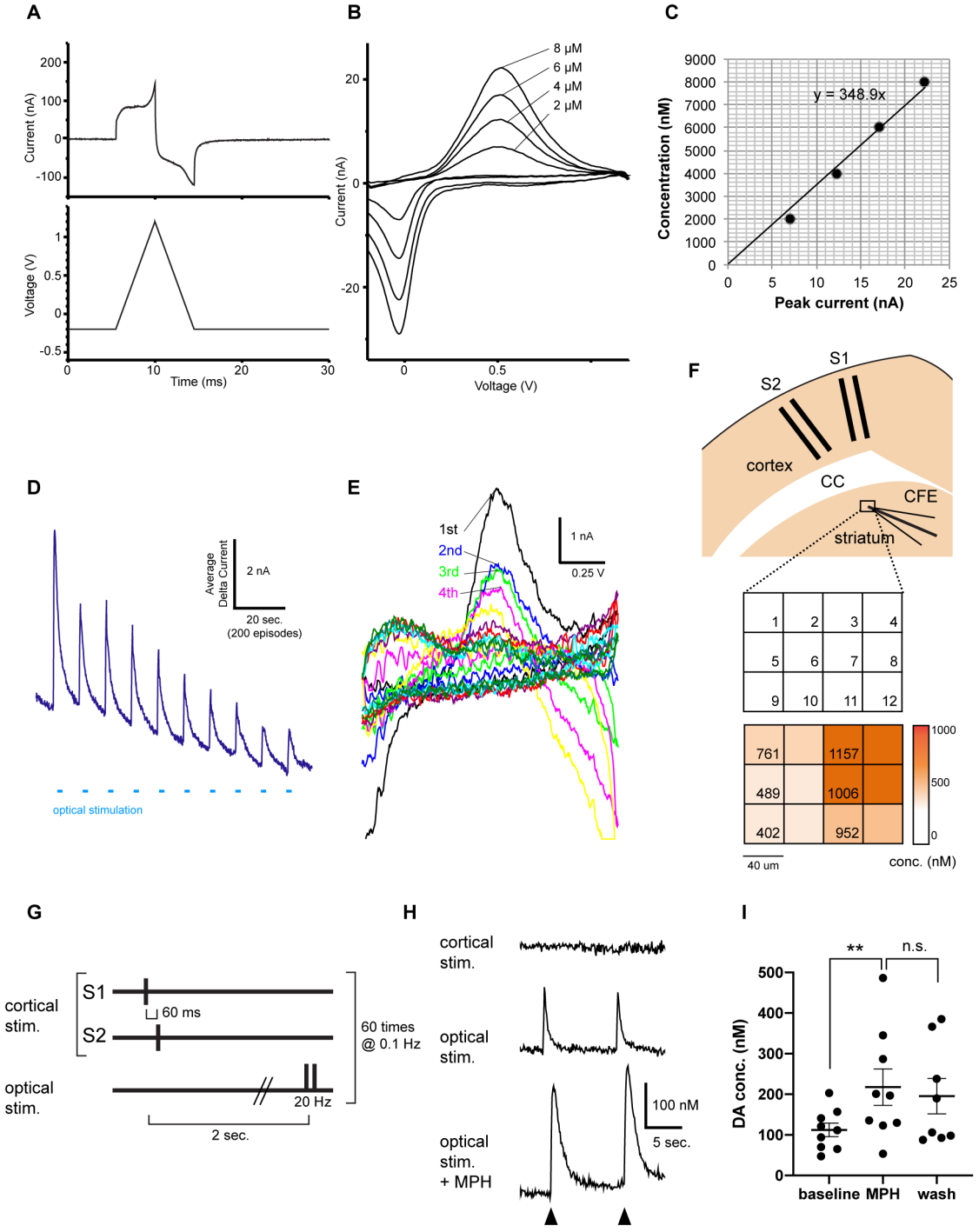

Figure 6.1. Confirmation of dopamine release by optical stimulation using fast scan cyclic voltammetry. (A) Current response (nA) to voltage applied (from -0.2 V to 1.2 V) to carbon fiber electrode (CFE) inserted in the striatum. (B) Voltammogram response to known dopamine concentration (in 2 μM increments) to calibrate glass CFE. (C) Peak current and concentration were plotted to estimate dopamine concentration from the measurements. (D) Optical dopamine release measured at 0.1 Hz for 10 times. (E) Voltammogram showing the dopamine response to optical stimulation. (F) Schematic diagram showing the location of bipolar electrodes (S1 & S2) and the placement of CFE. Rectangle indicates area of stimulation under the CCD camera. Heatmap showing the concentration (in nM) measured at each subarea to visualize spatial distribution of dopamine under optical stimulation. (G) Cortical and optical stimulation protocol. Cortical stimulation with two sets of bipolar electrodes (S1 & S2) was applied with 60 ms interval, followed by optical stimulation of 2x 10 ms pulse at 20 Hz 2 sec. later, repeated 60 times at 0.1 Hz. (H) Sample traces

(Figure 6.1 continued) of cortical, optical, optical + MPH stimulation. Black triangles indicate light flash. (I) Dopamine concentration (nM) of the baseline, MPH application, and after wash. Each dot indicates individual values, lines indicate mean ± SEM. **: $p<0.01$, n.s.: not significant.

6.3.2. Excitatory postsynaptic potentials (EPSPs) upon optogenetic dopamine release

To exclude the possibility that optical dopamine release would have an immediate effect on synaptic potentials, EPSPs were measured during optical stimulation. Firstly, EPSPs were measured for 10 times at 0.05 Hz without optical stimulation, and the same cell was stimulated with the same intensity, but with concomitant optical stimulation (twice at 20 Hz) for 10 times at 0.05 Hz (n = 3). In other cases, EPSPs were measured every 500 ms for 6 times, and optical stimulation was given only at odd stimulation (1st, 3rd, 5th), and not at even stimulation (2nd, 4th, 6th), repeated 10 times at 0.05 Hz. EPSP size with or without optical stimulation was then compared (n = 3). When compared together (n = 6), the mean EPSP was 2.18 ± 0.76 mV without dopamine (control), and 2.30 ± 0.74 mV with optical dopamine release (+ opto). There was no significant difference between the mean EPSP with or without optical stimulation ($t_{(5)}$ = 0.81, p = 0.453, paired-sample t-test; Fig.6.2). The results suggest no immediate effect of dopamine on the size of synaptic potentials.

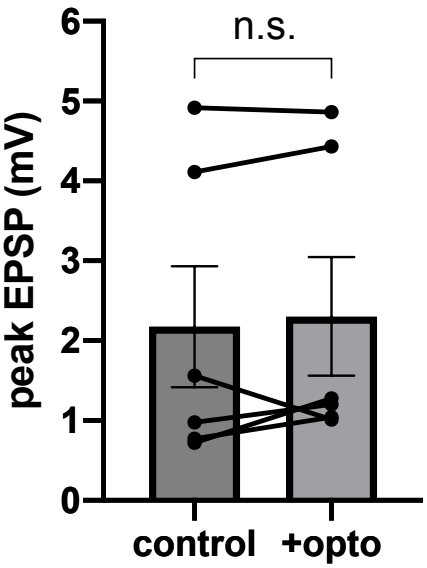

Figure 6.2. Effect of optical dopamine release on EPSP amplitudes. Each dot indicates individual values in control (without optical dopamine release) and with optical dopamine release (+ opto). Bars indicate the mean peak EPSP ± SEM (mV). n.s.: not significant.

6.3.3. Pre-post pairing with optogenetic dopamine release showed a mixed profile

For STDP experiments, I first tested pre-post pairing followed by optogenetic release of dopamine two sec. after pairing. Previous studies with similar paradigms have shown mixed results. Yagishita et al. (2014) showed no effect of optogenetically induced dopamine release when applied two sec. after pairing, and a potentiating effect when applied during pairing. In contrast, Shindou et al (2019) showed a potentiating effect of uncaging dopamine two sec. after pairing, but not when uncaging during pairing. In the present study, optogenetic release of dopamine two sec. after pairing caused a mixed profile (Fig.6.3). In three cases (25 %), an increase in normalized EPSP was observed (133.5 ± 21.7 %, Fig.6.3B), while nine cases showed a decrease in normalized EPSP (63.1 ± 3.7 %, Fig.6.3C). Overall (n = 12), there was no significant change in EPSPs after pairing (normalized EPSP was 80.7 ± 10.7 % of the baseline, $t_{(11)} = 1.81$, $p = 0.098$, n.s.), with mean EPSP showing a non-significant decrease from 2.6 ± 0.4 mV to 1.9 ± 0.2 mV.

Dopamine transporter (DAT)-Cre mice may have increased DAT activity, resulting in a decrease in available dopamine level (Chouinard & Wickens, personal communication). Hence, to boost up the amount of available dopamine, 10 μM MPH was applied during pairing of pre-post STDP experiments with delayed optogenetic dopamine release (n = 2). There was an increase in S1 EPSP in one cell (123.0 %), and no change in another (86.3 %), with the mean normalized EPSP of 104.6 ± 18.3% (data not shown). Although the sample size is too small to draw a conclusion, even in the presence of MPH, a mixed plasticity profile was still observed.

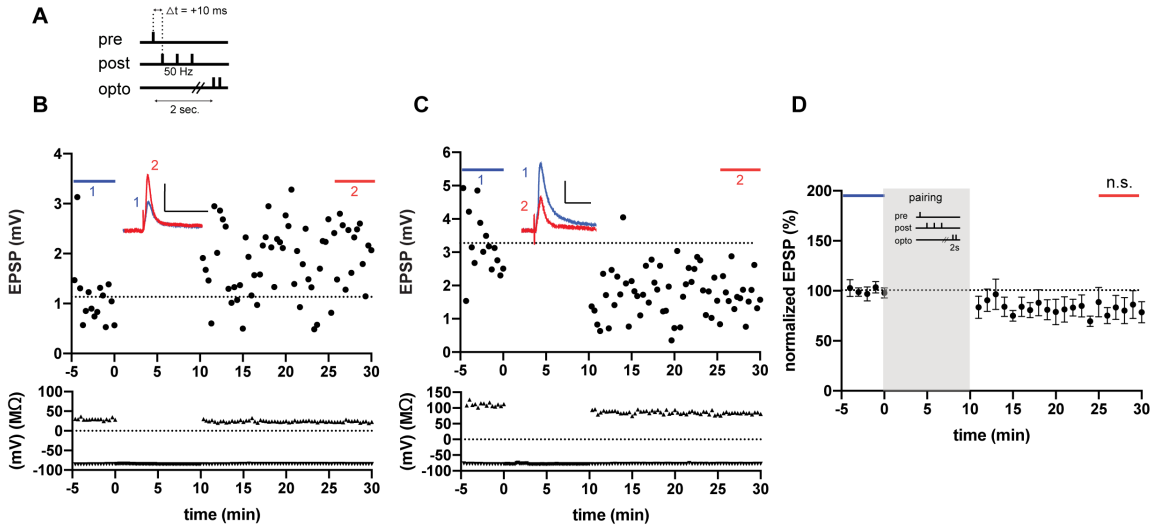

Figure 6.3. Pre-post pairing STDP with optogenetic dopamine release. (A) Schematic diagram of the experimental protocol. (B, C) Two representative examples of changes in EPSP amplitude (mV, filled circles, top), input resistance (Ri, MΩ, upright triangles, middle), and resting membrane potential (RMP, mV, downward triangles, bottom). Sample traces show averages of EPSP over 5 min. before (blue, 1) pairing and after (red, 2) pairing. Scale bars = 1 mV (vertical) and 50 ms (horizontal). Dotted line indicates the baseline EPSP. (C) Group averages (n = 12) of normalized EPSPs. Overall, after pre-post pairing followed by optogenetic dopamine release, not plasticity was observed. Data displayed as mean over 1 min. ± SEM. n.s.: not significant.

6.3.4. Post-pre pairing with optogenetic dopamine release caused robust LTD

Although it seems reasonable that pre-post pairing should cause an eligibility trace, it is also possible that post-pre pairing could cause eligibility. To test this possibility, optogenetically controlled release of dopamine was combined with post-pre pairing. When dopamine was applied optogenetically two seconds after each post-pre pairing, a significant decrease in normalized EPSP was observed (69.1 ± 4.3 % of the baseline, n = 6), indicating a robust LTD ($t_{(5)} = 7.12$, $p = 0.001$; Fig.6.4). EPSP before pairing was 2.8 ± 0.4 mV, which was reduced to 1.9 ± 0.3 mV after pairing. Previously, Shindou et al. (2019) showed that post-pre pairing induced no plasticity in dSPNs or iSPNs, without dopamine release (Shindou et al., 2019). The current results suggest that an eligibility trace for dopamine-dependent LTD was turned on by post-pre pairing.

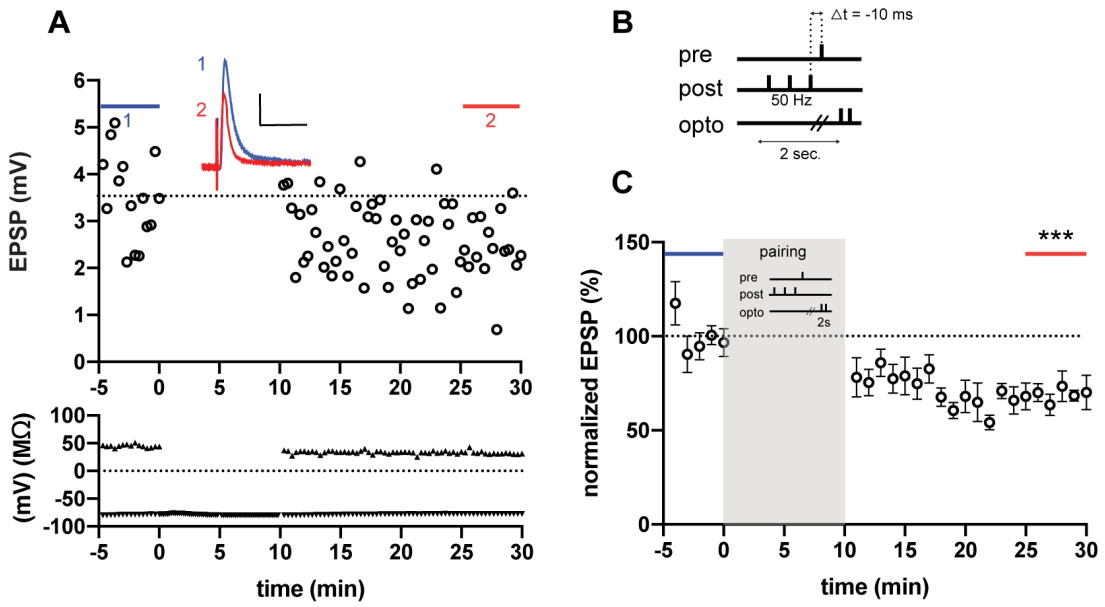

Figure 6.4. Post-pre pairing STDP with optogenetic dopamine release. (A) Representative examples of changes in EPSP amplitude (mV), Ri (MΩ), and RMP (mV). Sample traces show averages of EPSP over 5 min. before (blue, 1) pairing and after (red, 2) pairing. Scale bars = 1 mV (vertical) and 50 ms (horizontal). Dotted line indicates the baseline EPSP. (B) Schematic diagram of the experimental protocol. (C) Group averages (n = 6) of normalized EPSPs. After post-pre pairing followed by optogenetic dopamine release, LTD was induced. Data displayed as mean over 1 min. ± SEM. ***: $p < 0.001$.

6.3.5. Two-input STDP with optogenetic dopamine release showed a mixed profile

The results reported so far show that when separately tested, pre-post pairing causes both LTP and LTD, whereas post-pre pairing causes a robust LTD. Theoretically, if two inputs are independent, dopamine would differentially modify each input and similar plasticity profiles should be observed in each input depending on the timing (LTP & LTD for pre-post pairing, and LTD for post-pre pairing). To test this, the effects of retroactive application of dopamine on two different inputs (S1 & S2) were investigated using the 2-input STDP protocol.

When the 2-input STDP protocol was combined with retroactive application of dopamine, the effect was different from when pre-post and post-pre STDP protocols were applied separately (Fig.6.5A). As in Chapter 5, the independence of the two inputs was tested, with some showing linear summation, and others showing sublinear or supralinear summation. These cases were analyzed separately. In the case of linear summation (n = 5), there was a significant decrease in S1 EPSP, 56.3 ± 10.6 % of the baseline ($t_{(4)} = 4.13$, $p = 0.028$) after pre-post pairing (Fig.6.5B, C). Mean S1 EPSP decreased from 4.3 ± 0.7 mV to 2.2 ± 0.3 mV. On the other hand, after post-pre pairing, there was a decreasing trend (normalized EPSP reduced to 63.1 ± 11.0 %), but it was not significant ($t_{(4)} = 3.35$, $p = 0.056$; Fig.6.5B, D). Mean S2 EPSP before pairing was 4.2 ± 1.1 mV and 2.6 ± 0.7 mV after pairing.

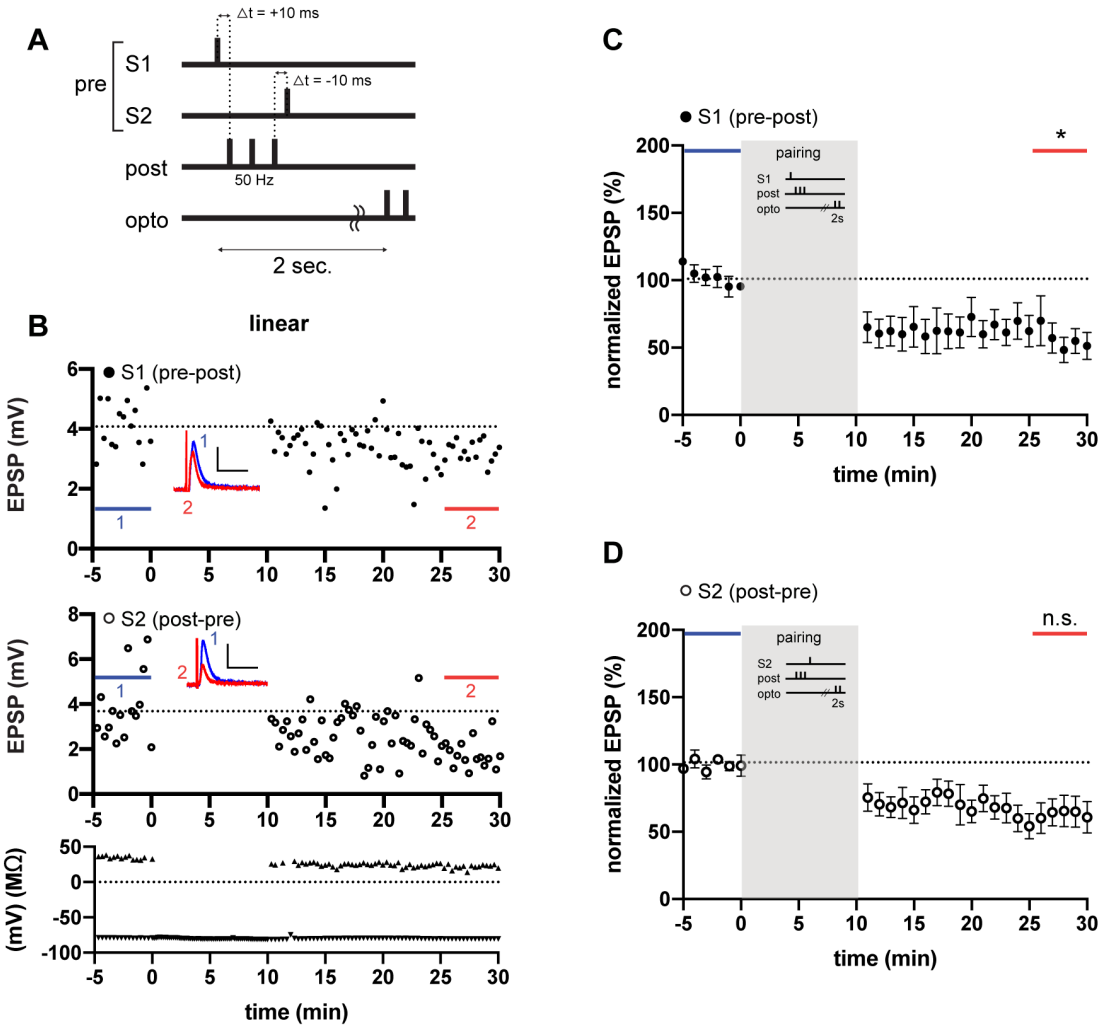

Figure 6.5. Two-input STDP with optogenetic dopamine release in cells with linearly summating inputs. (A) Experimental protocol. S1 came at pre-post timing (t = +10 ms), and S2 at post-pre timing (t = -10 ms), relative to postsynaptic action potential triplets (50Hz, post). Blue light was flashed (2 times at 20 Hz) two seconds after the beginning of pairing to release dopamine (opto). (B) Representative examples of changes in S1 EPSP amplitude (mV), S2 EPSP amplitude (mV), Ri (MΩ), and RMP (mV). Sample traces show averages of EPSP over 5 min. before (blue, 1) pairing and after (red, 2) pairing. Scale bars = 2 mV (vertical) and 40 ms (horizontal). (C, D) Group averages (n = 5) of (C) S1 and (D) S2 normalized EPSPs, in which each dot indicates the mean normalized EPSPs over 1 min. ± SEM. In cells with linearly summating inputs, LTD was induced after pre-post pairing, but not after post-pre pairing, when followed by dopamine release. *: $p < 0.05$, n.s.: not significant.

Separate analysis on the cases of inputs with sublinear or supralinear summation revealed no overall plasticity. However, this was not due to lack of plasticity, but due to their huge variability. From the sublinear summation group, one cell showed pre-post LTD and post-pre LTP (Fig.6.6A). Another cell showed LTP after both pre-post and post-pre pairing (Fig.6.6B). The other eight cells showed an overall decrease (Fig.6.6C). Taken together, in cells with sublinearly summating inputs (n = 10), S1 EPSP showed a non-significant decrease (82.5 ± 8.0 %, $t_{(9)} = 2.17$, $p = 0.116$; Fig.6.6). Mean S1 EPSP before pairing was 3.6 ± 0.7 mV, and 2.9 ± 0.5 mV after pairing. S2 EPSP change was also not significant ($t_{(9)} = 1.52$, $p = 0.324$), with normalized EPSP changed to 83.8 ± 10.7 % of the baseline. Mean S2 EPSP reduced from 2.9 ± 0.4 mV to 2.4 ± 0.5 mV.

In the case of supralinear summation, one cell showed pre-post LTD and post-pre LTP (Fig.6.7A). Another cell showed pre-post LTP and post-pre LTD (Fig.6.7B). The other four cells showed an overall decrease (Fig.6.7C). When statistically analyzed together, cells with supralinearly summating inputs (n = 6) showed no overall plasticity. S1 EPSP showed a non-significant decrease to 77.2 ± 13.4 % of the baseline ($t_{(5)} = 1.71$, $p = 0.298$; Fig.6.7). Mean S1 EPSP was 2.3 ± 0.4 mV before, and 1.9 ± 0.6 mV after. S2 EPSP also showed a non-significant decrease to 87.8 ± 7.4 % of the baseline ($t_{(5)} = 1.64$, $p = 0.326$). Mean S2 EPSP was 1.8 ± 0.4 mV before and 1.5 ± 0.3 mV after. This suggests that interaction of synaptic inputs introduced another variable, in addition to the timing of pre and postsynaptic spikes and dopamine release, that changes the direction of synaptic plasticity.

Overall, in all the dSPNs tested (n = 21), significant LTD was observed after both pre-post and post-pre pairing. After pre-post pairing (S1, Fig.6.8 left), normalized EPSP was reduced to 74.8 ± 6.1 % ($t_{(20)} = 4.12$, $p = 0.002$). Mean S1 EPSP was 3.4 ± 0.4 mV before, and 2.4 ± 0.3 mV after pairing. After post-pre pairing (S2, Fig.6.8 right), normalized EPSP was also significantly reduced to 80.0 ± 6.2 % ($t_{(20)} = 3.21$, $p = 0.008$). Mean S2 EPSP was reduced from 2.9 ± 0.4 mV to 2.2 ± 0.3 mV.

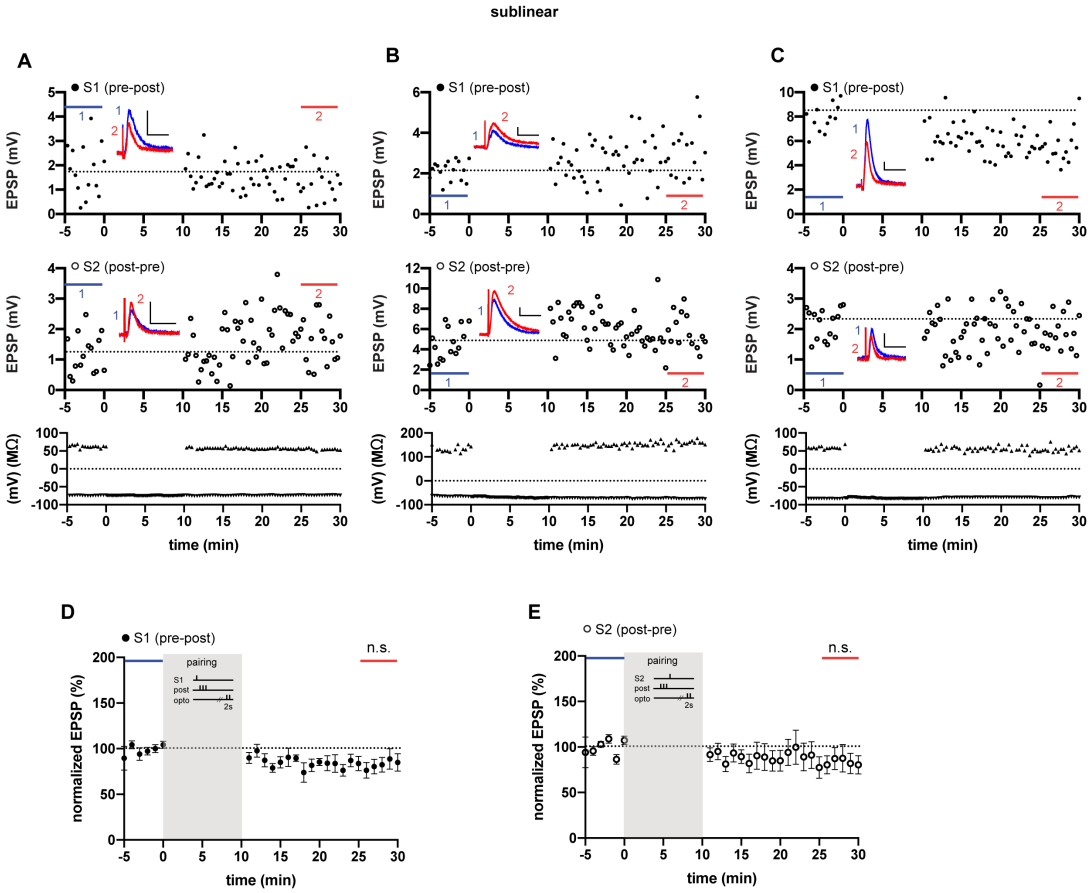

Figure 6.6. Two-input STDP with optogenetic dopamine release in cells with sublinearly summating inputs. (A, B, C) Three representative examples of changes in S1 EPSP amplitude (mV), S2 EPSP amplitude (mV), Ri (MΩ), and RMP (mV). Sample traces show averages of EPSP over 5 min. before (blue, 1) pairing and after (red, 2) pairing. Scale bars = 1 mV (vertical) and 50 ms (horizontal). (D, E) Group averages (n = 10) of (D) S1 and (E) S2 normalized EPSPs, in which each dot indicates the mean normalized EPSPs over 1 min. period ± SEM. In cells with sublinearly summating inputs, no plasticity was induced after pre-post or post-pre pairing, when followed by dopamine release. n.s.: not significant.

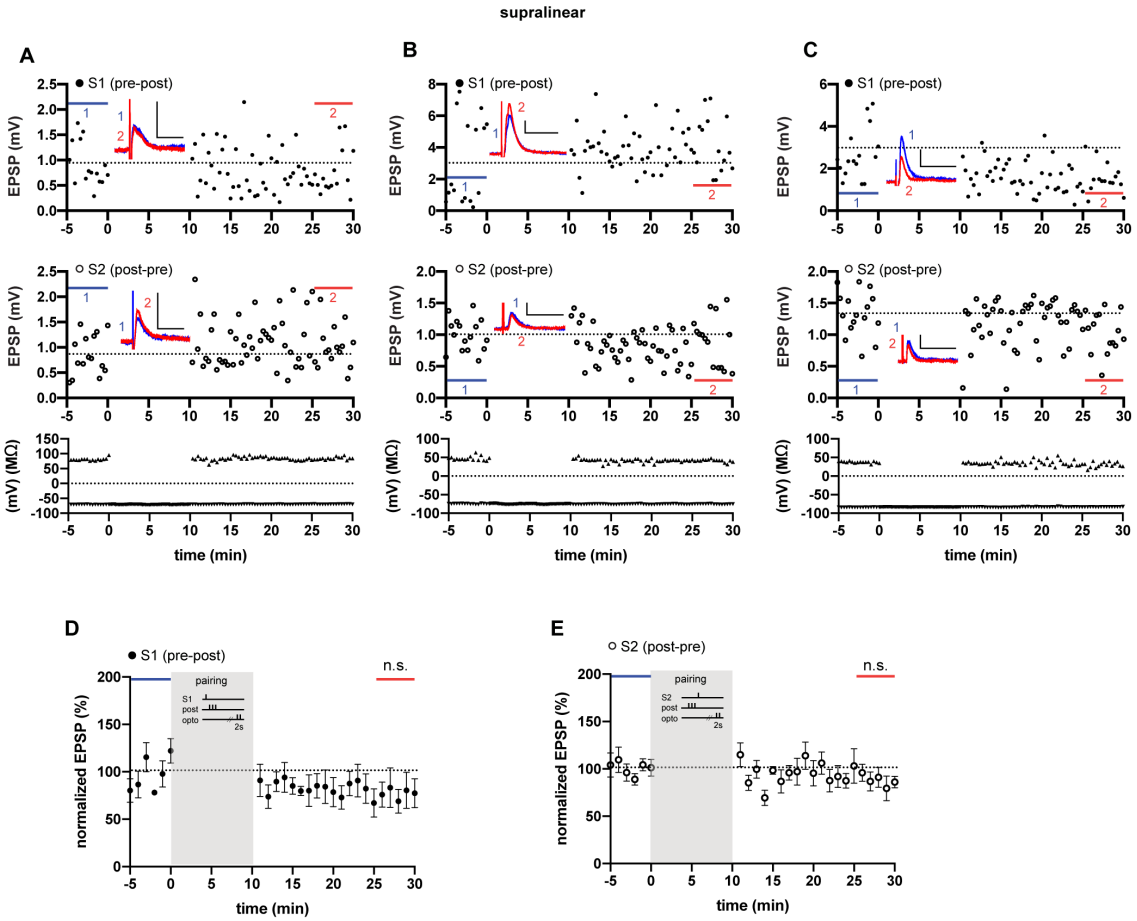

Figure 6.7. Two-input STDP with optogenetic dopamine release in cells with supralinearly summating inputs. (A, B, C) Three representative examples of changes in S1 EPSP amplitude (mV), S2 EPSP amplitude (mV), Ri (MΩ), and RMP (mV). Sample traces show averages of EPSP over 5 min. before (blue, 1) pairing and after (red, 2) pairing. Scale bars = 1 mV (vertical) and 50 ms (horizontal). (D, E) Group averages (n = 6) of (D) S1 and (E) S2 normalized EPSPs, in which each dot indicates the mean normalized EPSPs over 1 min. period ± SEM. In cells with supralinearly summating inputs, no plasticity was induced after pre-post or post-pre pairing, when followed by dopamine release. n.s.: not significant.

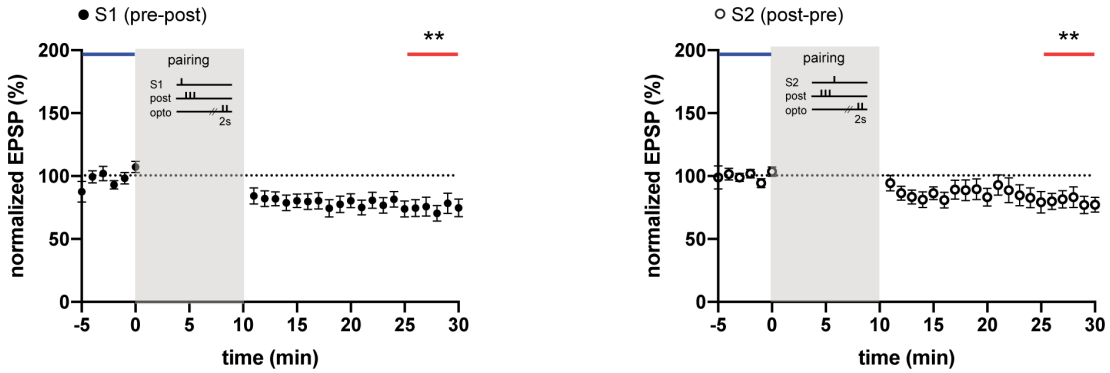

Figure 6.8. Two-input STDP with optogenetic dopamine release. Averages over all dSPNs (n = 21) of normalized EPSPs in S1 input (pre-post timing, left) and S2 input (post-pre timing, right). Data displayed as the mean over 1 min. ± SEM. When all the inputs were analyzed together LTD was observed after both pre-post and post-pre pairing. **: $p < 0.01$.

6.3.6. Pairing of two inputs without postsynaptic spikes with optogenetic dopamine release showed mixed profiles

As described in Chapter 5, pairing two inputs in the absence of spiking activity resulted in robust LTD, a different plasticity profile from the results of 2-input STDP. This was referred to as associative STDP. In the present experiment, associative STDP was investigated in the presence of temporally controlled release of dopamine. As before, the input interactions were categorized as linear, supralinear and sublinear and analyzed separately.

In the case of linear summation (n = 7) with optogenetic dopamine release, a significant decrease in normalized S1 EPSP was observed (66.7 ± 7.5 % of the baseline, $t_{(6)}$ = 4.43, p = 0.008, Fig.6.9). Mean S1 EPSP was reduced from 6.4 ± 1.0 mV to 4.3 ± 0.8 mV. On the other hand, S2 EPSP remained unchanged (100.7 ± 33.6 %, $t_{(6)}$ = 0.02, p = 0.984). Mean S2 EPSP before pairing was 3.6 ± 0.6 mV and 3.1 ± 0.7 mV after pairing. However, this lack of plasticity was also due to high variability. One example showed over 300% increase in S2 EPSP (Fig. 6.9B), whereas other cells showed decreasing trends (Fig. 6.9C).

In contrast to the associative LTD seen in non-linearly summating inputs (both sublinear and supralinear) in the absence of dopamine, with optogenetic dopamine release, differences in plasticity were observed between cells that had sublinearly and supralinearly summating inputs. From the sublinear summation group (n = 9), both S1 and S2 EPSP showed robust LTD (Fig.6.10). S1 EPSP showed a significant decrease (60.8 ± 4.5 %, $t_{(8)}$ = 8.74, p = 0.000046). Mean S1 EPSP was reduced 4.0 ± 0.5 mV to 2.4 ± 0.3mV. S2 EPSP also showed a significant decrease ($t_{(8)}$ = 11.62, p = 0.000006), with normalized EPSP reduced to 59.5 ± 3.5 % of the baseline. Mean S2 EPSP was reduced from 2.8 ± 0.4 mV to 1.6 ± 0.2 mV. In the case of supralinear summation, two cells (50%) showed an LTP in S1 input (S1 normalized EPSP was 118.9 ± 2.3 % of the baseline; Fig.6.11A), while the other two (50%) showed an LTD in S1 input (S1 normalized EPSP was 71.4 ± 11.3 % of the baseline; Fig.6.11B). Due to this huge variability, in the case of supralinear summation (n = 4), the change was not statistically significant (Fig.6.11). S1 EPSP remained unchanged (95.2 ± 14.5 % of the baseline, $t_{(3)}$ = 0.33, p = 0.761). Mean S1 EPSP was 4.7 ± 0.8 mV before, and 4.7 ± 1.3 mV after pairing. S2 EPSP also showed a non-significant decrease to 74.6 ± 10.6 % of the baseline ($t_{(3)}$ = 2.41, p = 0.095). Mean S2 EPSP was 3.5 ± 0.9 mV before and 2.7 ± 0.9 mV after.

Overall (n = 20), significant LTD was observed in S1 EPSP (normalized EPSP reduced to 69.8 ± 5.1 %, $t_{(19)}$ = 5.98, p = 0.000018; Fig.6.12 left), mean EPSP was reduced from 5.0 ± 0.5 mV to 3.5 ± 0.5 mV. S2 EPSP also showed a decrease (Fig.6.12 right), but it was not statistically significant (76.9 ± 12.2 %, $t_{(19)}$ = 1.90, p = 0.146). Mean S2 EPSP was reduced from 3.2 ± 0.3 mV to 2.4 ± 0.3 mV.

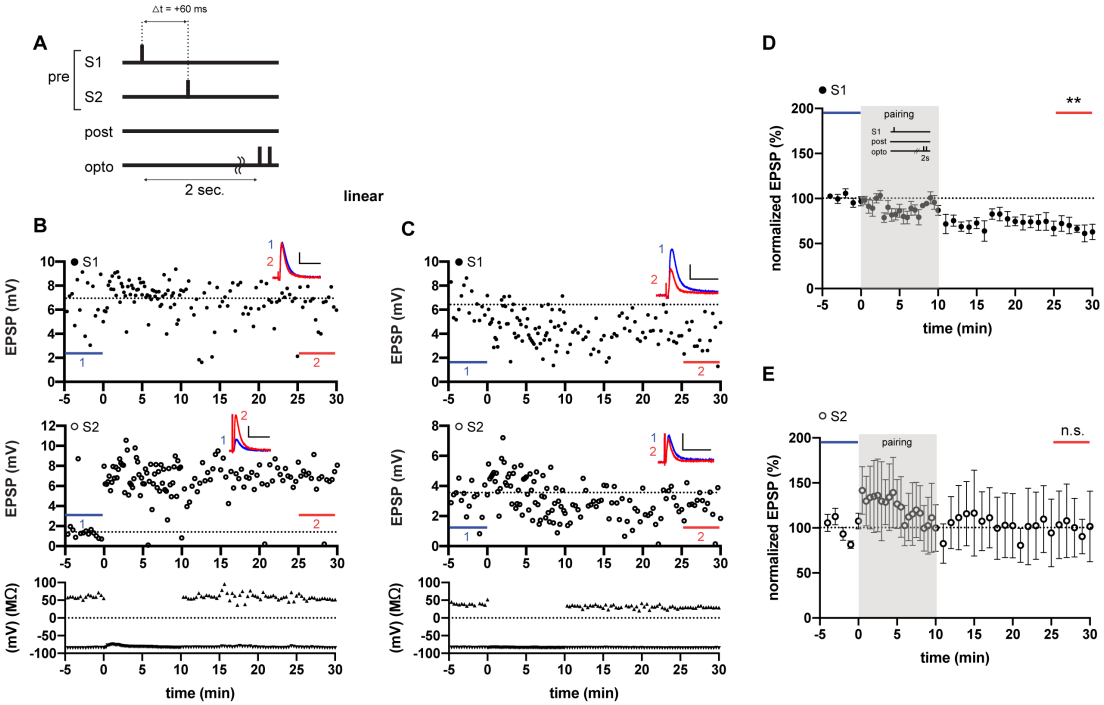

Figure 6.9. Associative STDP with optogenetic dopamine release in cells with linearly summating inputs. (A) Experimental protocol. S1 and S2 EPSPs were paired at a 60 ms interval without pairing with postsynaptic spikes (post). Blue light was flushed (2 times at 20 Hz) two seconds after the beginning of pairing to release dopamine (opto). In dSPNs that showed linear summation of two inputs, (B, C) Two representative examples of result showing S1 and S2 EPSP amplitude (mV), Ri (MΩ), and RMP (mV). Sample traces show averages of EPSP over 5 min. before (blue, 1) pairing and after (red, 2) pairing. Scale bars = 2 mV (vertical) and 50 ms (horizontal). (D, E) Group averages (n = 7) of (D) S1 and (E) S2 normalized EPSPs, in which each dot indicates the mean normalized EPSPs over 1 min. ± SEM. In cells with linearly summating inputs, pairing two presynaptic inputs followed by dopamine release caused LTD in S1 but no change in S2. **: $p < 0.01$, n.s.: not significant.

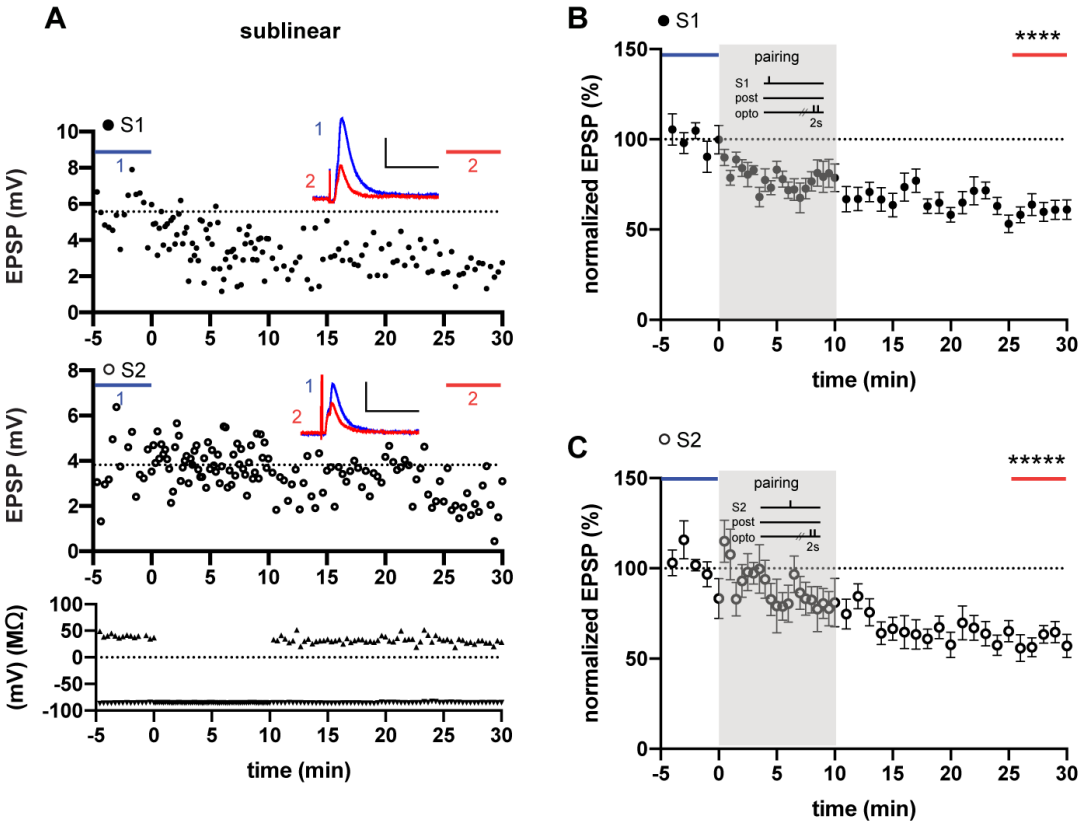

Figure 6.10. Associative STDP with optogenetic dopamine release in cells with sublinearly summating inputs. (A) representative example of sublinear summation category. Graphs show S1 and S2 EPSP amplitude (mV), Ri (MΩ), and RMP (mV). Sample traces show averages of EPSP over 5 min. before (blue, 1) pairing and after (red, 2) pairing. Scale bars = 2 mV (vertical) and 50 ms (horizontal). (B, C) Group averages (n = 9) of (B) S1 and (C) S2 normalized EPSPs, in which each dot indicates the mean normalized EPSPs over 1 min. ± SEM. In cells with sublinearly summating inputs, pairing two presynaptic inputs followed by dopamine release caused LTD in both S1 and S2 inputs. ****: $p < 0.0001$, *****: $p < 0.00001$.

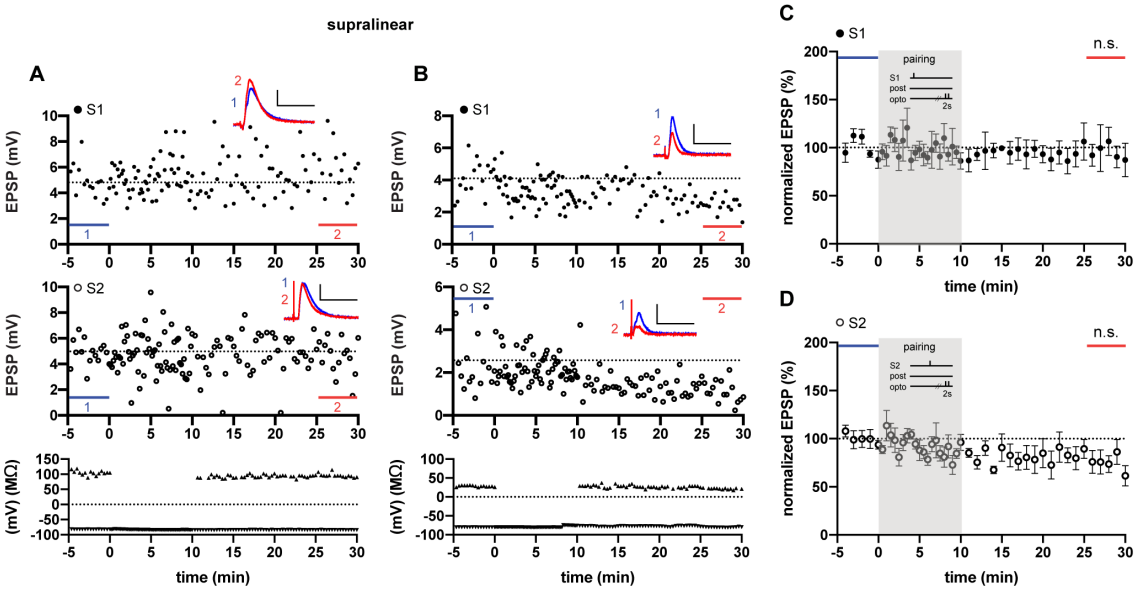

Figure 6.11. Associative STDP with optogenetic dopamine release in cells with supralinearly summating inputs. (A, B) Two representative examples of results that showed supralinear summation. Graphs show S1 and S2 EPSP amplitude (mV), Ri (MΩ), and RMP (mV). Sample traces show averages of EPSP over 5 min. before (blue, 1) pairing and after (red, 2) pairing. Scale bars = 2 mV (vertical) and 50 ms (horizontal). (C, D) Group averages (n = 4) of (C) S1 and (D) S2 normalized EPSPs, in which each dot indicates the mean normalized EPSPs over 1 min. ± SEM. In cells with supralinearly summating inputs, pairing two presynaptic inputs followed by dopamine release caused no significant change. n.s. : not significant.

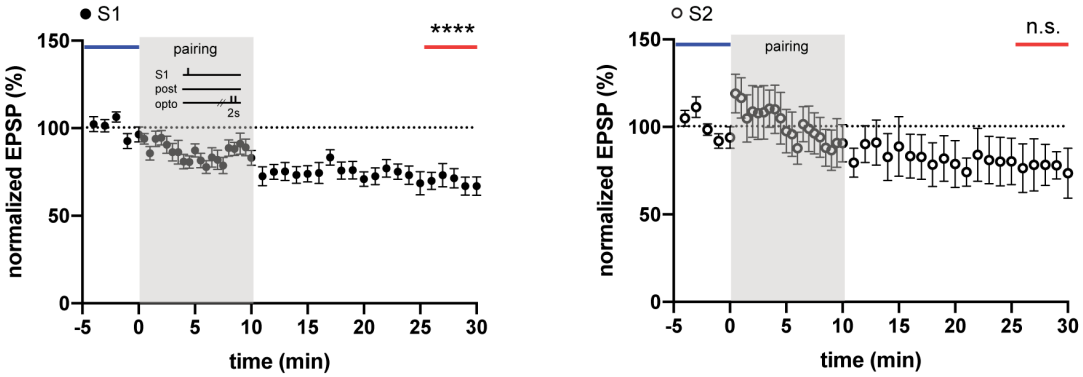

Figure 6.12. Associative STDP with optogenetic dopamine release. (A) Averages over all dSPNs (n = 20) of normalized EPSPs in S1 input (left) and S2 input (right). Data displayed as mean over 1 min. ± SEM. When all dSPNs were analyzed together, pairing two inputs followed by dopamine release cause LTD in S1 and no change in S2 inputs. ****: $p < 0.0001$. n.s.: not significant.

6.4. Discussion

The experiments reported in this chapter showed that the relative timing of inputs influenced the way subsequent optogenetic release of dopamine modulated corticostriatal STDP in those inputs. Single inputs exposed to pre-post pairing, followed by dopamine release, showed no plasticity in the group average. This is consistent with previous reports showing that pre-post protocols followed by dopamine uncaging resulted in no net change, whereas pre-post stimulation without dopamine caused LTD (Shindou et al., 2019). In relation to the reversed relative timing of inputs, the present results showed that post-pre pairing followed by dopamine release caused robust LTD. Compared with post-pre timing by itself, in the absence of dopamine release, which produced no change (Shindou et al., 2011), the present findings suggest that post-pre pairing caused eligibility for later dopamine-induced LTD. Together, these findings suggest that both pre-post and post-pre pairing cause an eligibility trace, but subsequent dopamine release has different effects in each case. Further experiments examined the STDP when two inputs to the same cell were stimulated at different timing. Under 2-input conditions, the effect of the precise timing of inputs prior to dopamine release was complicated. As with pairing in the case of single inputs, the 2-input pairing plus dopamine release caused different plasticity profiles depending on the relative timing of presynaptic and postsynaptic activity at each input (pre-post vs. post-pre). These results confirm that the effects of dopamine are differentiated according to the relative timing of prior synaptic input and cell firing. However, different plasticity was observed according to the summation profiles of the two inputs. Finally, an associative pairing protocol involving two inputs but without postsynaptic firing, followed by dopamine release, showed even greater dependence on the summation profiles of the two inputs. These findings indicate that dopamine-modulated corticostriatal STDP depends not only on the timing of different inputs, but also whether those inputs interact linearly, sublinearly or supralinearly.

The finding that pre-post pairing followed by dopamine release two seconds after each pairing induced no overall plasticity is consistent with a previous study in which pre-post pairing was followed by UV uncaging of dopamine two seconds after each pairing (Shindou et al., 2019). Despite some differences – such as using different methods to cause dopamine release (optogenetics vs. UV uncaging) and a slight difference in the experimental protocol (spike triplets induced at 50 Hz vs. 100 Hz) – with the present protocol no plasticity was observed, in agreement with the previous study. Shindou et al. (2019) attributed this apparent lack of plasticity to a combination of t-LTD and t-LTP resulting in a net absence of change. In support of that interpretation, when they applied the L-VGCC blocker (10 μM nimodipine), which blocked t-LTD, reliable t-LTP was observed (Shindou et al., 2019). In future experiments, it would be useful to test whether repeating the pre-post pairing plus dopamine release experiment in the presence of an L-VGCC blocker would produce a different result.

In addition to replicating the previous findings with single pre-post pairing plus dopamine release (Shindou et al., 2019; Yagishita et al., 2014), experiments were conducted using post-pre pairing followed by dopamine release. Post-pre pairing has previously been shown to produce an eligibility trace (He et al., 2015), but post-pre pairing followed by dopamine release has not previously been directly tested in the striatum. Although Shindou et al. (2011) showed that post-pre timing by itself, in the absence of dopamine release, produced no change, other reports showed a post-pre LTD, consistent with the present finding (Pawlak & Kerr, 2008; Shen et al., 2008). The present experiments showed that post-pre pairing followed by dopamine release caused LTD. Shindou et al. (2019) argued that the stimulation protocols used by Pawlak and Kerr (2008) and Shen et al. (2008) caused

dopamine release. In addition, the LTD was blocked by dopamine antagonists in both Pawlak and Kerr (2008) and Shen et al. (2008). In the present experiments, LTD was caused by post-pre timing followed by dopamine release, suggesting that post-pre timing can also induce an eligibility trace, with different outcomes from pre-post timing-induced eligibility. The current protocols did not reliably induce LTP, unlike Pawlak and Kerr (2008) and Shen et al. (2008). Differences in patch-clamp methods could be a possibility. Shen et al. (2008) used perforated patch and reliably induced LTP, whereas the current protocols used whole-cell recordings, which could lead to dilution of cytosolic ions and molecules. However, Fino et al. (2010) used both perforated patch and whole-cell patch clamp recordings in their STDP studies and showed no differences in plasticity (Fino et al., 2010). In addition, Pawlak and Kerr (2008) also used whole-cell recordings and the series resistance of the recording pipettes were lower in the current protocol (2 – 10 MΩ) but overlapped in range (8 – 30 MΩ, Pawlak & Kerr, 2008).

In the present study, after the 2-input STDP protocol with optogenetic dopamine release, different plasticity profiles were observed depending on the summation profiles of two inputs. The reasons for these differences are not immediately obvious. Few previous studies of corticostriatal plasticity testing more than one input are available for comparison. However, linear, sublinear and supralinear summation profiles may suggest differences in the degree of overlap of stimulated axons, or locality of the stimulated synapses, which might account for some of these differences. These will be discussed in the general discussion (Chapter 7) along with the effects of these profiles on 2-input stimulation without dopamine described in Chapter 5.

Chapter 7. General discussion

"If I have seen further, it is by standing on the shoulders of giants."
– Isaac Newton

7.1. Introduction

The overall aim of the research reported in this thesis was to study whether the activation of multiple synaptic inputs alters the characteristics of STDP in the corticostriatal pathway. There appear to have been no previous studies of corticostriatal STDP using multiple inputs, yet it is the convergence of multiple inputs to a cell that engages plasticity mechanisms *in vivo*. A comparison of the spikes induced by afferent stimulation and somatic current injection showed that electrical and chemical properties significantly differed, but despite the differences, STDP induced by afferently stimulated spikes showed LTD after pre-post pairing in dSPNs, consistent with the results using a similar standard STDP protocol paired with firing induced by postsynaptic current injection. When two different electrodes were used to stimulate two separate inputs to a recorded cell, different plasticity profiles were observed in dSPNs depending on the timing of inputs relative to firing. However, the relative timing of inputs was not the only factor determining the direction and extent of synaptic plasticity. Cells with nonlinear summation profiles showed different plasticity profiles from cells with linearly summating inputs. Surprisingly, pairing two inputs without postsynaptic spikes induced robust LTD, but with different plasticity profiles from 2-input STDP. These results highlight the effects of interaction of multiple inputs on corticostriatal STDP. When the effects of multiple inputs on eligibility traces were studied, 2-input STDP protocol with optical dopamine release showed different plasticity profiles depending on the timing and summation profiles of the two inputs. In addition, pairing of two inputs without spiking with optogenetic dopamine release also caused associative plasticity, but with variable results between different summation profiles. Although the results were not consistent, with mixed profiles of LTP and LTD, two inputs were differentially modified by dopamine depending on their relative timing. These findings are summarized in Table 7.1. They indicate that striatal STDP and associative plasticity phenomena are sensitive to many factors, which will be discussed in the next sections.

Table 7.1. Plasticity profiles of the STDP experiments with two (S1 & S2) inputs in dSPNs.

summation	**linear**		**sublinear**		**supralinear**	
	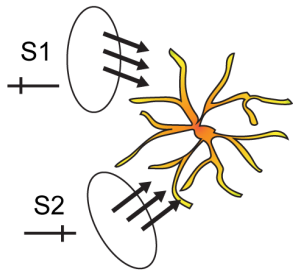		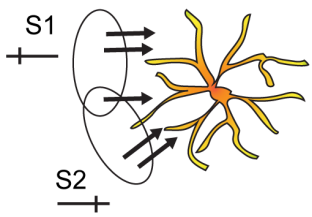		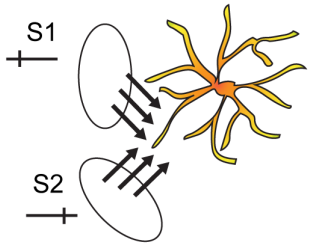	
conditions	**S1**	**S2**	**S1**	**S2**	**S1**	**S2**
S1-S2	ns	LTD	LTD	LTD	LTD	LTD
S1-spike-S2	LTD	ns	ns	LTD	ns	LTD
with dopamine						
S1-S2	LTD	ns (mixed)	LTD	LTD	ns (mixed)	ns (mixed)
S1-spike-S2	LTD	ns	ns (mixed)	ns (mixed)	ns (mixed)	ns (mixed)
S1-spike	ns (mixed)					
spike-S2		LTD				

spike = postsynaptic spiking. ns = not significant.

7.2. Biological interpretation of linear, sublinear and supralinear summation

One question raised in Chapter 2 was whether, given the biophysical activity that occurs in dendrites, inputs with different spike timing could express plasticity in a specific way, a property known as "specificity". Experiments in which two inputs were used showed that different inputs to the same cell could display changes in synaptic efficacy that were not correlated with each other. This is most evident when the two inputs showed linear summation, in which case there was little or no overlap in the axons stimulated or in the dendritic terminations. In these cases, the changes in S1 were different from the changes in S2, indicating specificity (see Table 7.1). Different plasticity profiles induced in a single cell by two near-simultaneous inputs (S1-spike-S2 sequence) were first demonstrated in the cortex by He et al. (2015). The present results are the first demonstration of such specificity in striatal STDP.

Comparison of the plasticity observed when there are two inputs with that seen when only one input is tested, revealed some similarities and differences. For linearly summating inputs, the input exposed to pre-post stimulation (S1 followed by spike) expressed LTD, similar to that described previously for a single pre-post input (Shindou et al., 2011). In other words, the subsequent exposure of the cell to post-pre stimulation (spike followed by S2) in the S1-spike-S2 sequence did not alter the plasticity normally seen in S1 with pre-post stimulation. Similarly, the S2 input in the S1-spike-S2 sequence showed no change, as previously reported for single post-pre inputs (Shindou et al., 2011, 2019). This finding indicates that in the case of linearly summating inputs, the induction and expression of synaptic plasticity was independent of the activity at other inputs.

In the present study, it was often found that two inputs showed nonlinear interactions when the summation test was used (see Fig.A.1 & Table A.1 in Appendix 1). From all the experimental results that had two inputs (n = 117 from Chapters 5 & 6), sublinear summation was the major form of interaction, with 43.6% (n = 54) showing sublinear interaction. Supralinear summation was most rare and accounted for 21.4% (n = 25) of all the inputs. When combined together, nonlinear summation accounted for 65%. In those cases, there appeared to be interactions in the induction of plasticity. Even though the two inputs could change differently, the presence of another input could change the plasticity compared to a single input case, which implies interaction in induction mechanisms. The fact that this interaction occurred when there was non-linear summation suggests that the interaction might be due to overlap and/or repeated stimulation. The use of multiple input stimuli does not automatically ensure that the inputs are perfectly independent, because current spread from each stimulating electrode may result in an overlap of the field of stimulation. On the other hand, the stimulated synapses converging on adjacent parts of a dendrite might interact in complex ways.

The test for linear summation used in the present study made it possible to analyze interacting inputs as separate cases. Sublinear summation – identified when both stimuli given together produce responses less than the algebraic sum of the individual responses – implies that there may be overlap among the stimulated axons. On the other hand, supralinear summation of inputs implies that some type of regenerative interaction occurs among the synapses at the level of the dendrites. These interpretations are simplifications because combinations of these effects might exist. However, this classification provides an empirical basis for inferring these different types of overlap and interaction.

According to this reasoning, with dual stimulation, sublinearity in the tested responses implies that a subset of the same axons, and hence, synapses, is stimulated twice, first by S1 and then by S2. This dual stimulation means that a subset of the synapses contributing to the net change measured with whole-cell recordings, experiences two successive stimuli, and in

the case of postsynaptic spiking, a combination of pre-post and post-pre stimulation. This could cause the co-occurrence of LTP and LTD. Glutamate release on the same, shared synapses by repeated inputs may have enabled an activation of NMDAR due to temporal summation causing increased depolarization, which underlies LTP induction (Fino et al. 2010). This might explain why in the sublinear case of S1-spike-S2, S1 shows no change, in contrast to the linear case, and also in contrast to the single input pre-post LTD. The absence of pre-post LTD in this case may be due to the effects of S2 on some of the same synapses that were activated by S1, if the sublinearity is due to overlap of axons stimulated by S1 and S2. For example, the repeated stimulation might have caused a mixture of LTP (of the overlapped and hence repetitively stimulated inputs) and LTD (of the non-overlapping inputs) and hence no net change.

A different explanation is needed to explain the plasticity in S2 in the sublinear case. In this case S2 showed LTD, in contrast to S2 in the linear case, and also in contrast to the single input post-pre stimulation, that caused no change. Logically, the LTD seen in S2 in this sublinear case could not be due to the repeated stimulation of the overlapping inputs by S1 and S2, which was just hypothesized to cause LTP. A plausible alternative explanation is that the S1 causes depolarization of the dendrites that are receiving S2, so that S2 is more able to initiate voltage-dependent Ca^{2+} entry. Increased local dendritic depolarization might activate L-VGCC contributing to LTD induction (Adermark & Lovinger, 2007). The direct effect of this depolarization would not influence S1 in the same way, because by definition this depolarization comes later.

This explanation is highly speculative and *post-hoc*, in that these changes would not have been predicted before they were observed. However, it may be possible, in the future, to test the plausibility and internal consistency of such scenarios using a detailed computational model or imaging of dendritic activity and synaptic inputs during 2-input STDP protocols.

In the supralinear case, I also saw that S1 showed no change while S2 showed LTD. Supralinearity might arise if multiple synaptic contacts are made in a clustered manner in the same dendrite (Polsky et al., 2004). This could lead to interactive effects because the depolarizing effects of one synaptic input could cause a reduction in membrane potassium currents, which would facilitate the depolarization caused by other inputs (Mahon, Deniau, Charpier, & Delord, 2000; Nisenbaum & Wilson, 1995). With further input the membrane potential could depolarize enough to activate voltage-dependent excitatory conductances. A recent computational study suggested that supralinear Ca^{2+} increase in dendritic spines of SPNs occur if multiple synaptic contacts are made in a clustered manner in the same distal dendrites (Dorman et al., 2018). Interaction of such multiple synaptic inputs at distal dendrites may explain the supralinear summation, and result in greater LTD of the later S2 input. This does not, however, explain why S1 shows no change. The lack of change in S1 could be due to insufficient activation of LTD mechanisms, or alternatively to coactivation of LTP and LTD mechanisms. It is possible that the placement of stimulating electrodes, or the placement of the postsynaptic neuron, that results in non-linear summation, causes one of these possibilities. Further work is needed to explain these findings, which may be possible using two-photon imaging of local dendritic spines to determine the precise location of stimulated synaptic inputs (Weber et al., 2016).

The current results suggest that the interaction of multiple cortical inputs both temporally and spatially alters plasticity. Temporally, interaction of synaptic inputs by sequential stimulation (S1-spike-S2) can cause an accumulation of depolarization. Spatially, interaction of multiple inputs onto dendrites by two stimulations may contribute to prolonged depolarization and a supralinear Ca^{2+} increase. A combination of these temporal and spatial

interactions contributing to nonlinear summation seems to underlie their complex synaptic plasticity profiles.

7.3. Dopamine and eligibility in multiple inputs

The present study investigated the effects on striatal STDP of multiple inputs and different pre-post or post-pre timing. Previous work has shown that dopamine modulates synaptic plasticity in dSPNs when applied by UV uncaging of dopamine after pre-post pairing (Shindou et al., 2019). In this previous study, varying the timing of dopamine uncaging showed that dopamine applied two sec. after pairing, but not at other times, reversed the LTD that normally occurs after pre-post pairing. However, until now there has been no exploration of the effects of dopamine on pairing of multiple inputs or effects of different pre-post or post-pre timing in the corticostriatal pathway. The biophysical considerations calling into question the specificity of STDP – when there are multiple inputs – also apply to the eligibility trace. Is it possible for a cell to have synaptic eligibility traces at multiple inputs and preserve their input specificity?

In the present experiments, pre-post pairing (S1-spike) followed by dopamine release induced no overall plasticity. This is consistent with the effect of uncaging dopamine reported previously (Shindou et al., 2019). It may indicate that this protocol induces both LTD and LTP with net zero change. On the other hand, post-pre pairing (spike-S2) without dopamine caused no plasticity, but when it was followed by optogenetic dopamine release, robust LTD was induced. This suggests that the sequence of post-pre activity also turns on a silent eligibility trace, which is later converted to LTD by the action of dopamine. A similar finding was reported by He et al. (2015) in the cortex, showing that post-pre pairing induced LTD with retroactive serotonin application, but no plasticity in the absence of serotonin.

Dopamine was released optogenetically two seconds after pairing in the present experiments. In the single input condition, this caused the LTD that normally followed pre-post timing to become no change. In an STDP study which also used optogenetic release of dopamine, if dopamine was applied two seconds after the onset of pre-post pairing, no change in plasticity was observed (Yagishita et al., 2014). However, potentiation occurred when the timing of dopamine was 0.6 - 1 sec. after the start of pairing, which was still during pairing (Yagishita et al., 2014). In contrast, after pre-post pairing, application of dopamine via UV uncaging two seconds after pairing resulted in no change, or LTP if LTD was blocked by L-VGCC blocker (Shindou et al., 2019). These findings indicate that there may be differences in the effects of optogenetically released dopamine compared to UV uncaging, possibly related to the different time course of spread of dopamine. Other differences, including the protocol (60 pairing at 0.1 Hz vs. 15 trains of 10 spike triplet bursts at 10 Hz) and the location within striatum (DMS vs. VS), may also contribute to the difference in temporal window (Shindou et al., 2019; Yagishita et al., 2014). For future experiments, it would be useful to investigate different, in particular a shorter (0.6 - 1 sec.) timing of optogenetic dopamine release.

Induction of the eligibility trace when multiple inputs were applied was different from what was observed with only single inputs. In 2-input stimulation, application of dopamine after pairing (S1-spike-S2) had no effect on linearly summating inputs. S1 showed LTD, and S2 showed no change, similar to the results obtained with 2-inputs STDP without application of dopamine as reported in Chapter 5. On the other hand, non-linearly summating inputs showed huge variability in S1 and S2 after dopamine application. This suggests that the initiation, maintenance, or translation of the eligibility trace into plasticity by retroactive actions of dopamine was totally disrupted by having multiple inputs. This was different from the profile of STDP seen with two inputs, which seemed to follow the expected pattern.

Although these results defy simple interpretation, they may indicate that eligibility obeys different rules from STDP. Shindou et al. (2019) suggested that eligibility was not based on Ca^{2+} entry through VSCCs like LTD, but rather involved Ca^{2+}-permeable AMPAR allowing Ca^{2+} into a different subcellular compartment.

Corticostriatal STDP is highly susceptible to subtle differences in experimental conditions, and some electrical stimulation caused dopamine release during the STDP protocols (Pawlak & Kerr, 2008; Shen et al., 2008; Shindou et al., 2019). Dopamine can widen a temporal window for t-LTP, and lower the minimum pairing numbers to induce plasticity in the striatum (Pawlak, Wickens, Kirkwood, & Kerr, 2010; Xu et al., 2018). Eligibility traces are also highly susceptible to subtle differences in experimental conditions and timing, especially when there are multiple inputs. Brzosko et al. (2015, 2017) showed that neuromodulators can retroactively modify the fate of plasticity set up by the initial eligibility traces, showing malleability. In the hippocampus where normally Hebbian STDP is observed, Brzosko et al. (2015) showed that dopamine applied immediately after the end of pairing protocol converted post-pre t-LTD to t-LTP, but not after 10 or 20 minutes after the pairing (Brzosko, Schultz, & Paulsen, 2015). Brzosko et al. (2017) also showed that acetylcholine could convert pre-post t-LTP to t-LTD. This acetylcholine-mediated pre-post t-LTD can further be turned to t-LTP with a retroactive application of dopamine (Brzosko, Zannone, Schultz, Clopath, & Paulsen, 2017). This suggests that dopamine can retroactively modulate plasticity irrespective of the precise order of pairing. The variability between laboratories, and even between synapses on the same neuron, may indicate that the rules for synaptic plasticity are more complicated than assumed in existing computational models.

7.4. What is happening in the associative plasticity?

A surprising finding of the present study was that stimulation of two synaptic inputs in the same temporal sequence as used in STDP induction, but without spiking in the postsynaptic neuron, was sufficient to induce LTD. I refer to this as associative plasticity (S1-S2). This pairing was sufficient to induce LTD, provided the two inputs occurred within a narrow time window of 60 ms. Comparison with controls in which a wider time window was tested (500 ms), and no LTD occurred, showed that the associative LTD was genuinely related to the pairing protocol and not an effect of time, or repeated test stimulation.

To the best of our knowledge, there have been no previous reports of associative LTD in the corticostriatal pathway. However, earlier work has shown that action potentials are not always required for synaptic plasticity. Calabresi et al. (1994) showed that action potentials themselves are unnecessary for LTD but depolarizing current injection was needed to achieve Ca^{2+} influx (Calabresi, Pisani, Mercuri, & Bernardi, 1994). Similarly, Adermark and Lovinger (2007) showed that activation of L-VGCC with membrane depolarization and afferent stimulation was sufficient to induce LTD (Adermark & Lovinger, 2007). With protocols that concern precise timing of pre- and postsynaptic activity, Fino et al. (2009) showed that pairing synaptic inputs with subthreshold depolarization in postsynaptic cells induced plasticity (termed subthreshold depolarization dependent plasticity, SDDP) (Fino et al., 2009). These experimental studies support the idea that a sufficient increase in Ca^{2+} may lead to associative LTD due to the depolarizing effects of the inputs, even in the absence of postsynaptic firing. Control experiments of pairing two inputs with a larger temporal window (500 ms) without postsynaptic spikes caused no plasticity, suggesting that it was the temporal proximity of two inputs (60 ms) that enabled plasticity.

As with STDP, analysis of the degree of overlap or separation of inputs contributing to the associative S1-S2 LTD phenomenon can provide some insight into mechanisms. I

found that cells with linearly summating inputs showed LTD in the later S2, but not in S1, while cells with nonlinearly summating inputs showed LTD in both S1 and S2 inputs.

A potential mechanism for associative plasticity of two inputs without postsynaptic spiking is a local supralinear Ca^{2+} increase. In the absence of backpropagation from somatic spikes, local dendritic summation is likely to play an important role. A detailed biophysical model of SPN predicted that sequential stimulation of clustered distal spines followed by a proximal spine can facilitate Ca^{2+} entry into the proximal spine (Fino et al., 2010; Fino & Venance, 2010; Shindou et al., 2019). The sequential stimulation of two inputs with 60 ms in the present study may have been within the temporal window for such facilitation. Thus, in the case of linear summation, LTD may have occurred in S2 but not in S1 because the sequence S1-S2 is expected to cause increased activation of dendritic currents in S2.

In the case of sublinear summation, if the sublinearity is due to an overlap then some spines can be assumed to be repetitively stimulated at both S1 and S2 timing, which may facilitate accumulation of Ca^{2+} influx. On the other hand, in the case of supralinear summation, as discussed earlier, modelling suggests that activation of clustered distal inputs can also facilitate Ca^{2+} increase in local dendritic spines (Dorman et al., 2018). Experimentally, activation of different dendritic spines on the same dendritic branch by synaptic inputs can facilitate spine activation via local depolarizing events, as recorded in hippocampal pyramidal neurons (Magó, Weber, Ujfalussy, & Makara, 2020). Similarly, synaptic cooperativity of two neighboring inputs onto spines can extend the plasticity time window (Tazerart et al., 2020). Stimulating an additional spine during STDP induction altered Ca^{2+} dynamics and the induction of t-LTP and t-LTD (Tazerart et al., 2020). In this study, Ca^{2+} accumulation due to stimulation of clustered spines was NMDAR-dependent (Tazerart et al., 2020). These experimental and theoretical studies suggest that facilitation of spine Ca^{2+} increase when there are multiple inputs may induce associative plasticity in the absence of postsynaptic firing, provided that the inputs occur within a 60 ms temporal window for facilitation.

Associative plasticity (S1-S2) of two inputs without postsynaptic spiking paired with optogenetic dopamine release showed different profiles from the results without dopamine application. Plasticity was affected by dopamine release in inputs that had linear or supralinear summation. In the case of linear summation, in the absence of dopamine, S1 was unchanged but S2 showed LTD. In the presence of dopamine this was reversed, with S1 showing LTD and S2 showing no change. In the case of supralinear summation, both S1 and S2 showed LTD in the absence of dopamine, and no plasticity in the presence of dopamine. On the other hand, in the case of sublinear summation, both S1 and S2 showed LTD, which was not changed by dopamine. Associative plasticity rules were also disrupted by retroactive actions of dopamine. Dopamine changed the profile of associative plasticity from that seen in the absence of dopamine.

The finding that a postsynaptic spike is not necessary for induction of plasticity may have theoretical importance. It is generally assumed that the rules for STDP embody the essential Hebbian requirement of “takes part in firing” the postsynaptic neuron. The associative plasticity described depends on subthreshold membrane potential changes and not postsynaptic cell firing. There are very few reports of induction of synaptic plasticity by subthreshold stimulation (Fino et al., 2009; Soldado-Magraner et al., 2020; Weber et al., 2016).

Because this form of LTD has not been described previously, there is little theoretical consideration of the possible function of such a mechanism in the striatum. However, changes driven by the subthreshold behavior of a neuron could be sensitive to network dynamics driving the afferents. Correlations among these inputs contain information even if they do not result in postsynaptic cell firing. In addition, the finding is important for the

interpretation of STDP, because associative plasticity presumably occurs in parallel with STDP when there are multiple inputs, and thus STDP includes a component of associative plasticity. This may also co-occur with dopamine- and spiking-dependent synaptic plasticity, for example, by selectively depressing local inputs.

The associative nature of the plasticity together with its sensitivity to subsequent dopamine application suggest that it may play a functional role in certain forms of reward-related learning. Electrophysiological studies in awake animals indicate that corticostriatal synaptic plasticity is necessary for learning (Koralek et al., 2012; Yin et al., 2009). The present study introduces the additional possibility that the integration of local synaptic inputs is sufficient to trigger plasticity, in particular LTD. Both LTD and LTP are involved during learning, but a different plasticity is involved at different stages of learning. For instance, in the DMS, LTP is engaged in the early phase, and LTD is engaged in the late phase of T-maze learning (Hawes et al., 2015). Associative LTD found in the present study is an effective plasticity induction mechanism that bypasses postsynaptic firing. Stimulus-stimulus associations, in the absence of responses, may play an important role in latent learning or cognitive function. Modification of these responses by reward-related dopamine release may help to learn about motivationally significant inputs to the striatum. Associative LTD may thus serve as a filtering mechanism for effective learning.

7.5. Limitations, methodological issues, and recommendations for future experiments

The present study was phenomenological. In order to reveal underlying molecular mechanisms, use of pharmacological agents will be necessary. For future experiments, it will be useful to apply L-VGCC blocker in the presence of optogenetic dopamine release to investigate whether LTD blockade would occur and whether LTP would be induced. However, as reported in Chapter 5, 2-input STDP in the presence of L-VGCC blocker and D1 agonist induced LTD in inputs with linear and supralinear summation. Thus, the plasticity observed in the present study might be independent of L-VGCC, but further studies are needed to confirm this possibility. Other potential sources of Ca^{2+} increase include NMDAR, Ca^{2+}-permeable AMPAR, other types of VGCCs (e.g. R- and T-types) and Ca^{2+} release from inositol triphosphate receptor (IP_3R)-dependent stores (Fino et al., 2010; Fino & Venance, 2010; Shindou et al., 2019). LTD also depends on CB1R and mGluRs (Mathur & Lovinger, 2012). Pharmacological agents for these aforementioned channels and receptors will be useful to identify the underlying molecular mechanisms.

The present study revealed a new form of plasticity, an associative plasticity, which bypasses pairing with postsynaptic spiking. As associative plasticity does not require postsynaptic current injection through whole-cell recordings, long-term changes induced by associative synaptic inputs in multiple neurons could, in principle, be monitored simultaneously by optical means. This would reveal whether different plasticity can be induced in subsets of neurons by the same induction protocol in a striatal microcircuit in brain slices. A voltage or Ca^{2+} sensitive dye (voltage sensor di-4-ANEPPS or Ca^{2+}-indicator Fluo-4FF or Fluo-5F) together with a dopamine sensor (dLight1 or RdLight1) would allow such monitoring of activity of multiple neurons (Gandolfi, Mapelli, & D'Angelo, 2015; Patriarchi et al., 2018; Shindou et al., 2011; Yagishita et al., 2014).

The present study used electrical stimulation to recruit cortical axons. However, the spread of current that occurs with electrical field stimulation means that the stimulated axons cannot be precisely localized. In addition, during electrical stimulation, S1 was always inserted in a more medial part of the cortex and applied at pre-post timing, while S2 was always inserted in a more lateral part and was applied at post-pre timing. This makes it harder

to compare two conditions. In the future, S1 and S2 should be counterbalanced. Instead of electrical stimulation, two-photon imaging of local dendritic spines may provide more precise location of synaptic inputs, and interactions of cortical afferents and dopaminergic inputs may also be identified (Carter et al., 2007; Yagishita et al., 2014). This may also be complemented by the use of a computational model. With the model used in the present study, I was unable to specifically monitor the synapses that were stimulated during the induction protocol, or to incorporate synaptic plasticity. Monitoring behavior of a single spine using a detailed biophysical model incorporating Ca^{2+} dynamics may be useful (Evans et al., 2013; Jędrzejewska-Szmek et al., 2017).

Despite the limitations of the study, it has produced new knowledge about STDP and associative plasticity in the corticostriatal pathway. It has shown that two inputs to the same neuron can change their synaptic efficacy in different ways. This independence is, however, accompanied by a sensitivity to other inputs depending on the degree to which they interact. Thus, the rules for synaptic plasticity observed with multiple inputs activated in different temporal relationships to the postsynaptic spike are not identical to those observed when inputs are tested one at a time per neuron. This is important for placing STDP in the context of whole brain activity. Furthermore, it was observed that plasticity could occur even in the absence of a postsynaptic spike, and that this plasticity could be modulated by dopamine. Further work to clarify the rules for associative plasticity may lead to revisions of current assumptions about the neural substrates of associative learning.

Bibliography

Adermark, L., & Lovinger, D. M. (2007). Combined activation of L-type Ca2+ channels and synaptic transmission is sufficient to induce striatal long-term depression. *The Journal of Neuroscience*, *27*(25), 6781–6787.

Araya, R., Jiang, J., Eisenthal, K. B., & Yuste, R. (2006). The spine neck filters membrane potentials. *Proceedings of the National Academy of Sciences of the United States of America*, *103*(47), 17961–17966.

Arbuthnott, G. W., & Wickens, J. (2007). Space, time and dopamine. *Trends in Neurosciences*, *30*(2), 62–69.

Augustin, S. M., Chancey, J. H., & Lovinger, D. M. (2018). Dual Dopaminergic Regulation of Corticostriatal Plasticity by Cholinergic Interneurons and Indirect Pathway Medium Spiny Neurons. *Cell Reports*, *24*(11), 2883–2893.

Barto, A. G., Sutton, R. S., & Brouwer, P. S. (1981). Associative search network: A reinforcement learning associative memory. *Biological Cybernetics*, *40*(3), 201–211.

Bi, G. Q., & Poo, M. M. (1998). Synaptic modifications in cultured hippocampal neurons: dependence on spike timing, synaptic strength, and postsynaptic cell type. *The Journal of Neuroscience*, *18*(24), 10464–10472.

Bliss, T. V., & Lomo, T. (1973). Long-lasting potentiation of synaptic transmission in the dentate area of the anaesthetized rabbit following stimulation of the perforant path. *The Journal of Physiology*, *232*(2), 331–356.

Bolam, J. P., Hanley, J. J., Booth, P. A., & Bevan, M. D. (2000). Synaptic organisation of the basal ganglia. *Journal of Anatomy*, *196 (4)*, 527–542.

Branco, T., & Häusser, M. (2010). The single dendritic branch as a fundamental functional unit in the nervous system. *Current Opinion in Neurobiology*, *20*(4), 494–502.

Brembs, B., Lorenzetti, F. D., Reyes, F. D., Baxter, D. A., & Byrne, J. H. (2002). Operant reward learning in Aplysia: neuronal correlates and mechanisms. *Science*, *296*(5573), 1706–1709.

Brzosko, Z., Schultz, W., & Paulsen, O. (2015). Retroactive modulation of spike timing-dependent plasticity by dopamine. *ELife*, *4*. doi:10.7554/eLife.09685

Brzosko, Z., Zannone, S., Schultz, W., Clopath, C., & Paulsen, O. (2017). Sequential neuromodulation of Hebbian plasticity offers mechanism for effective reward-based navigation. *ELife*, *6*. doi:10.7554/eLife.27756

Calabresi, P., Maj, R., Pisani, A., Mercuri, N. B., & Bernardi, G. (1992). Long-term synaptic depression in the striatum: physiological and pharmacological characterization. *The Journal of Neuroscience*, *12*(11), 4224–4233.

Calabresi, P., Pisani, A., Mercuri, N. B., & Bernardi, G. (1992). Long-term Potentiation in the Striatum is Unmasked by Removing the Voltage-dependent Magnesium Block of NMDA Receptor Channels. *The European Journal of Neuroscience*, *4*(10), 929–935.

Calabresi, P., Pisani, A., Mercuri, N. B., & Bernardi, G. (1994). Post-receptor mechanisms underlying striatal long-term depression. *The Journal of Neuroscience*, *14*(8), 4871–4881.

Calabresi, P., Saulle, E., Centonze, D., Pisani, A., Marfia, G. A., & Bernardi, G. (2002). Post-ischaemic long-term synaptic potentiation in the striatum: a putative mechanism for cell type- specific vulnerability. *Brain*, *125*, 844–860.

Carew, T. J., Hawkins, R. D., & Kandel, E. R. (1983). Differential classical conditioning of a defensive withdrawal reflex in Aplysia californica. *Science*, *219*(4583), 397–400.

Carter, A. G., & Sabatini, B. L. (2004). State-dependent calcium signaling in dendritic spines of striatal medium spiny neurons. *Neuron*, *44*(3), 483–493.

Carter, A. G., Soler-Llavina, G. J., & Sabatini, B. L. (2007). Timing and location of synaptic inputs determine modes of subthreshold integration in striatal medium spiny neurons. *The Journal of Neuroscience*, *27*(33), 8967–8977.

Cassenaer, S., & Laurent, G. (2012). Conditional modulation of spike-timing-dependent plasticity for olfactory learning. *Nature*, *482*(7383), 47–52.

Charpier, S., & Deniau, J. M. (1997). In vivo activity-dependent plasticity at cortico-striatal connections: evidence for physiological long-term potentiation. *Proceedings of the National Academy of Sciences of the United States of America*, *94*(13), 7036–7040.

Cui, Y., Paillé, V., Xu, H., Genet, S., Delord, B., Fino, E., … Venance, L. (2015). Endocannabinoids mediate bidirectional striatal spike-timing-dependent plasticity. *The Journal of Physiology*, *593*(13), 2833–2849.

Di Filippo, M., Picconi, B., Tantucci, M., Ghiglieri, V., Bagetta, V., Sgobio, C., … Calabresi, P. (2009). Short-term and long-term plasticity at corticostriatal synapses: implications for learning and memory. *Behavioural Brain Research*, *199*(1), 108–118.

Dorman, D. B., Jędrzejewska-Szmek, J., & Blackwell, K. T. (2018). Inhibition enhances spatially-specific calcium encoding of synaptic input patterns in a biologically constrained model. *ELife*, *7*. doi:10.7554/eLife.38588

Doya, K. (2007). Reinforcement learning: Computational theory and biological mechanisms. *HFSP Journal*, *1*(1), 30–40.

Dudek, S. M., & Bear, M. F. (1992). Homosynaptic long-term depression in area CA1 of hippocampus and effects of N-methyl-D-aspartate receptor blockade. *Proceedings of the National Academy of Sciences of the United States of America*, *89*(10), 4363–4367.

Eichenbaum, H. (2018). Barlow versus Hebb: When is it time to abandon the notion of feature detectors and adopt the cell assembly as the unit of cognition? *Neuroscience Letters*, *680*, 88–93.

Evans, R. C., Maniar, Y. M., & Blackwell, K. T. (2013). Dynamic modulation of spike timing-dependent calcium influx during corticostriatal upstates. *Journal of Neurophysiology*, *110*(7), 1631–1645.

Feldman, D. E. (2012). The spike-timing dependence of plasticity. *Neuron*, *75*(4), 556–571.

Fino, E., Deniau, J.-M., & Venance, L. (2008). Cell-specific spike-timing-dependent plasticity in GABAergic and cholinergic interneurons in corticostriatal rat brain slices. *The Journal of Physiology*, *586*(1), 265–282.

Fino, E., Deniau, J.-M., & Venance, L. (2009). Brief subthreshold events can act as Hebbian signals for long-term plasticity. *PloS One*, *4*(8), e6557.

Fino, E., Glowinski, J., & Venance, L. (2005). Bidirectional activity-dependent plasticity at corticostriatal synapses. *The Journal of Neuroscience*, *25*(49), 11279–11287.

Fino, E., Paille, V., Cui, Y., Morera-Herreras, T., Deniau, J.-M., & Venance, L. (2010). Distinct coincidence detectors govern the corticostriatal spike timing-dependent plasticity. *The Journal of Physiology*, *588*(Pt 16), 3045–3062.

Fino, E., & Venance, L. (2010). Spike-timing dependent plasticity in the striatum. *Frontiers in Synaptic Neuroscience*, *2*, 6.

Frémaux, N., & Gerstner, W. (2015). Neuromodulated Spike-timing-Dependent Plasticity, and theory of three-factor learning rules. *Frontiers in Neural Circuits*, *9*, 85.

Freund, T. F., Powell, J. F., & Smith, A. D. (1984). Tyrosine hydroxylase-immunoreactive boutons in synaptic contact with identified striatonigral neurons, with particular reference to dendritic spines. *Neuroscience*, *13*(4), 1189–1215.

Frey, U., & Morris, R. G. (1997). Synaptic tagging and long-term potentiation. *Nature*, *385*(6616), 533–536.

Fuller, J. A., Burrell, M. H., Yee, A. G., Liyanagama, K., Lipski, J., Wickens, J. R., & Hyland, B. I. (2019). Role of homeostatic feedback mechanisms in modulating methylphenidate actions on phasic dopamine signaling in the striatum of awake behaving rats. *Progress in Neurobiology*, *182*, 101681.

Gandolfi, D., Mapelli, J., & D'Angelo, E. (2015). Long-Term Spatiotemporal Reconfiguration of Neuronal Activity Revealed by Voltage-Sensitive Dye Imaging in the Cerebellar Granular Layer. *Neural Plasticity*, *2015*, 284986.

Gerfen, C. R., & Surmeier, D. J. (2011). Modulation of striatal projection systems by dopamine. *Annual Review of Neuroscience*, *34*, 441–466.

Gong, S., Zheng, C., Doughty, M. L., Losos, K., Didkovsky, N., Schambra, U. B., … Heintz, N. (2003). A gene expression atlas of the central nervous system based on bacterial artificial chromosomes. *Nature*, *425*(6961), 917–925.

Graybiel, A. M. (1998). The basal ganglia and chunking of action repertoires. *Neurobiology of Learning and Memory*, *70*(1–2), 119–136.

Gruber, A. J., & McDonald, R. J. (2012). Context, emotion, and the strategic pursuit of goals: interactions among multiple brain systems controlling motivated behavior. *Frontiers in Behavioral Neuroscience*, *6*, 50.

Gulledge, A. T., Kampa, B. M., & Stuart, G. J. (2005). Synaptic integration in dendritic trees. *Journal of Neurobiology*, *64*(1), 75–90.

Hardie, J., & Spruston, N. (2009). Synaptic depolarization is more effective than back-propagating action potentials during induction of associative long-term potentiation in hippocampal pyramidal neurons. *The Journal of Neuroscience*, *29*(10), 3233–3241.

Hawes, S. L., Evans, R. C., Unruh, B. A., Benkert, E. E., Gillani, F., Dumas, T. C., & Blackwell, K. T. (2015). Multimodal Plasticity in Dorsal Striatum While Learning a Lateralized Navigation Task. *The Journal of Neuroscience*, *35*(29), 10535–10549.

Hawkins, R. D., Abrams, T. W., Carew, T. J., & Kandel, E. R. (1983). A cellular mechanism of classical conditioning in Aplysia: activity-dependent amplification of presynaptic facilitation. *Science*, *219*(4583), 400–405.

He, K., Huertas, M., Hong, S. Z., Tie, X., Hell, J. W., Shouval, H., & Kirkwood, A. (2015). Distinct Eligibility Traces for LTP and LTD in Cortical Synapses. *Neuron*, *88*(3), 528–538.

Hebb, D. O. (1949). *The organization of behavior: a neuropsychological theory*. J. Wiley; Chapman & Hall.

Higley, M. J., & Sabatini, B. L. (2008). Calcium signaling in dendrites and spines: practical and functional considerations. *Neuron*, *59*(6), 902–913.

Hille, B. (2001). *Ion channels of excitable membranes* (3rd ed.). Sunderland, MA: Sinauer Press.

Izhikevich, E. M. (2007). Solving the distal reward problem through linkage of STDP and dopamine signaling. *Cerebral Cortex* , *17*(10), 2443–2452.

Jędrzejewska-Szmek, J., Damodaran, S., Dorman, D. B., & Blackwell, K. T. (2017). Calcium dynamics predict direction of synaptic plasticity in striatal spiny projection neurons. *The European Journal of Neuroscience*, *45*(8), 1044–1056.

Kamijo, T. C., Hayakawa, H., Fukushima, Y., Kubota, Y., Isomura, Y., Tsukada, M., & Aihara, T. (2014). Input integration around the dendritic branches in hippocampal dentate granule cells. *Cognitive Neurodynamics*, *8*(4), 267–276.

Kerr, J. N. D. & Plenz, D. (2002). Dendritic calcium encodes striatal neuron output during up-states. *The Journal of Neuroscience*, *22*(5), 1499–1512.

Kerr, J. N. D.& Plenz, D. (2004). Action potential timing determines dendritic calcium during striatal up-states. *The Journal of Neuroscience*, *24*(4), 877–885.

Kerr, J. N. D. & Wickens, J. R. (2001). Dopamine D-1/D-5 receptor activation is required for long-term potentiation in the rat neostriatum in vitro. *Journal of Neurophysiology*, *85*(1), 117–124.

Kincaid, A. E., Zheng, T., & Wilson, C. J. (1998). Connectivity and convergence of single corticostriatal axons. *The Journal of Neuroscience*, *18*(12), 4722–4731.

Koralek, A. C., Jin, X., Long, J. D., 2nd, Costa, R. M., & Carmena, J. M. (2012). Corticostriatal plasticity is necessary for learning intentional neuroprosthetic skills. *Nature*, *483*(7389), 331–335.

Larkum, M. E., & Nevian, T. (2008). Synaptic clustering by dendritic signalling mechanisms. *Current Opinion in Neurobiology*, *18*(3), 321–331.

Letzkus, J. J., Kampa, B. M., & Stuart, G. J. (2006). Learning rules for spike timing-dependent plasticity depend on dendritic synapse location. *The Journal of Neuroscience*, *26*(41), 10420–10429.

Levy, W. B., & Steward, O. (1983). Temporal contiguity requirements for long-term associative potentiation/depression in the hippocampus. *Neuroscience*, *8*(4), 791–797.

Lin, J. Y. (2011). A user's guide to channelrhodopsin variants: features, limitations and future developments. *Experimental Physiology*, *96*(1), 19–25.

Lovinger, D. M. (2010). Neurotransmitter roles in synaptic modulation, plasticity and learning in the dorsal striatum. *Neuropharmacology*, *58*(7), 951–961.

Lynch, G. S., Dunwiddie, T., & Gribkoff, V. (1977). Heterosynaptic depression: a postsynaptic correlate of long-term potentiation. *Nature*, *266*(5604), 737–739.

Magee, J. C., & Johnston, D. (1997). A synaptically controlled, associative signal for Hebbian plasticity in hippocampal neurons. *Science*, *275*(5297), 209–213.

Magó, Á., Weber, J. P., Ujfalussy, B. B., & Makara, J. K. (2020). Synaptic Plasticity Depends on the Fine-Scale Input Pattern in Thin Dendrites of CA1 Pyramidal Neurons. *The Journal of Neuroscience*, *40*(13), 2593–2605.

Mahon, S., Deniau, J. M., Charpier, S., & Delord, B. (2000). Role of a striatal slowly inactivating potassium current in short-term facilitation of corticostriatal inputs: a computer simulation study. *Learning & Memory* , *7*(5), 357–362.

Mahon, S., Deniau, J.-M., & Charpier, S. (2004). Corticostriatal plasticity: life after the depression. *Trends in Neurosciences*, *27*(8), 460–467.

Markram, H., Lübke, J., Frotscher, M., & Sakmann, B. (1997). Regulation of synaptic efficacy by coincidence of postsynaptic APs and EPSPs. *Science*, *275*(5297), 213–215.

Martin, S. J., Grimwood, P. D., & Morris, R. G. M. (2000). An Evaluation of the Hypothesis. *Annual Review of Neuroscience*, *23*, 649–711.

Mathur, B. N., & Lovinger, D. M. (2012). Endocannabinoid-dopamine interactions in striatal synaptic plasticity. *Frontiers in Pharmacology*, *3*, 66.

Matsuzaki, M., Honkura, N., Ellis-Davies, G. C. R., & Kasai, H. (2004). Structural basis of long-term potentiation in single dendritic spines. *Nature*, *429*(6993), 761–766.

Mcgeorge, A. J., & Faull, R. L. M. (1989). The organization of the projection from the cerebral cortex to the striatum in the rat. *Neuroscience*, *29*(3), 503–537.

Molyneaux, B. J., Arlotta, P., Menezes, J. R. L., & Macklis, J. D. (2007). Neuronal subtype specification in the cerebral cortex. *Nature Reviews. Neuroscience*, *8*(6), 427–437.

Moyer, J. T., Wolf, J. A., & Finkel, L. H. (2007). Effects of dopaminergic modulation on the integrative properties of the ventral striatal medium spiny neuron. *Journal of Neurophysiology*, *98*(6), 3731–3748.

Nakano, T., Doi, T., Yoshimoto, J., & Doya, K. (2010). A kinetic model of dopamine- and calcium-dependent striatal synaptic plasticity. *PLoS Computational Biology*, *6*(2), e1000670.

Nevian, T., & Sakmann, B. (2004). Single spine Ca2+ signals evoked by coincident EPSPs and backpropagating action potentials in spiny stellate cells of layer 4 in the juvenile rat somatosensory barrel cortex. *The Journal of Neuroscience*, *24*(7), 1689–1699.

Nevian, T., & Sakmann, B. (2006). Spine Ca2+ signaling in spike-timing-dependent plasticity. *The Journal of Neuroscience*, *26*(43), 11001–11013.

Nisenbaum, E. S., & Wilson, C. J. (1995). Potassium currents responsible for inward and outward rectification in rat neostriatal spiny projection neurons. *The Journal of Neuroscience*, *15*(6), 4449–4463.

Nisenbaum, E. S., Xu, Z. C., & Wilson, C. J. (1994). Contribution of a slowly inactivating potassium current to the transition to firing of neostriatal spiny projection neurons. *Journal of Neurophysiology*, *71*(3), 1174–1189.

Packard, M. G., & Knowlton, B. J. (2002). Learning and memory functions of the Basal Ganglia. *Annual Review of Neuroscience*, *25*, 563–593.

Paille, V., Fino, E., Du, K., Morera-Herreras, T., Perez, S., Kotaleski, J. H., & Venance, L. (2013). GABAergic circuits control spike-timing-dependent plasticity. *The Journal of Neuroscience*, *33*(22), 9353–9363.

Partridge, J. G., Tang, K. C., & Lovinger, D. M. (2000). Regional and postnatal heterogeneity of activity-dependent long-term changes in synaptic efficacy in the dorsal striatum. *Journal of Neurophysiology*, *84*(3), 1422–1429.

Patriarchi, T., Cho, J. R., Merten, K., Howe, M. W., Marley, A., Xiong, W.-H., … Tian, L. (2018). Ultrafast neuronal imaging of dopamine dynamics with designed genetically encoded sensors. *Science*, *360*(6396). doi:10.1126/science.aat4422

Pawlak, V., & Kerr, J. N. D. (2008). Dopamine receptor activation is required for corticostriatal spike-timing-dependent plasticity. *The Journal of Neuroscience*, *28*(10), 2435–2446.

Pawlak, V., Wickens, J. R., Kirkwood, A., & Kerr, J. N. D. (2010). Timing is not Everything: Neuromodulation Opens the STDP Gate. *Frontiers in Synaptic Neuroscience*, *2*, 146.

Polsky, A., Mel, B. W., & Schiller, J. (2004). Computational subunits in thin dendrites of pyramidal cells. *Nature Neuroscience*, *7*(6), 621–627.

Reig, R., & Silberberg, G. (2014). Multisensory integration in the mouse striatum. *Neuron*, *83*(5), 1200–1212.

Reynolds, J. N. J., Hyland, B. I., & Wickens, J. R. (2001). A cellular mechanism of reward-related learning. *Nature*, *413*(6851), 67–70.

Reynolds, J. N. J. & Wickens, J. R. (2002). Dopamine-dependent plasticity of corticostriatal synapses. *Neural Networks*, *15*(4–6), 507–521.

Schultz, W. (1997). Dopamine neurons and their role in reward mechanisms. *Current Opinion in Neurobiology*, *7*(2), 191–197.

Schultz, W., Dayan, P., & Montague, P. R. (1997). A neural substrate of prediction and reward. *Science*, *275*(5306), 1593–1599.

Shen, W., Flajolet, M., Greengard, P., & Surmeier, D. J. (2008). Dichotomous dopaminergic control of striatal synaptic plasticity. *Science*, *321*(5890), 848–851.

Shen, W., Tian, X., Day, M., Ulrich, S., Tkatch, T., Nathanson, N. M., & Surmeier, D. J. (2007). Cholinergic modulation of Kir2 channels selectively elevates dendritic excitability in striatopallidal neurons. *Nature Neuroscience*, *10*(11), 1458–1466.

Sherrington, C. (1942). *Man on His Nature*. Cambridge: Cambridge University Press.

Shindou, T., Ochi-Shindou, M., & Wickens, J. R. (2011). A Ca(2+) threshold for induction of spike-timing-dependent depression in the mouse striatum. *The Journal of Neuroscience*, *31*(36), 13015–13022.

Shindou, T., Shindou, M., Watanabe, S., & Wickens, J. (2019). A silent eligibility trace enables dopamine-dependent synaptic plasticity for reinforcement learning in the mouse striatum. *The European Journal of Neuroscience*, *49*(5), 726–736.

Smith, A. D., & Bolam, J. P. (1990). The neural network of the basal ganglia as revealed by the study of synaptic connections of identified neurones. *Trends in Neurosciences*, *13*(7), 259–265.

Sohur, U. S., Padmanabhan, H. K., Kotchetkov, I. S., Menezes, J. R. L., & Macklis, J. D. (2014). Anatomic and molecular development of corticostriatal projection neurons in mice. *Cerebral Cortex* , *24*(2), 293–303.

Soldado-Magraner, S., Brandalise, F., Honnuraiah, S., Pfeiffer, M., Moulinier, M., Gerber, U., & Douglas, R. (2020). Conditioning by subthreshold synaptic input changes the intrinsic firing pattern of CA3 hippocampal neurons. *Journal of Neurophysiology*, *123*(1), 90–106.

Song, S., Miller, K. D., & Abbott, L. F. (2000). Competitive Hebbian learning through spike-timing-dependent synaptic plasticity. *Nature Neuroscience*, *3*(9), 919–926.

Stern, E. A., Jaeger, D., & Wilson, C. J. (1998). Membrane potential synchrony of simultaneously recorded striatal spiny neurons in vivo. *Nature*, *394*(6692), 475–478.

Stern, E. A., Kincaid, A. E., & Wilson, C. J. (1997). Spontaneous subthreshold membrane potential fluctuations and action potential variability of rat corticostriatal and striatal neurons in vivo. *Journal of Neurophysiology*, *77*(4), 1697–1715.

Stolyarova, A. (2018). Solving the Credit Assignment Problem With the Prefrontal Cortex. *Frontiers in Neuroscience*, *12*, 182.

Stuart, G., Spruston, N., Sakmann, B., & Häusser, M. (1997). Action potential initiation and backpropagation in neurons of the mammalian CNS. *Trends in Neurosciences*, *20*(3), 125–131.

Sutton, R. S., & Barto, A. G. (1992). *Reinforcement Learning: An Introduction*. The MIT Press.

Suvrathan, A., Payne, H. L., & Raymond, J. L. (2016). Timing rules for synaptic plasticity matched to behavioral function. *Neuron*, *92*(5), 959–967.

Tazerart, S., Mitchell, D. E., Miranda-Rottmann, S., & Araya, R. (2020). A spike-timing-dependent plasticity rule for dendritic spines. *Nature Communications*, *11*(1), 4276.

Ting, J. T., Daigle, T. L., Chen, Q., & Feng, G. (2014). Acute brain slice methods for adult and aging animals: application of targeted patch clamp analysis and optogenetics. *Methods in Molecular Biology* , *1183*, 221–242.

Tran-Van-Minh, A., Cazé, R. D., Abrahamsson, T., Cathala, L., Gutkin, B. S., & DiGregorio, D. A. (2015). Contribution of sublinear and supralinear dendritic integration to neuronal computations. *Frontiers in Cellular Neuroscience*, *9*, 67.

Turner, R. S., & DeLong, M. R. (2000). Corticostriatal activity in primary motor cortex of the macaque. *The Journal of Neuroscience*, *20*(18), 7096–7108.

Valtcheva, S., Paillé, V., Dembitskaya, Y., Perez, S., Gangarossa, G., Fino, E., & Venance, L. (2017). Developmental control of spike-timing-dependent plasticity by tonic GABAergic signaling in striatum. *Neuropharmacology*, *121*, 261–277.

Voorn, P., Vanderschuren, L. J. M. J., Groenewegen, H. J., Robbins, T. W., & Pennartz, C. M. A. (2004). Putting a spin on the dorsal-ventral divide of the striatum. *Trends in Neurosciences*, *27*(8), 468–474.

Wanjerkhede, S. M., & Bapi, R. S. (2011). Role of CAMKII in reinforcement learning: a computational model of glutamate and dopamine signaling pathways. *Biological Cybernetics*, *104*(6), 397–424.

Waters. R. H. (1934). The law of effect as a principle of learning. *Psychological Bulletin*, *31*(6), 408.

Waters, J., Nevian, T., Sakmann, B., Helmchen, F., Byrne, J. H., & Sweatt, J. D. (2008). Action potentials in dendrites and spike-timing-dependent plasticity. In J. H. Byrne & J. D. Sweatt (Eds.), *Molecular mechanisms of memory* (pp. 803–828). Amsterdam, NL: Elsevier.

Weber, J. P., Andrásfalvy, B. K., Polito, M., Magó, Á., Ujfalussy, B. B., & Makara, J. K. (2016). Location-dependent synaptic plasticity rules by dendritic spine cooperativity. *Nature Communications*, *7*, 11380.

Wickens. J. R. (2009). Synaptic plasticity in the basal ganglia. *Behavioural Brain Research*, *199*(1), 119–128.

Wickens, J. R., Begg, A. J., & Arbuthnott, G. W. (1996). Dopamine reverses the depression of rat corticostriatal synapses which normally follows high-frequency stimulation of cortex In vitro. *Neuroscience*, *70*(1), 1–5.

Wickens, J. R. & Kötter, R. (1995). Cellular models of reinforcement. In J. C. Houk, J. L. Davis, & D. G. Beiser (Ed.), *Models of Information Processing in the Basal Ganglia.* (pp. 187–214). MIT Press.

Wickens, J. R. & Wilson, C. J. (1998). Regulation of action-potential firing in spiny neurons of the rat neostriatum in vivo. *Journal of Neurophysiology*, *79*(5), 2358–2364.

Wilson. C. J. (1992). Dendritic morphology, inward rectification, and the functional properties of neostriatal neurons. In McKenna,T., Davis, J., Zornetzer, S. F. (Ed.), *Single Neuron Computation*. San Diego: Academic Press.

Wilson. C. J. (2008). Up and down states. *Scholarpedia Journal*, *3*(6), 1410.

Wilson, C. J. & Groves, P. M. (1981). Spontaneous firing patterns of identified spiny neurons in the rat neostriatum. *Brain Research*, *220*(1), 67–80.

Wilson, C. J., Groves, P. M., Kitai, S. T., & Linder, J. C. (1983). Three-dimensional structure of dendritic spines in the rat neostriatum. *The Journal of Neuroscience*, *3*(2), 383–388.

Wolf, J. A., Moyer, J. T., Lazarewicz, M. T., Contreras, D., Benoit-Marand, M., O'Donnell, P., & Finkel, L. H. (2005). NMDA/AMPA ratio impacts state transitions and entrainment to oscillations in a computational model of the nucleus accumbens medium spiny projection neuron. *The Journal of Neuroscience*, *25*(40), 9080–9095.

Xu, H., Perez, S., Cornil, A., Detraux, B., Prokin, I., Cui, Y., … Venance, L. (2018). Dopamine-endocannabinoid interactions mediate spike-timing-dependent potentiation in the striatum. *Nature Communications*, *9*(1), 4118.

Yagishita, S., Hayashi-Takagi, A., Ellis-Davies, G. C. R., Urakubo, H., Ishii, S., & Kasai, H. (2014). A critical time window for dopamine actions on the structural plasticity of dendritic spines. *Science*, *345*(6204), 1616–1620.

Yin, H. H., & Knowlton, B. J. (2006). The role of the basal ganglia in habit formation. *Nature Reviews. Neuroscience*, *7*(6), 464–476.

Yin, H. H., Mulcare, S. P., Hilário, M. R. F., Clouse, E., Holloway, T., Davis, M. I., … Costa, R. M. (2009). Dynamic reorganization of striatal circuits during the acquisition and consolidation of a skill. *Nature Neuroscience*, *12*(3), 333–341.

Yuste, R. (2013). Electrical compartmentalization in dendritic spines. *Annual Review of Neuroscience*, *36*, 429–449.

Yuste, R. & Denk, W. (1995). Dendritic spines as basic functional units of neuronal integration. *Nature*, *375*(6533), 682–684.

Yuste, R. (2010). *Dendritic spines*. The MIT Press.
Zheng, T., & Wilson, C. J. (2002). Corticostriatal combinatorics: the implications of corticostriatal axonal arborizations. *Journal of Neurophysiology*, *87*(2), 1007–1017.

Appendix 1. Supplemental data on EPSP summation

Summation profiles of two EPSPs from all the experimental results that had two inputs (n = 117, results from Chapters 5 & 6) were analyzed (summarized in Table A1). They were classified into three categories, namely, cells showing sublinear, linear, and supralinear summation. Sublinear summation (Fig.A1B) was the major form of interaction, with 43.6% (n = 54) showing sublinear interaction. Sublinear summation occurs if two stimulation electrodes activate some overlapping cortical axons. Sublinear summation was defined as the combined EPSP by simultaneous stimulation below 90% of the arithmetic sum of the two EPSPs. Considering the spatial restriction of electrode placement within the layer V cortex projecting to the DMS and the spread of electricity from two sets of bipolar electrodes, it is reasonable to assume some overlap of cortical axons. Linear summation (Fig.A1C) comprises 35% (n = 41) of all the interactions. Linear summation implies that two stimulating electrodes activate independent sets of cortical axons, which then innervate different branches of dendrites (Polsky et al., 2004). Supralinear summation (Fig.A1C) was most rare form of interaction, with only 21.4% (n = 25). Supralinear summation occurs when multiple inputs are clustered on the same dendritic branches (Dorman et al., 2018; Polsky et al., 2004). Supralinear summation was assumed to have occurred when combined EPSP was 110% or larger than the arithmetic sum.

Table A.1. Summation profiles of two EPSPs.

	All (n = 117)			Sublinear (n = 54)			Linear (n = 41)			Supralinear (n = 25)		
	mean		SEM	mean		SEM	mean		SEM	mean		SEM
S1 (mV)	3.6	±	0.2	3.8	±	0.3	3.7	±	0.3	3.3	±	0.3
S2 (mV)	3.0	±	0.2	3.2	±	0.2	3.0	±	0.3	2.5	±	0.3
arithmetic sum (mV)	6.6	±	0.3	6.9	±	0.4	6.7	±	0.5	5.8	±	0.6
combined EPSP (mV)	6.2	±	0.3	5.0	±	0.4	6.4	±	0.5	8.4	±	0.8
combined EPSP / sum (%)	97.4	±	4.1	71.0	±	2.5	96.5	±	0.9	152.8	±	12.9
S1 stimulus intensity (μA)	311.9	±	27.0	317.5	±	38.1	338.8	±	49.3	256.4	±	59.4
S2 stimulus intensity (μA)	560.3	±	42.1	650.0	±	70.1	530.5	±	66.2	426.0	±	75.8

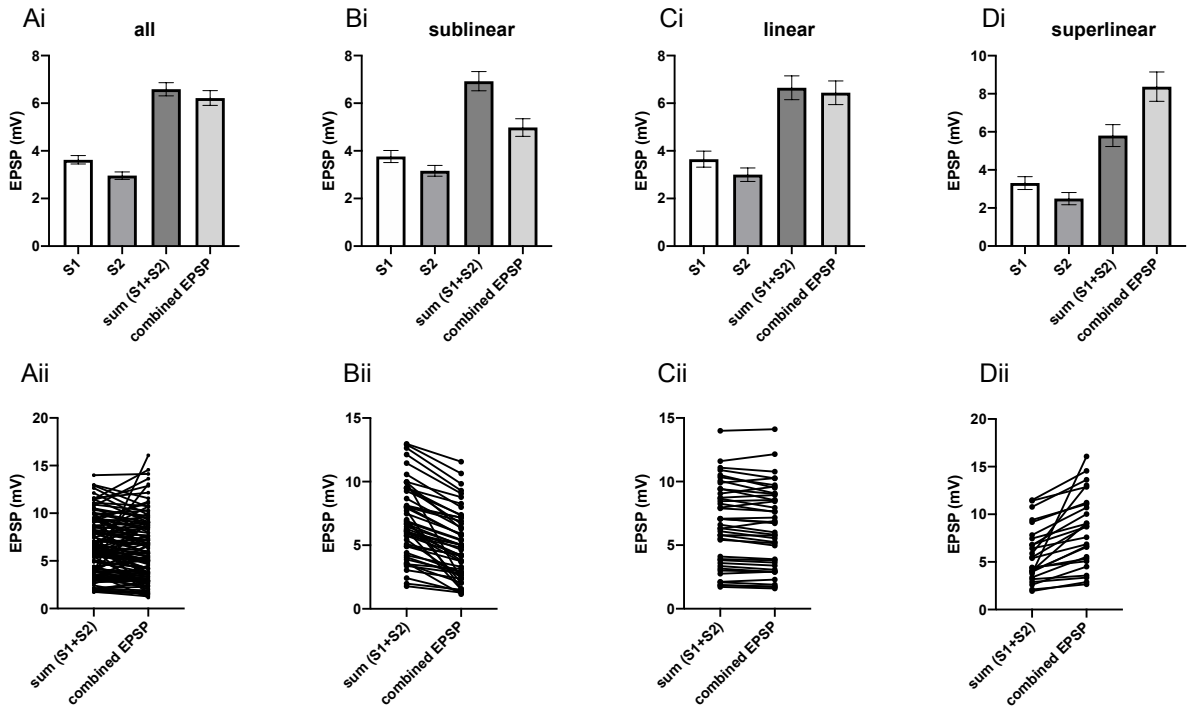

Figure A.1. Simultaneous stimulation of two EPSPs shows sublinear, linear or supralinear summation. (A) S1 EPSP (mV, white), S2 EPSP (mV, mid gray), arithmetic sum of S1 and S2 (mV, dark gray), and combined EPSP by simultaneous stimulation (mV, light grey) from all the experiments with two inputs (n = 17) were plotted. (B) Inputs with sublinear summation (n = 51). (C) Inputs with linear summation (n = 41) and (D) Inputs with superliner summation (n = 25). (i) Bars indicate mean ± SEM. (ii) Dots indicate individual values, line connecting arithmetic sum of two EPSPs and combined EPSP.